Insights Into Mitochondrial Genetic and Morphologic Dynamics Gained by Stochastic Simulation

Harsha Karur Rajasimha

Dissertation submitted to the faculty of the Virginia Polytechnic Institute and State University in partial fulfillment of the requirements for the degree of

**Doctor of Philosophy
In
Genetics, Bioinformatics and Computational Biology**

Dr. David C. Samuels (Committee Chair)
Dr. David R. Bevan
Dr. Alexey Onufriev
Dr. John J. Tyson
Dr. Anilkumar Vullikanti S

Wednesday, the 5th of December, 2007
Virginia Tech, Blacksburg, VA 24061

Keywords: ageing, blood, fission, fusion, heteroplasmy, inheritance, model, morphology, mtDNA, mutations, oogenesis, segregation, stem cells,

**Insights Into Mitochondrial Genetic and Morphologic Dynamics
Gained by Stochastic Simulation**

Harsha Karur Rajasimha

ABSTRACT

MtDNA mutations in mammalian cells are implicated in cellular ageing and encephalomyopathies, although mechanisms involved are not completely understood. The mitochondrial genetic bottleneck has puzzled biologists for a long time. Approximate models of genetic bottleneck proposed in the literature do not accurately model underlying biology. Recent studies indicate mitochondrial morphology changes during cellular ageing in culture. In particular, the rates of mitochondrial fission and fusion are shown to be in tight balance, though this rate decreases with age. Some proteins involved in mitochondrial morphology maintenance are implicated in *apoptosis*. Hence, mitochondrial genetic and morphologic dynamics are critical to the life and death of cells.

By working closely with experimental collaborators and by utilizing data derived from literature, we have developed stochastic simulation models of mitochondrial genetic and morphologic dynamics.

Hypotheses from the mitochondrial genetic dynamics model include: (1) the decay of mtDNA heteroplasmy in blood is exponential and not linear as reported in literature. (2) Blood heteroplasmy measurements are a good proxy for the blood stem cell heteroplasmy. (3) By analyzing our simulation results in tandem with published longitudinal clinical data, we propose for the first time, a way to correct for the patient's age in the analysis of heteroplasmy data. (4) We develop a direct model of the genetic bottleneck process during mouse embryogenesis. (5) Partitioning of mtDNA into daughter cells during blastocyst formation and relaxed replication of mtDNA during the exponential growth phase of primordial germ cells leads to the variation in heteroplasmy inherited by offspring from the same mother. (6) We develop a "simulation control" for experimental studies on mtDNA heteroplasmy variation in cell cultures.

Hypothesis from the mitochondrial morphologic dynamics model: (7) A cell adjusts the mitochondrial fusion rate to compensate for the fluctuations in the fission rate, but not vice versa. A deterministic model for this control is proposed.

Contributions: extensible simulation models of mitochondrial genetic and morphologic dynamics to aide in the powerful analysis of published and new experimental data. Our results have direct relevance to cell biology and clinical diagnosis. The work also illustrates scientific success by tight integration of theory with practice.

Dedication

To my mother

Vani Rajasimha,

and father

late Karur Rajasimha, *M.Sc.* (1950 – 2007)

Author's Acknowledgements

I would like to thank my advisor Dr. David C. Samuels for his invaluable guidance and scientific temperament without which this dissertation would not have been possible. I would like to thank him for his (successful!) attempts at transforming an engineer into a scientist and for making my doctoral research, a rewarding experience.

I am thankful to our experimental collaborators from the Dr. Patrick F. Chinnery laboratory for their timely experiments and allowing us advanced access to the experimental data. I also thank Dr. Anton K. Raap group for giving us the opportunity to develop simulation controls for their cell culture experiments.

I thank each of my committee members (including former committee member Dr. Karen Duca) for their valuable inputs and advise both during individual meetings and during committee meetings.

I thank my long time friends Chetan Shiva Shankar, Nitin Goel, and Shishir Bhatia. Extra thanks are due to Chetan for always being online through the inevitable mood swings during my doctoral research. I thank my former room mates Bhadri Kubendran, Srihari Raghavan, Naveen Srinivasan, Satish Tadepalli, Vedavyas Duggirala, Brijesh Sirpatil, Kishore Sirvole, Sudheer Dhulipala, Raghavendra Nyamagoudar, and Swaroop Neti for cooking delicious food when ever I returned apartment. Long thoughtful conversations with them on various topics especially make my graduate school experience memorable.

I thank Dr. Bruno Sobral's cyber infrastructure group for supporting my doctoral research while I was employed full time in the group. Specifically, I thank Mr. Eric Nordberg, Ms. Rebecca Will, Dr. Dana Eckart and all managers for allowing flexible work schedule to accommodate my doctoral research that had little overlap with my job duties. Special thanks to my present and former colleagues Maulik Shukla, Mudita Singhal, Nishant Vaghela, Chaitanya Kommidi, Bharat Mehrotra, Anand Rathi and Patrick Bradshaw.

I thank all the faculty, staff and students of Virginia Tech, especially of VBI. I especially thank Ms. Dennie Munson for her ever helping attitude and taking care of all the administrative and graduate school paperwork for me. I am grateful to the core computation facility at VBI for their IT support throughout this study. I also thank VBI receptionists and administrative staff for reserving rooms and resources for PhD related meetings.

I thank my brothers Mr. Tejasimha and Mr. Santosh, my sister-in-law Ramya and my little nephew Mr. Abhay. Words cannot thank enough, my mother Vani Rajasimha Karur and father late Mr. Karur Rajasimha for their unconditional love, support and inspiration without which I would not have undertaken this seemingly daunting task.

Very warm thanks to my wife Ashwini and my tiny little daughter Amulya for being so lovely and patient, making my doctoral journey a smooth ride, especially towards the end.

Finally, I thank all persons who may have knowingly or unknowingly contributed to the dissertation in any way. I thank my grandparents in heaven and the almighty for giving me the strength and wisdom to succeed in graduate school.

Grant Information

Table of Contents

List of Figures

List of Tables

1 Chapter 1: Introduction

Chapter 1 introduces the general background concepts in biology and simulation relevant to the dissertation. In particular, the chapter introduces basic mitochondrial biology, mitochondrial DNA (mtDNA) dynamics and its clinical relevance, mitochondrial morphologic dynamics, and the general simulation philosophy. Concepts relevant only to a specific chapter are covered in the introductory section of that chapter.

1.1 Section 1.1: Mitochondrial biology

Mitochondria Structural Features

Figure 1

http://micro.magnet.fsu.edu/
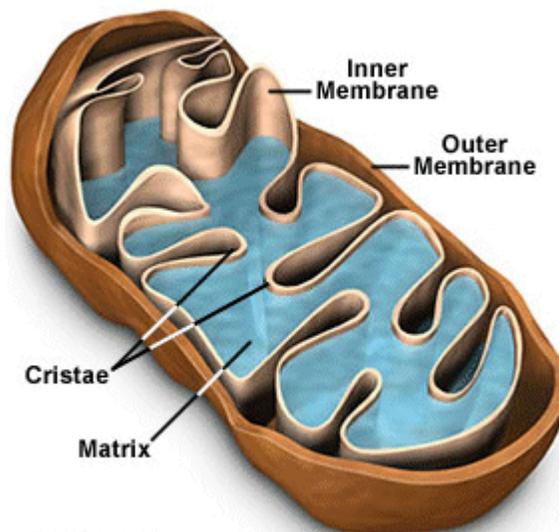
Figure 1: The fine structure of a mitochondrion. Reproduced with permission from Dr. Michael W. Davidson.

Mitochondria are known to be key cellular organelles responsible for central metabolism and energy production in mammalian cells. Mitochondria are now known to also play a role in catabolism of fatty acids, citric acid cycle, nitrogen metabolism, amino acid metabolism, part of urea cycle, inheritance and segregation of mtDNA, apoptosis, ageing, cancer, and other cellular processes and diseases [1, 2]. The typical textbook structure of a mitochondrion resembles a slipper with the mitochondrial matrix enclosed by inner and outer membranes (Figure 1). The two membranes are separated by an inter-membrane space. The inner mitochondrial membrane convolutes into the matrix to form what are called *cristae*. The outer and inner mitochondrial membranes are connected at several points called contact sites [3, 4]. Reichert and Neupert [3], provide an excellent review of the different kinds of contact sites and their known roles. Despite being an important cellular organelle, a lot of open questions are yet to be answered about mitochondrial genetics, morphology and function. Recently, mitochondrial

compartmentalization, mitochondrial dynamic networks, intermembrane bridges, their contacts with endoplasmic reticulum, and mtDNA segregation patterns have been microscopically observed [4]. The elucidation of a variety of mitochondrial diseases and a central role for mitochondria in apoptosis have revived interest in the organelle in the late 1990s [1, 5, 6].

1.2 Section 1.2: Mitochondrial genetics

Mitochondria have their own copy of DNA (mtDNA) [7, 8], separate from the organism's genome, the nuclear DNA. Mitochondria, and hence mtDNA are almost entirely maternally inherited [7, 9-11]. Evolutionary analysis of mtDNA strongly supports the idea that mitochondria originated in evolution as prokaryotic endosymbionts, whose closest contemporaries are purple photosynthetic bacteria [12]. The human mtDNA is a tightly packed 16,569 bp circular loop encoding for 13 polypeptides, 22 tRNAs, and 2 rRNAs [13]. Almost all of the ~16 kbp mtDNA sequence is coding DNA with a very high gene density compared to the nuclear DNA [13]. MtDNA encodes for several protein subunits of the protein complexes critical to energy production by the electron transport chain. MtDNA and nuclear DNA work in close coordination to encode the protein complex subunits involved in energy production and other cellular functions [14]. This is enforced by evidence from Moraes, *et al.* [15-17] that mitochondria from one mammalian species are generally incompatible with the nuclear genome of the other. The mechanisms and the extent of this coordination are not completely understood.

Typically, a human mitochondrion contains 2-10 mtDNA molecules in its matrix and there are several hundreds to thousands of mitochondria in a cell. Hence, a human cell may contain several thousand copies of mtDNA, a state called *polyploidy*. Under certain conditions, groups of a certain number of mtDNA molecules form protein-DNA complexes called *nucleoids*. It is not clear whether mtDNA segregate as individual molecules or as groups of mtDNA compartmentalized into nucleoids or mitochondria during cell division. The number of mtDNA in a cell correlates with the energy needs of the particular cell type. For example, muscular and neuronal cells require more mitochondria for their higher energy needs compared to skin cells. The mtDNA copy number can vary from about a couple hundred in skin cells up to 100,000 cells in primary oocytes. Moraes, *et al.* [17-19] study the factors controlling mtDNA copy number in cells and suggest the idea that shorter mtDNA molecules (mtDNA with large deletions, e.g. 5kb deletion) replicate and repopulate the cell faster compared to the full-length mtDNA. They propose that mtDNA sequence and length contribute more towards mtDNA maintenance than do their functional responsibilities. A cell needs to replicate mtDNA to compensate for the loss of mtDNA due to degradation and due to mtDNA segregation during cell divisions. However, not all mtDNA are replicating simultaneously. Rather, each mtDNA replicates independently of other mtDNA in the cell. Hence the replication process is defined as *relaxed replication of mtDNA [20]*.

Figure 2 taken from MITOMAP [21], shows the popular picture of human mtDNA with some of the known pathogenic mutations marked on it [22]. These pathogenic mutations are shown to cause loss of cellular function, neurodegenerative, and muscular diseases [1, 6, 23]. An exhaustive listing of all known *encephalomyopathies* caused by mutations in mtDNA genes is tabulated by Servidei [24]. Kujoth, *et al.* [23] present the idea of "accelerated ageing" in mice with mutant mtDNA polymerase that accumulate mtDNA mutations and die at an early age. Interpretations in the study have sparked criticisms and discussions [25, 26] in the literature. Pathogenic mtDNA mutations are thus of great importance. Since many of the disease-causing mtDNA mutations are maternally transmitted over generations, it is critical to understand the mechanisms controlling mtDNA segregation not only in somatic cells but also in germ line cells. Improved understanding of mtDNA segregation can assist in providing proper reproductive counseling to women carrying heteroplasmic mtDNA [11, 27].
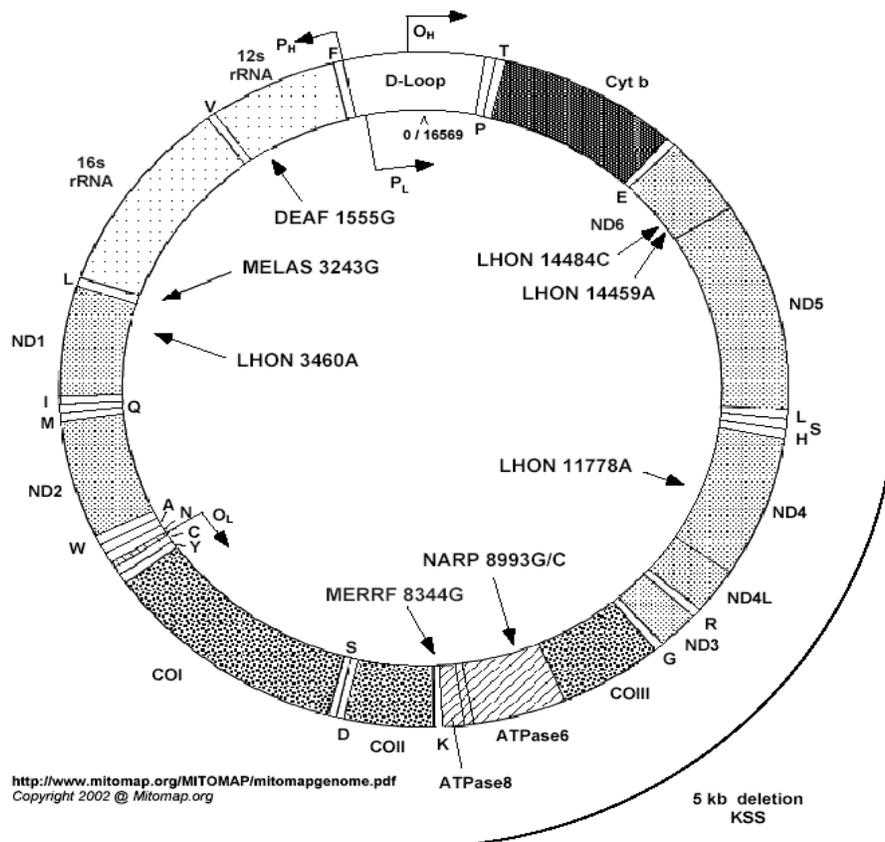
Figure 2: Image of human mitochondrial DNA (mtDNA) of length 16,569 bp, with some pathogenic mutations marked on it. Picture is reproduced with permission from MITOMAP [21].

Individuals harboring pathogenic mutations in their mtDNA typically have a mixture of mutant and wild-type mtDNA in each cell, a condition called *heteroplasmy* [28]. A heteroplasmic cell can function normally until a certain threshold heteroplasmy

level is reached, beyond which cell function is compromised [29-35]. This threshold level depends on the particular mutation and can vary from 60% to 95% (Table 1). *High penetrance mutations* are defined as those mtDNA mutations that can cause disease phenotypes or symptoms consistently above a certain threshold heteroplasmy in an individual. An example of a high penetrance mutation is the most common *MELAS* (mitochondrial encephalomyopathy, lactic acidosis and stroke) mutation 3243A>G (OMIM # 590050.0001) [36, 37]. *Low penetrance mutations* may not always show disease phenotypes even when an individual is homoplasmic to a certain mtDNA mutation. An example for low penetrance mutation is the *MERRF* (Myoclonus Epilepsy associated with Ragged-Red Fibers) mutation 8344A>G (OMIM # 590060.0001).

Table 1: Some of the mtDNA mutations and their threshold derived from literature. The table draws the link between simulation and reality. The only change we do to our model to simulate a mutation is setting the threshold for loss of cell function derived from literature. Note that for certain mutations, the heteroplasmy threshold for cell death may vary among individuals.

MtDNA mutation	Heteroplasmy Threshold (%)	Tissue	In vivo or in vitro	Reference
LHON 3460G>A	60	Cultured Fibroblasts	*In vitro*	[38]
MELAS 3243A>G	95	Osteosarcoma cell cybrids	*In vitro*	[30]
MERRF 8344A>G	95.3 – 97.7	Skeletal muscle	NA	[32]
NARP 8993T>G	90	NA	NA	[34]
LHON 11778G>A	90	Blood	*In vivo*	[29, 39]

LHON: Leber's Hereditary Optic Neuropathy;
NARP: Neuropathy, Ataxia and Retinitis Pigmentosa.

The level of heteroplasmy can vary across cells within a single tissue [40-42], and can vary across tissues in an individual [43-46]. A general pattern to this tissue variation can be deciphered in the most commonly reported mtDNA mutation, 3243A>G. The level of heteroplasmy for this *MELAS* mutation is lower in dividing cell types than it is in long-lived post-mitotic cells in the same individual. The extent of this tissue variation depends on the particular mutation. Specifically, the 3243A>G mtDNA mutation heteroplasmy measured in blood samples are almost always lower than those determined

from muscle biopsies [44, 47]. For some mtDNA mutations, particularly 8993T>G or C, the heteroplasmy is usually fairly uniform across tissue types [48].

1.3 Section 1.3: MtDNA mutations and ageing

The role of mtDNA mutations in human ageing [49] has been a topic of research for several decades. Two theories emerge from the literature on this subject. The *error cascade theory* is based on the assumption that mtDNA mutations disrupt the energy production by the electron transport chain. This disruption subjects the electrons to increased probability of being diverted to *reactive oxygen species* (ROS) production. ROS are highly reactive species that can react with a wide variety of chemicals including the nucleotide makeup of DNA causing new mutations in mtDNA. Orrenius [50] provides a good review on the harmful effects of ROS in the cell. This increases the rate of mtDNA mutation resulting in a vicious cycle of increasing ROS production and increasing mtDNA mutations. Although the *error cascade theory* is reasonable in explaining the accumulation of different mtDNA mutations in the cell, there is doubt that this process plays a significant role in ageing. This is because the error cascade process results in various different mtDNA mutations in the mtDNA of a single cell. However, in elderly cells, a large number of copies of mtDNA with the same mutation are generally found, not the wide range of different mtDNA mutations that would result from the error cascade process [51].

The *clonal expansion theory* presumes that a single mutation event is responsible for all of the identical copies of mutated mtDNA molecules found in older cells. This may be merely due to *random genetic drift* or due to *selection*. As a result, other acquired mtDNA mutations that may occur are eventually lost due to selection or random genetic drift. One question of interest here is whether random genetic drift is enough to explain the clonal expansion of mutant human mtDNA in a typical population of about 1000 mtDNA per cell, within a realistic timescale of less than 100 years.

1.4 Section 1.4: Mitochondrial morphology

Mitochondria are dynamic cellular organelles that move in the cytoplasm and undergo frequent fission and fusion [52, 53]. Mitochondrial movement, fusion, and fission have been extensively reported and reviewed in various eukaryotes ranging from yeast to humans [4, 52, 54-62]. Mitochondrial morphology, motility, and distribution depend on the actin and myosin cytoskeleton and related motors in yeast [54, 63, 64]. Typically, mitochondria form about 15-22% of the cell volume. In somatic cells, the ratio of nucleo-cytoplasm and mitochondria remains approximately constant [65, 66]. Mitochondrial morphologic aspects also depend on cell cycle phase, tissue, and affect the accumulation of mtDNA mutations [67]. Cell cycle linked mitochondrial morphologic dynamics are reported in yeast [54, 63]. Arakaki, *et al.* [68] report that mitochondria appear small and fragmented in early G1 phase but appear bigger and reticular in G1/S phase in HeLa

cells. This is conflicting with Margineantu [69] who report reticular mitochondria in G1 phase and fragmented peri-nuclear mitochondria in S phase of osteosarcoma 143b cells in culture. Hermann and Shaw [54] report studies on mutations that affect mitochondrial morphology and inheritance in temperature sensitive yeast at 37°C. The study demonstrates the importance of the distribution of mitochondria between daughter cells during yeast cell division. Although some of the protein machinery involved in mitochondrial dynamics is highly conserved, the mitochondrial system is complicated and varies across species. We are mainly concerned with human mitochondria in this study.

There is growing evidence in the literature that mitochondrial function is closely linked with its morphology [70, 71]. There are several aspects of mitochondria that affect its morphology and hence its function in the cell. One aspect is the *size or mass* distribution for mitochondria in a cell. The total mitochondrial mass in a cell is fairly stable with slight increase with age [72-75]. Second aspect is the mitochondrial *inner membrane potential*. This potential is shown to be necessary for mitochondrial fission and fusion [57, 71, 76, 77]. Studies [78, 79] of the changes in mitochondrial membrane potential suggest the existence of underlying transient electrically coupled mitochondrial network. Another aspect of mitochondria is the oxidative damage accumulating in them over time. The reason for the accumulation of damaged mitochondria in older cells is not clear. The prevailing theory is *the Lysosomal-Axis theory of ageing* described in Section 1.5.

Figure 3 shows a pictorial representation of the mitochondrial morphologic dynamics. Mitochondria in three polarization states are depicted. The dark green mitochondria are the polarized ones. The majority of mitochondria in a healthy young cell are in a polarized state, meaning that their inner membrane potential is intact. The light green mitochondria are depolarized mitochondria. Depolarization in mitochondria is shown to be reversible [79]. However, some mitochondria in older cells appear to lose all their membrane potential, do not participate in fusion or fission events, swell and cease to function. Such mitochondria are said to have zero polarization (red colored) and are good candidates for lysosomal degradation. Figure 3 shows the fission and fusion events occurring only in polarized mitochondria. The following sections describe in greater detail, what is known about mitochondrial morphologic dynamics.
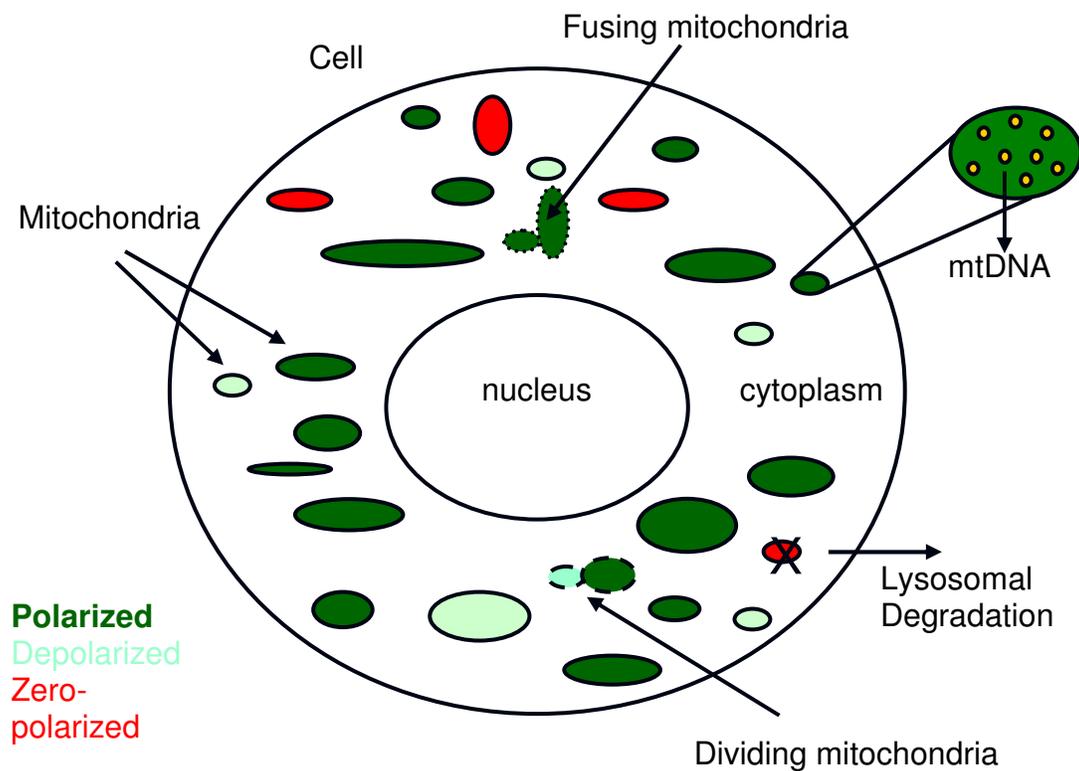
Figure 3: Diagrammatic representation of the mitochondrial morphologic dynamics. Mitochondria of different masses and polarization states are shown. Mitochondrial morphologic events fusion, fission and degradation are depicted. MtDNA are not modeled. (Note: this figure is intended for illustration purposes only and is not drawn to scale).

1.4.1 Mitochondrial motility

Typically, mitochondria do not move freely in the cytoplasm, but rather strictly along the cytoskeleton using actin and myosin motors [65, 80-82]. The polarity of the specific motor on which the mitochondria are riding determines the direction of their motion. Characterization of a signal for energy requirement and its effects on mitochondrial movement can establish the concerted mitochondrial motion, or lack thereof. It is not clear whether mitochondria form a single population or many based on morphologic criteria, differing fate, or genetic differences. Mitochondria are generally assumed to be distributed across the cytoplasm as a single dynamic population [83]. Mitochondrial localization is shown to vary depending on the cell type and energy requirements [84]. There are strict spatial and functional requirements for mitochondria in neurons [85]. Peripheral mitochondria tend to have high membrane potential but peri-nuclear mitochondria have lower membrane potential due to the lesser availability of O_2 [86].

1.4.2 Mitochondrial growth, damage, and degradation

A cell cannot synthesize mitochondria *de novo*. Mitochondria have to be inherited maternally and mitochondrial biogenesis or growth mainly relies on protein import (matrix expansion) and marginally on mtDNA transcription [65]. Mitochondrial growth is coordinated with cell cycle, with mitochondrial mass approximately doubling before cell division [69, 87].

Mitochondria are also major sources of *reactive oxygen species (ROS)*. Since ROS can readily react with almost any entity, they cause damage by reacting with mtDNA and proteins in the mitochondria (*error cascade theory*, Section 1.3). Due to ROS, mtDNA are at risk of pathogenic mutations or degradation. Polarized mitochondria are more active (or functional) and are hence capable of undergoing more damage than depolarized mitochondria. Efficient fusion of mitochondria has been shown to slow down the process of damage accumulation due to rescue of damaged mitochondria by fusion with healthy mitochondria [76, 88].

Damaged mitochondria are degraded or eaten up by the lysosomes in the cell. Lysosomes are efficient in degrading small damaged mitochondria. But, it is proposed that larger mitochondria are not easily degradable by lysosomes [89] implying fission is critical for recycling of (smaller) damaged mitochondria [90]. This also suggests that there is a threshold size for mitochondria to get degraded [91]. Artificially blocking mitochondrial degradation accelerates accumulation of damaged mitochondria [75].

1.4.3 Mitochondrial fission

Mitochondria undergo rapid fission in 3-10 seconds [65, 81]. Bereiter-Hahn and Voth [65], report about 40 fission events per hour per about 100 mitochondria which approximates to about 1 fission event occurring every 1.5 minute in mammalian cells [65]. Blocking fission (e.g., by mutating the Drp1 protein required for mitochondrial fission) blocks the collapse of membrane potential [71]. It is generally assumed that mitochondrial inner membrane potential is required for fission, though there is no direct evidence to support this.

1.4.4 Mitochondrial fusion

Mitochondria fuse together rapidly in a matter of 3-10 seconds [65, 81]. Bereiter-Hahn and Voth [65], report about 40 fusion events per hour per about 100 mitochondria which reduces to about 1 fusion event occurring every 1.5 minute in mammalian cells [65]. Fusion achieves complete mixing of the two mitochondrial matrices in about 12 hours in human cells. However, not every fusion attempt is successful in mixing matrices. Mitochondria have been observed to successfully fuse after several failed attempts [65, 79]. Sequences of fission and fusion at the same site are common. Mitochondrial fusion has been observed at outer and inner membrane contact sites that exhibit high electron

density [65]. Since several contact sites are located along the mitochondrial periphery, it is still not clear where exactly mitochondrial fusion occurs. Some evidences support the idea that fusion occurs only at specific contact sites on the mitochondrial surface [3]. Mitochondrial fusion requires inner membrane potential on both fusing mitochondria [57, 71, 77]. Depolarization of mitochondrial inner membrane blocks inner membrane fusion only, but not outer membrane fusion in human cells [92]. Blocking mitochondrial fusion results in several smaller dysfunctional mitochondria [93]. Maintenance of mitochondrial morphology is tightly linked with mitochondrial function [70]. Mutation in fusion genes are shown to cause diseases [85, 94]. Hence, fusion is required for maintaining both the structure and function of mitochondria.

1.4.5 Mitochondrial morphology during cell division

It is not clearly known how mitochondria are segregated during cell division to daughter cells. In budding yeast, there is evidence [95] that mitochondria are almost equally divided between the mother and bud controlled by actin dependent processes.

1.5 Section 1.5: Mitochondrial morphology and ageing

A balance in the mitochondrial fission and fusion events, maintained by complex protein machinery, is critical for their normal functioning and morphology maintenance [96]. Jendrach, *et al.* [55] show the tight balance between fusion and fission events and how this balance decreases with age. The authors [97] report (Figure 4) higher rates of fusion and fission events in young human proliferative cells (2.16 and 2.19 /10 min/10 μm^2 respectively) in culture. With ageing cells, tight balance in the rates of fusion and fission is still maintained, but at a much lower rate (0.34 /10 min/10 μm^2). Jendrach, *et al.* [55] also report mitochondrial morphologic changes and cristae remodeling in ageing cells. In young proliferative cells in culture, they observe numerous, well structured mitochondria with clearly visible cristae. But with ageing in culture, the cristae undergo remodeling, are degenerate and are barely visible with some mitochondria even showing swollen regions [97]. Various studies [51, 73, 98-108] confirm the ageing related mitochondrial morphologic changes.

An emerging theory to explain the mitochondrial morphologic changes associated with ageing is the *mitochondrial-lysosomal axis theory of ageing* [109]. The theory states that large, damaged mitochondria are formed during cellular ageing either due to defects or inefficiency in fusion and fission of mitochondria or due to defects in the autophagy machinery. Lysosomes are unable to break down and degrade these large mitochondria. Hence, accumulation of such large, damaged, and depolarized mitochondria leads to cellular ageing. This theory is still being tested [110] and faces the criticism that mitotic activity protects cells from death induced by inhibition of autophagy. Hence, it is important to unravel the mechanisms of mitochondrial morphologic degeneration during ageing. Another intriguing question here is, whether mitochondrial morphology degeneration causes ageing or if it is an effect of the ageing process?
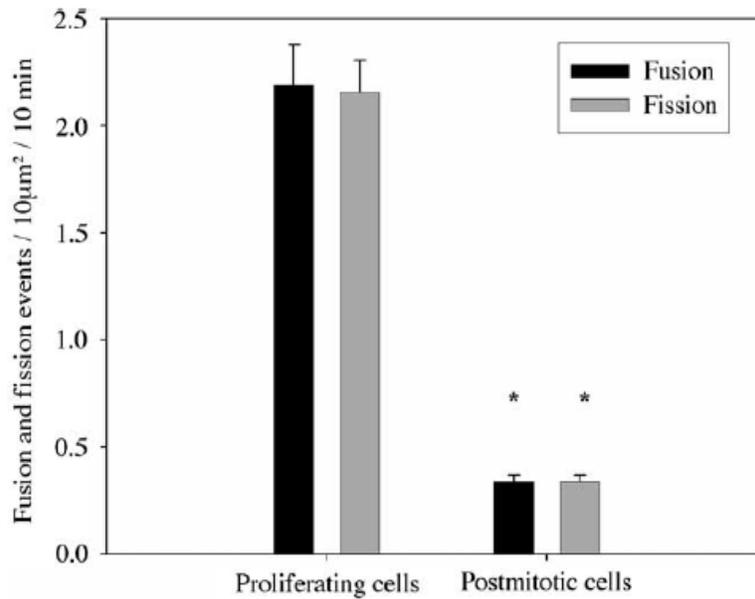
Figure 4: Fission and fusion rates of mitochondria during cellular ageing in culture (Reproduced with permission from Jendrach, *et al.* [111]). Proliferating cells in the figure refer to young and differentiating cells in culture while the post-mitotic cells refer to old (~4 months) non-dividing cells in culture.

1.6 Section 1.6: Mitochondrial fission and fusion machinery

The rates of mitochondrial fission and fusion are tightly coupled in human cells [97]. Increased fission or decreased fusion results in fragmented mitochondria [112] whereas increased fusion or decreased fission results in elongated mitochondria [112]. Increased mitochondrial fragmentation causes a decrease in the mitochondrial inner membrane potential [112]. Whether this decrease in membrane potential is reversible or if it is an irreversible loss of membrane potential is still not clear. It is proposed [77] that slight changes in inner membrane potential could serve to fine-tune fusion rates. These observations suggest that complex protein machinery and signaling mechanisms are involved in mitochondrial fission and fusion events. Several proteins are being identified and implicated a role in fission and fusion machinery [96, 113-115]. The details of the roles of all these proteins [116] involved in mitochondrial morphology are beyond the focus of this study. However, two highly conserved proteins in this machinery deserve mention: a dynamin related protein (Dnm1) that is shown to have a direct mechanistic role in mitochondrial fission [117-119] and a fuzzy onion protein (Fzo1) implicated a definitive role in fusion [120].

Figure 5 shows the mutant phenotypes for *ΔDnm1* and *ΔFzo1* proteins [60]. With the *ΔDnm1*, fission is blocked, and mitochondria assume a mesh like network structure. On the other hand, with the *ΔFzo1*, mitochondrial fusion is blocked, and mitochondria assume a split mitochondrial network. Dnm1 and Fzo1 are thus implicated as key proteins required for fission and fusion events to occur respectively. Interestingly, the ΔDnm1 and ΔFzo1 phenotypes correspond to the phenotypes in exponential and stationary phases of the budding yeast cell cycle respectively [60]. This is counter-intuitive because, we would expect a split mitochondrial phenotype during the phase when a cell is dividing, thereby enabling efficient distribution of mitochondria between daughter cells. One of the questions to answer is why do cells need to shift between the two mitochondrial morphologies? How does this happen in relation to cell cycle?

There is growing evidence [23, 96, 100, 107, 114, 121-162] in literature about the possible roles of mitochondrial morphologic dynamics in *apoptosis or programmed cell death*. Recent studies [163, 164] have confirmed a definite role, though controversial, for mitochondrial fission in apoptosis. Youle [165], Karbowski [166], Oakes [123], Perfettini, *et al.* [167] and Scorrano [125], provide their perspectives and hypotheses on how mitochondrial fission and fusion may mediate apoptosis. There is no clear message emerging on this role right now. Hence, an understanding of how mammalian cells control mitochondrial morphology can have far reaching implications for cancer research, ageing and death of an organism.
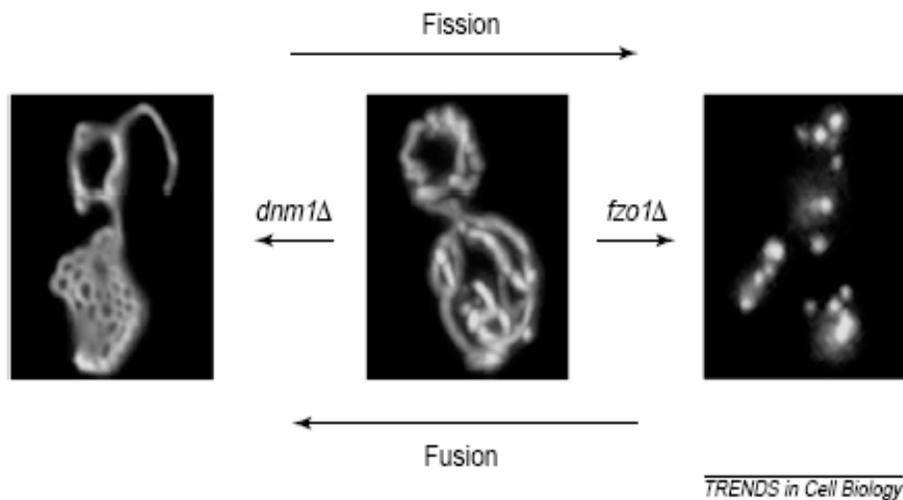
Figure 5: Mutant phenotypes of mitochondrial morphology for the *ΔDnm1* and *ΔFzo1* mutants [60]. This figure is reproduced with permission from Dr. Jodi Nunnari [168].

1.7 Section 1.7: Simulation and experimental interplay

Modeling and simulation is becoming an effective and integral tool for the experimental life sciences. Not only an increasing number of laboratory experiments are including simulation based controls in their study, but also simulation is starting to substitute as *in silico experimentation* [169]. Certain scientific experiments may not be practical in time and space to conduct in the laboratory in one's lifetime. Simulation can be a good alternative in providing approximate predictions in such cases. However, simulation models may not be useful if they are not developed with due consideration to the model's purpose and by utilizing available experimental data to drive the modeling. Building valid and scientifically useful simulation models is as much an art as it is science. The process involves learning from trial and error and needs to be incremental and iterative. It is both a necessary pre-requisite and a desired outcome to thoroughly understand the system to be modeled. A delicate balance is needed to define the boundary of the system to be modeled by avoiding unnecessary details and not ignoring relevant mechanisms and parameters.

1.8 Section 1.8: Cellular simulation initiatives from literature

Novel simulation-based research initiatives in mitochondria and cell biology are recently reported [170-173]. Most simulation efforts in biology are based on continuous modeling of a number of linked metabolic reactions grouped into pathways or a set of periodic cellular events such as those occurring in cell cycle. Examples include the mathematical model of cell division cycle in fission yeast developed at the Tyson laboratory [174-176]. Djafarzadeh, *et al.* [173] model the metabolic pathways in mitochondria using the DEVS formalisms [177] and the CD++ toolkit [173] for defining discrete event models. The Coller, *et al.* [178, 179] team at Harvard is actively pursuing research to understand mtDNA heteroplasmy and mutant homoplasmy in stem cells and tumors with a very similar computer modeling approach as ours. Reder [180] has proposed models to study the evolution of mitochondrial genetic state of a cell culture. We believe that the methods we develop here are computationally efficient in our software design enabling us to simulate much larger mtDNA numbers in many more cells over much larger time scales. Aimar-Beurton, *et al.* [181] aim to apply high-throughput experimental methods developed in genomics to construct complete metabolic maps of mitochondria from sequenced eukaryotic genomes. The authors plan to utilize such genome scale data to develop *virtual mitochondria* to eventually include as a module in a *virtual cell*. Takahashi, *et al.* [182] develop the E-CELL System: an open source software platform for modeling, simulation and mathematical analysis of the cell. Yugi and Tomita 2004 [183] develop kinetic models of metabolic pathways in mitochondria to study the pathological analyses of mitochondrial diseases. Whole cell simulation is a grand challenge both from the software engineering perspective [172] and the biological perspective. We believe that such endeavors will bear fruit only after smaller subsystems of the cellular system are well understood, the bottom-up approach. We hope that our

simulation models of mitochondria take us a step forward in the direction of achieving this grand goal. Here, we model the effects of genetic and physical events on cell fate using object-oriented design and implementation in C++.

1.9 Section 1.9: Insights gained or hypotheses arising from the simulations

In this section, we list the key contributions (or results or hypotheses or insights) from the dissertation. The detailed and integrative analyses of simulation and experimental data that lead us into these hypotheses are presented in Chapters 4, 5, and 7. Analyses leading to hypotheses 1, 2, and 3 are to appear in peer reviewed journals [184-186].

Hypothesis 1

Decay of mutant mtDNA proportion in hematopoietic stem cells is exponential [184, 185]. (Refer Section 4.5).

Hypothesis 2

The hematopoietic progenitor cell expansion process that forms mature blood cells does not significantly alter the mean mtDNA heteroplasmy compared to the exponential decay of heteroplasmy in the stem cell population over long time scales [184, 185].
(Refer Section 4.5).

Corollary 1 to Hypothesis 2

Mean mtDNA heteroplasmy measurement in peripheral blood is a good approximation for the mean heteroplasmy level in the hematopoietic stem cell population [184, 185].
(Refer Section 4.5).

Corollary 2 to Hypothesis 2

MtDNA selection occurs at the stem cell population level and not at the progenitor cell expansion level. Random genetic drift and selection at the cellular level together play a role in the exponential decay of the average blood heteroplasmy [184, 185].
(Refer Section 4.5).

Hypothesis 3

Partitioning of mtDNA molecules into different cells pre- and post-implantation with blocked mtDNA replication, followed by segregation of mtDNA between proliferating primordial germ cells with resumption of mtDNA replication explains the mitochondrial genetic bottleneck puzzle [186].

(Refer Section 5.3).

Hypothesis 4

The mitochondrial genetic dynamics model can be applied to study mtDNA segregation during growth of cell cultures.
(Refer Chapter 6).

Hypothesis 5

A mammalian cell controls mitochondrial morphology by controlling the rate of fission, the rate of fusion, or both. By altering the rate of fission, the cell can force the desired change in the rate of fusion. But the cell cannot control the rate of fission by altering the rate of fusion. This control mechanism can be described by a deterministic model.
(Refer Chapter 7).

2 Chapter 2: Research Focus

Chapter 1 provided an introduction to mitochondrial genetic and morphologic dynamics and set the stage for general research in the area. Chapter 2 motivates the specific research questions addressed in or relevant to the dissertation. Mutations in mtDNA are implicated in several encephalomyopathies and the protein machinery involved in mitochondrial morphology maintenance is also shown to play a role in apoptosis or programmed cell death. Hence, mitochondrial genetic and morphologic dynamics are critical to the life and death of cells.

2.1 Mitochondrial genetics

Chapter 1 provided literature references to the fact that mtDNA plays a critical role in the normal functioning of a cell and that mutations in mtDNA are implicated in several encephalomyopathies. Mitochondrial disease symptoms are visible only for heteroplasmy levels above a certain threshold (Table 1). Since mtDNA segregation patterns determine the heteroplasmy level in a cell, and because mtDNA are primarily maternally inherited, a clear understanding of mtDNA heteroplasmy segregation is needed not only in somatic cells but also in germ line cells.

2.1.1 Decay of mtDNA heteroplasmy in blood

Longitudinal clinical studies for the 3243A>G MELAS mtDNA mutation suggest that heteroplasmy levels in blood tend to slowly decrease over time [187-189]. Most of this data is based upon pairs of blood sample measurements separated by several years. These studies report a 0.5 to 2% decrease in heteroplasmy per year. Chinnery, *et al.* [190] suggest that this decrease occurs due to selection at the cellular level. However, it is not clear whether the selection occurs in the blood stem cell population or the proliferating and differentiating blood precursor cells. Hence, an answer to this question can help clinicians in the diagnosis of mitochondrial diseases.

Which cell type contributes more to the decay of mtDNA heteroplasmy in adult human blood? Is it the heteroplasmy changes in blood stem cells or the changes in proliferating and differentiating blood precursor cells?

To answer this question, we develop two separate simulations (Chapter 4) to understand the changes in heteroplasmy levels in blood. The first simulation models the heteroplasmy changes in the blood stem cell population and the second simulation models the heteroplasmy changes in the blood precursor cells. We show from our analysis of the simulation output data that heteroplasmy changes in the stem cell population significantly contribute to the decay of mean blood heteroplasmy and that the contribution of heteroplasmy changes in precursor cells is negligible. Meaning, selection

against mutant mtDNA occurs in the stem cell population and not significantly in the blood precursor cell population.

Since adult hematopoietic stem cells form the precursors of peripheral blood, we can answer a related question,

Can we predict the average mtDNA heteroplasmy for the 3243A>G mutation in adult human blood stem cells, given the average heteroplasmy in peripheral blood?

From our findings (Chapter 4), we hypothesize that heteroplasmy measurement in peripheral blood can serve as a good approximation to those in the stem cell population.

The longitudinal studies of 3243A>G MELAS mutation [187-189] have a limitation. They report 0.5 to 2% decrease in heteroplasmy per year based on blood heteroplasmy measurements in subjects at two different ages. This limited data suggest a linear decrease in heteroplasmy with age. Since many functions may appear as linear when analyzed within a narrow time range, we should look at this decrease over larger time scales. This raises the question,

Is the decay of blood mtDNA heteroplasmy for 3243A>G mutation linear as reported in the literature?

Our simulation-based collective analysis of old and new clinical data (Chapter 4) from literature shows that the decrease in the rate of heteroplasmy actually follows an exponential function and is not linear as presumed in literature.

Are the results for 3243A>G MELAS mutation also applicable to all mtDNA mutations?

Our analysis indicates that the results we obtain based on the analysis of clinical data for 3243A>G mutation but not for low penetrance mutations such as the 8344A>G MERRF mutation or any of the LHON mutations (Chapter 4).

2.1.2 Mitochondrial genetic bottleneck

Mammalian mtDNA is primarily maternally inherited. Heteroplasmic females transmit varying proportion of mutant mtDNA to their offspring. In humans with mtDNA disorders, there is evidence that disease severity correlates with the proportion of mutant mtDNA inherited from mother. Despite the high mtDNA copy number (10^5) in mature oocytes and the relatively small number of cell divisions in the female germ line, mtDNA genotypes segregate rapidly between generations [191]. Drastic changes in heteroplasmy levels can occur in a single generation. The general explanation for this variability is that only a very small number of mtDNA molecules per cell are passed on to the next generation during embryogenesis. This is termed as *the bottleneck*. Some important questions concerning the bottleneck are,

What is the size of the mitochondrial genetic bottleneck?

Earlier reports[192-194] based on complete switching in a single generation in cattle indicate that the bottleneck size can be as low as a 1 – 10 mtDNA molecules. Jenuth, *et al.* [191] estimate the genetic bottleneck size in murine models to be ~200 mtDNA molecules. However, they base this estimation on an approximate model of the bottleneck process explained in Chapter 5. We develop a direct model of the biological process leading to genetic bottleneck by working closely with experimental collaborators to estimate the bottleneck size.

What is the mechanism by which mammalian offspring from the same mother inherit dramatically variable levels of mtDNA heteroplasmy?

Based on our model of mtDNA dynamics in the mouse embryo during pre- and post-implantation, we show that the partitioning of non-replicating mtDNA into daughter cells during pre-implantation blastocyst formation and the exponential growth of primordial germ cells with the resumption of mtDNA replication is responsible for the variation in heteroplasmy transmitted to offspring by the heteroplasmic female mice. Values for our simulation parameters are derived from literature. The model clarifies the mechanism for rapid heteroplasmy shifts during mammalian embryogenesis (Chapter 5). These results have implications for pre-implantation genetic diagnosis for pregnant women carrying mtDNA mutations [195].

A related question is:

Do mtDNA segregate as individual molecules or as groups of mtDNA (nucleoids or mitochondria)?

Our experimental collaborators observe rapid changes in the heteroplasmy levels during the expansion of cells in cell cultures in the laboratory. We develop control simulations (Chapter 6) to test the hypothesis that mutant and wild-type mtDNA segregate individually to daughter cells with equal probability during cell division.

2.2 Mitochondrial morphology

2.2.1 Cell's control of mitochondrial fission and fusion rates

Recent literature [97] suggests that the rates of mitochondrial fission and fusion are strongly coupled. The rates of fission and fusion events are balanced at a much higher rate of occurrence in young proliferative cells in culture but the rates decrease significantly in old post-mitotic cells in culture, though the balance between fission and

fusion rates is maintained during ageing [97]. However, it is not clear how the cell controls the balance between the rates of fission and fusion events. Since changes in mitochondrial morphology have been implicated in ageing and apoptosis, it is important to understand how the cell controls mitochondrial morphology. Specifically, we need to understand the control mechanism by which the cell maintains the balance in fission and fusion rates.

How does the cell control the balance in the rates of mitochondrial fission and fusion events?

We develop a stochastic simulation model and a deterministic model of the mitochondrial morphologic dynamics by utilizing experimental data. Based on our analysis, we hypothesize that the cell controls the mitochondrial morphology by controlling the rate of fission.

A related question of interest is:

Why the balance in fission and fusion rates decreases with cellular ageing in culture?

3 Chapter 3: Research Methods

Chapter 3 introduces the general research approach to this study. The chapter describes the role of modeling and simulation as a discipline and tool in this research. It then presents the basic models and algorithms developed or borrowed from literature to simulate the basic cellular processes affecting mtDNA heteroplasmy and mitochondrial morphology. The models presented here are referred by the scientific models described in Chapters 4, 5, 6, and 7.

3.1 Section 3.1: Introduction

There is an enormous amount of published experimental data in the literature related to mitochondrial genetic and morphologic dynamics. This resource is, at best, only partially utilized, analyzed and applied in arriving at scientific conclusions. Our general philosophy is to utilize this data to develop predictive simulation models to hypothesize the mechanisms that underlie biology and to arrive at useful biological and clinical conclusions. This is especially illustrated in Chapter 4 where we analyze a large pool of clinical data based on the theoretical limit we computed from our simulations. The approach is to develop computational models of the biological subsystems by utilizing experimental data from literature and collaborators. While choosing the boundaries of the subsystem to model, we limit ourselves to those components that have good literature references. After verification and validation, we apply the models to answer specific scientific questions of interest. We highlight an instance where simulation based analysis leads to uncovering an experimental error in Chapter 4.

Balci [196] and Sargent [197] offer different perspectives on modeling methodologies. While we do not directly use a specific methodology from literature, the simulation model is developed with due consideration of the methodology and conceptual framework. Iterative enhancement with incremental builds constitutes the methodology of model development. We incrementally program and test individual subroutines such as random number generation and the required probability distributions. The algorithm used to generate a uniform random number taken from the book "Numerical Recipes in C" [198] is originally proposed by Park and Miller [199]. The subroutines for generating a Poisson distribution and binomial distribution are also taken from the same source. All these subroutines are implemented as 'C' functions and included in a header file. A Poisson distribution is used to choose the number of wild-type and mutant type mtDNA to be degraded during each time step. A binomial distribution is used to choose the number of wild-type and mutant-type mtDNA to be copied during a time step based on the current numbers in the cell.

Two of the popular modeling methods in practice are discrete and continuous modeling. Most published experimental data are measured at discrete time intervals rather than continuously. Hence, we choose the discrete modeling approach rather than

the continuous method as the system to model is discrete. For example, the number of mtDNA in a cell is a discrete number of mtDNA molecules and not a continuous function.

Another way of distinguishing simulation models is deterministic versus stochastic. In deterministic models, given a set of values for all input parameters, the output(s) can be accurately calculated. On the other hand, in stochastic models, one cannot calculate the output based on values of input parameters. There is stochasticity in these models in terms of the probabilities of events occurring in a given time period. The output of stochastic models will depend on these probabilities. In this study, we assume that the phenomena are stochastic [200] and adopt stochastic modeling over deterministic modeling.

We model the biological entities such as cell, mitochondria, mtDNA as agents or objects in C++. The events that these objects undergo such as cell division, cell death, mitochondria fission, fusion, mtDNA replication and degradation are modeled in subroutines. Algorithms for pseudo random number generation, Poisson distribution, and binomial distribution are directly borrowed and implemented as subroutines from a standard text book [198]. These routines are included in a header file and are used for calculating the number of events that should occur in a time step. All data analyses presented in this dissertation are performed using the package Origin from Origin lab.

3.2 Section 3.2: Conceptual framework

To implement the simulation model, we consider event scheduling and activity scanning conceptual frameworks [201]. Our objectives require that we perform statistical analysis on the state of the system at specific intervals of time in order to make valid predictions. For example, consider the following questions: Given an initial number of stem cells to start with, what is the number of simulated cells that are alive after 50 years? What is the average number of blood cells produced per day? Starting from a given initial mutation level in given number of cells, how does the mutation level change over a 5, 10, 20 year period? To answer such questions, activity scanning with fixed time increments allows a simple and logical design of the program flow. The simulation termination condition is time based and statistical routines are to be called at regular intervals of time in order to save the system state at those times. Since there are only a limited number of different events that can occur at each time point (cell division, cell death, mtDNA copy, and mtDNA degradation), it is inexpensive to scan through them. We deal with a large number of cells (millions), and an event scheduling approach would mean scheduling (or queuing) millions of events whenever an event occurs (since several events are expected to occur at each time step). This would be memory and CPU inefficient [202]. Activity scanning overcomes this inefficiency by assigning a probability of occurrence for each event in each time step. Also, we do not save all the attributes of the system at every time step, but only those averaged over intervals of time. Hence, we adopt the *activity scanning* conceptual framework [201] with fixed increment time flow mechanism.

3.3 Section 3.3: Model verification and validation

Model verification and validation techniques are included in the model development process. Two of these techniques taken from Law and Kelton [124] are presented here.

3.3.1 Analysis by plot

Individual subroutines such as random number generation, Poisson, binomial, cell division, and statistics subroutines are verified using short programs and plotting the output data. Subroutines derived from published sources [199] are subject to one time verification to eliminate any implementation errors. For the blood cell model, one of the verification and validation (V&V) procedures is to analyze the counts of the number of cells living and dying due to mutation threshold (Figure 6). We note that there is no cell death in the first twelve days and thereafter the death count rises exponentially as the simulated cell count does. In addition, the death events are small in number indicating that the cascaded cell divisions do not cause many cells to exceed the mutation threshold.
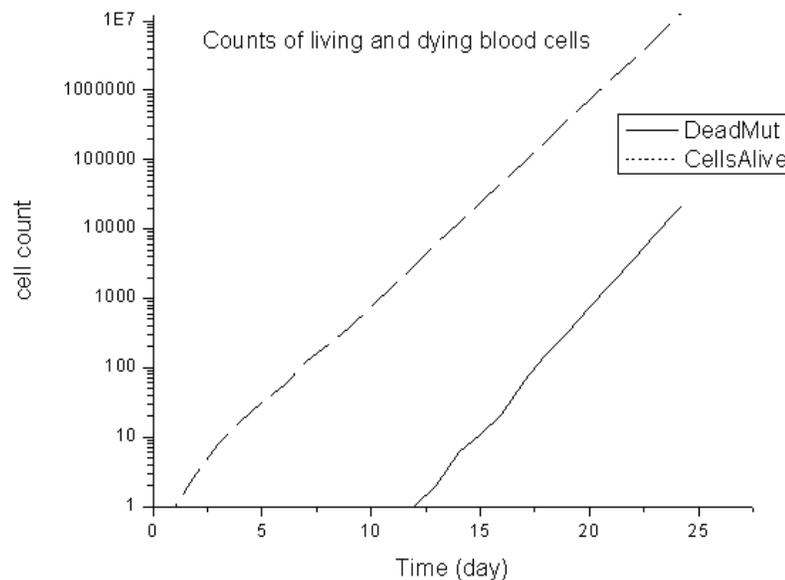
Figure 6: Analysis by plot: Exponential expansion of the blood progenitor cells and the number of cells dying due to mutation threshold over time. Cell death first begins after ~12 days when the heteroplasmy in cells begins to exceed threshold for cell death.

3.3.2 Desk checking

The simulations are subject to routine desk checking whenever model increments or modifications are made. *System behavior graphs* (e.g., Figure 7) are used to perform desk

checking to ensure that the data structures for the critical parameters are storing the right data. The validation criteria set for this model are based on the standard expectations or the biological scenario derived from literature. The total number of mtDNA in a cell (N = W+M) should be fairly constant (very little initial variation and then it stabilizes). If the model is implemented right, the average number of W and M type mtDNA in all living stem cells should behave as shown in Figure 7. We expect the total mtDNA count per cell to fluctuate slightly around the set number (5,000 in this case). The M count will start decreasing as the cells begin to die due to exceeding the mutation threshold and W counts start increasing. Simulation runs performed for exact parameter set with different random number seeds (idum) serve as a verification procedure.
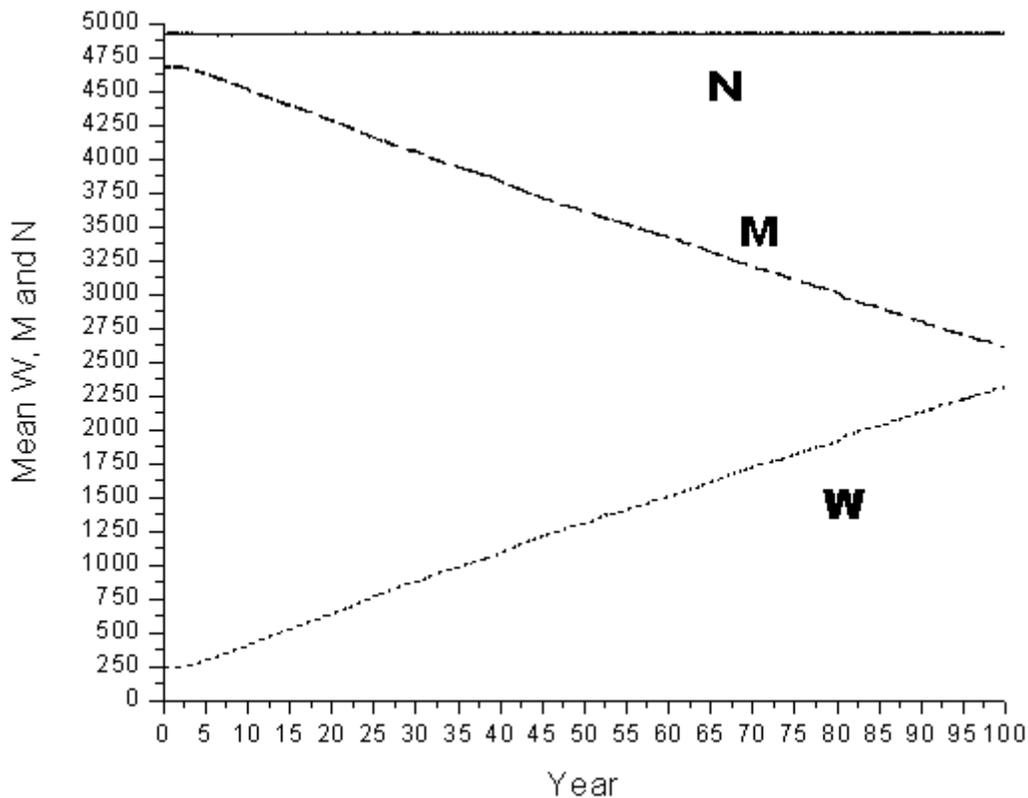
Figure 7: Desk checking: A plot of the mean values of W, M and N for a stem cell simulation run starting at 95% mutation level with the heteroplasmy threshold for loss of cell function set at 100%. N is initialized to 5000 and W and M are initialized to 5% and 95% of N respectively.

In Chapter 4, we apply the general research methods presented here to develop the mitochondrial genetic dynamics model. We show a powerful way of analyzing clinical heteroplasmy data together with simulation results. Applications of the mitochondrial genetic dynamics model to study mtDNA heteroplasmy segregation during mouse oogenesis and cell cultures are presented in Chapter 5 and Chapter 6 respectively.

4 Chapter 4: Blood Stem Cells Model

Chapter 4 describes in detail, the mitochondrial genetic dynamics model, its application to adult hematopoietic stem cell system and its usefulness in analyzing clinical heteroplasmy data for a MELAS mutation (3243A>G) from patients over a wide range of ages. The model aims to address specific questions motivated in Chapter 2. The simulation development methodology and preliminary results were presented at the winter simulation conference in 2004 [184]. The key results and conclusions from the model presented here, are to appear in the *American Journal of Human Genetics*, Feb 2008 [185].

4.1 Section 4.1: Hematopoietic stem cells
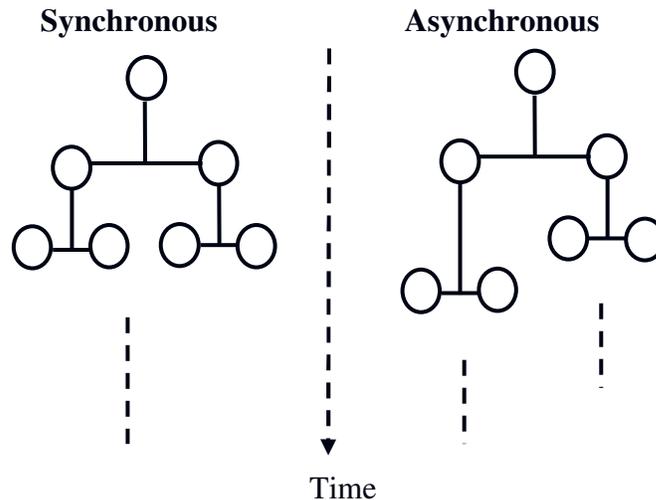
Figure 8: Synchronous and asynchronous cell division types. In synchronous cell division model, all cells in the system divide at the same time. Whereas in asynchronous cell division model, each cell divides independently with the mean time between cell divisions being the same for all cells in the system.

The hematopoietic stem cell system consists of about two million stem cells in the bone marrow [203]. The blood stem cells undergo rare cell divisions with an average time between cell divisions of about one year [204]. Blood stem cells follow asynchronous (Figure 8) and mixed (Figure 9) cell division patterns. Hence, a stem cell division can result in two stem cells, or two progenitor cells, or one stem cell and one progenitor cell (Figure 10). A blood progenitor cell, once formed, undergoes a series of rapid cell divisions at an average rate of one division per day [205] to yield mature blood cells after about 20 levels [171, 205] of cell divisions (Figure 10 and Figure 12).
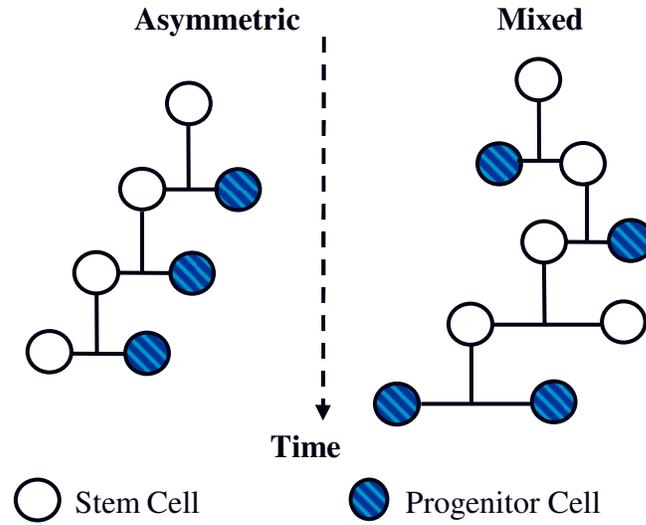
Figure 9: Asymmetric and mixed cell division types. An asymmetric cell division consistently results in two dissimilar daughter cells. A mixed cell division results in two similar or dissimilar daughter cells. In addition, one or both of the daughter cells may or may not be similar to the parent cell.

Cell Division Models
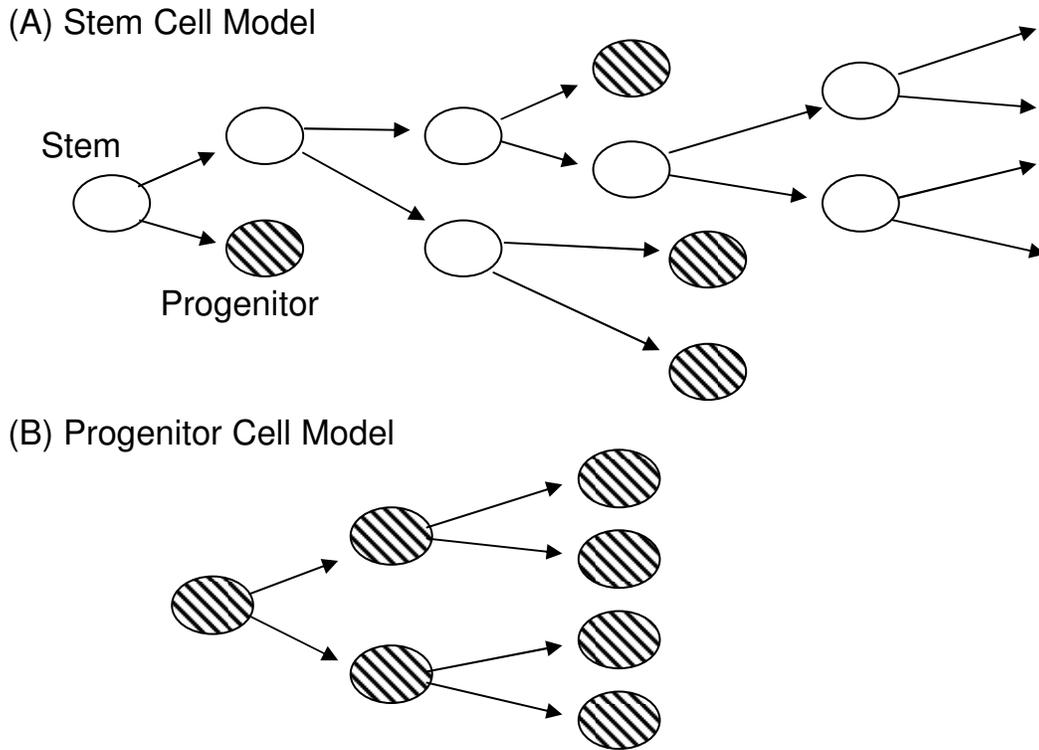
Figure 10: Schematic diagram of the two cell division models. Open ovals represent stem cells. Shaded ovals represent progenitor cells. Lengths of the edges indicate average time between cell divisions.

Mitochondrial DNA Dynamics

(A) Relaxed Replication
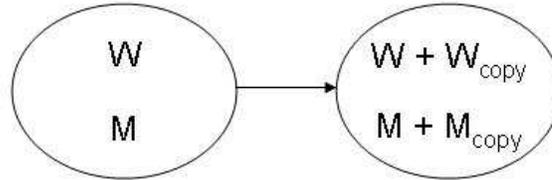
(B) Random Degradation
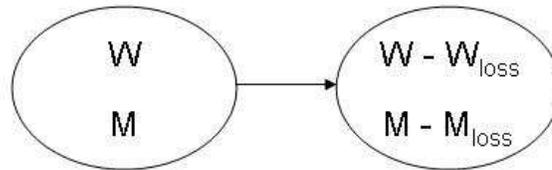
(C) Random Segregation
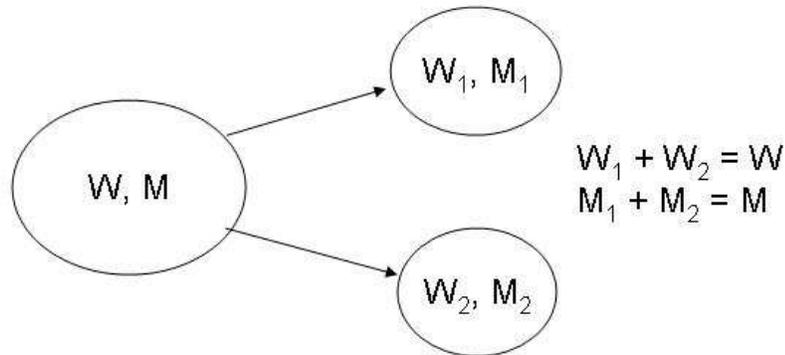
Figure 11: Schematic diagrams of the mtDNA dynamics in the models. (A) In relaxed replication of mtDNA, the number of wild-type, W, and mutant, M, mtDNA molecules is increased over one time step by the amounts W_{copy} and M_{copy} respectively. (B) In the random mtDNA degradation model, the numbers W and M are decreased over one time step by W_{loss} and M_{loss}. (C) At a cell division event, W and M are randomly distributed to the two daughter cells.

The exact number of mtDNA in a blood stem cell is not yet reported in literature. So, we assume each stem cell to have a few thousand mtDNA molecules and simulate for

a range of values. Each mtDNA molecule can be of either a wild-type (W: the normal type we would expect in a cell), or a mutant-type (M: abnormal due to point substitution of a nucleotide). The dynamics of insertion and deletion mutations may be different and are not considered in this study. Each mtDNA molecule undergoes relaxed replication and degradation events with a certain probability in a given time step. Each stem cell or progenitor cell undergoes cell division and cell death with a certain probability. The models for computing these probabilities are presented in Section 4.2.

4.2 Section 4.2: Simulation modules for mitochondrial genetic dynamics model

In this section, we present the basic modules we develop to simulate mitochondrial genetic dynamics. The mtDNA heteroplasmy in a cell varies due to stochastic and independent occurrence of various events. The probabilities for these events' occurrence (subroutine calls) are set based upon available experimental evidence from literature.

4.2.1 MtDNA degradation

MtDNA molecules degrade with a half life of T_{half} typically set in the range 10 to 20 days [206]. In our models, both wild-type and mutant mtDNA are degraded with the same half life. In a time step Δt, the number of wild-type mtDNA molecules lost to random degradation (the value W_{loss} in Figure 11) is calculated from a Poisson distribution with mean value of ($ln(2)\ W\ \Delta t\ /\ T_{half}$), where W is the number of wild-type mtDNA in the cell. A similar calculation ($ln\ (2)\ M\ \Delta t\ /\ T_{half}$) determines the number of mutant mtDNA molecules degraded (M_{loss}) in time step Δt.

4.2.2 Relaxed replication of mtDNA

The relaxed mtDNA replication rate R is given by:

$$R = \left(\ln(2)\, N_{target} \, / \, T_{half} \right) + \left(\ln(2)\, N_{target} \, / \, D \right) \qquad (1)$$

Where, N_{target} is the target total number of mtDNA in the cell. Note that N_{target} is merely a parameter used to calculate the mtDNA replication rate, and that it may be slightly different from the total number of mtDNA molecules actually present in the simulation at a given time t, $N_t = W_t + M_t$. In steady state the actual copy number N_t fluctuates around the target number N_{target}.

Equation (1) represents the mathematical model for relaxed replication of mtDNA. The first term in the Equation (1) replaces degraded mtDNA and the second

term compensates for the decrease in mtDNA number due to cell divisions. The replication rate is divided proportionally between the wild-type and mutant-type mtDNA in a cell. A Binomial distribution is used to make this distribution.

If W_{copy} and M_{copy} represent the number of wild-type and mutant-type mtDNA copied in a single time step of length Δt, then the total number of mtDNA that replicate in time step Δt is given by:

$$R \times \Delta t = W_{copy} + M_{copy} \tag{2}$$

4.2.3 Model of mtDNA changes during cell division

At cell division, we assume that the mtDNA from the dividing cell are randomly distributed to daughter cells with equal probability. We model cell division as a Poisson distribution separately for wild-type and mutant-type mtDNA, with mean values of *W/2* and *M/2* distributed to each of the two daughter cells, where *W* and *M* are the numbers of wild-type and mutant-type mtDNA in the dividing cell. The occurrence of cell division events is stochastic with mean time between cell divisions = *D*. *D* is set to a value derived from literature for the cell type. For example, *D* = 1 year for blood stem cells and *D* = 1 day for blood progenitor cells.

4.2.4 Cell loss due to mutation threshold

From experiments [29-34], it is known that cells can survive and even function normally with mutation levels of up to 85% or higher (Table 1). When the mutation level in a cell exceeds a certain threshold value m_{thresh}, the cell function is compromised and it starts showing pathogenic symptoms. We model this pathogenic effect by removing such cells from the simulation. The value of m_{thresh} depends on the particular mutation and other environmental factors. We simulate for a range of m_{thresh} values in the range 60% to 100% are used in the simulation covering the range of values reported for the threshold of 3243A>G [207, 208] mutation.

4.3 Section 4.3: Hematopoietic stem cell model

We develop and use two related simulations; a *blood stem cell model* (Figure 10A) and a *blood progenitor cell model* (Figure 10B). In both simulations, we consider only point substitution mutations as the dynamics of deletion mutations may be different. Each simulated cell has integer values for wild-type (*W*) and mutant (*M*) mtDNA molecules respectively. These numbers change over time due to relaxed replication of mtDNA (Figure 11A), mtDNA degradation (Figure 11B), and cell divisions (Figure 11C). Note that the total number N_t of mtDNA molecules in the simulated cell at time t, $N_t = W_t + M_t$

is not held constant over time but varies as W_t and M_t vary independently with time. W and M are the basic variables in these two models. A simplified version of the formation of blood from adult blood stem cells is shown in Figure 12. A description of all the simulation parameters and typical ranges for their values derived from literature is tabulated in Table 2.
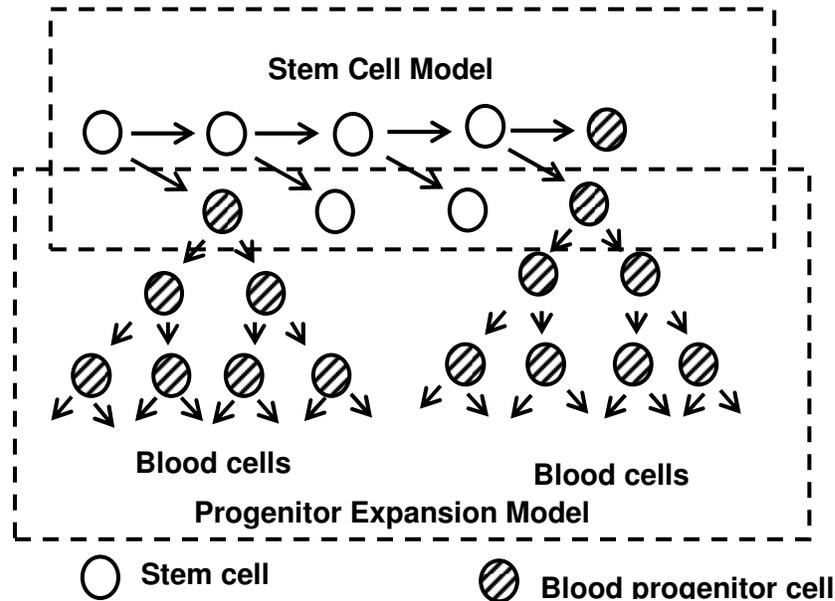
Figure 12: The model of peripheral blood formation from stem cells. This combines both the stem cell model (upper dotted rectangle) and the progenitor cell model (lower dotted rectangle).

The stem cell and progenitor models together represent the formation of blood in the blood stem cell system with at least the following simplifications:

1. During cell division, roughly half of W and M mtDNA are distributed to daughter cells.
2. When the heteroplasmy level in a cell exceeds the threshold for an mtDNA mutation, the cell ceases to function and is hence removed from the population.
3. MtDNA replication, mtDNA degradation, cell division and cell death are the only events that affect the mtDNA mutation load in the cell.
4. The blood progenitor cells in reality divide to produce several specialized blood cell types, namely, red blood cells, white blood cells, and platelets. However, our model does not differentiate the different blood cell types.
5. We do not model the complicated feedback mechanisms controlling stem cell self-renewal [209] as these detailed mechanisms are not considered relevant to this problem.

Table 2: Simulation parameters for the stem cell and progenitor cell models and their typical values

Parameter	Meaning	Values
D	Mean time between cell divisions	1 year for stem cells [210] 1 day for progenitor cells [205]
T_{half}	MtDNA half life	10 to 20 days [206]
m_{thresh}	Cells with mutation level greater than m_{thresh} were removed from the simulation	60% to 100% [29, 30, 32, 34, 38, 39]
N_{target}	Target number of mtDNA molecules in simulated cell (used to set replication rate). Also used to set the initial copy number in the cell.	1,000 to 2,000
P_0	Initial mutation level in cell.	0% to 100%
Δt	Simulation time step	1 hour
No symbol	Total simulation duration	100 years (stem cell model) or 20 to 25 days (progenitor model)
N_t	Total number of cells as a function of time 't'	Around 20,000 or 2,000,000 (stem cell model) or 1 to 7,000,000 (progenitor model)

4.4 Section 4.4: Data collection

By performing a systematic search of the literature, papers containing both, the blood heteroplasmy measurements for an mtDNA point substitution mutation and the subject's age at sample collection were identified. Based on the availability of such data for multiple subjects, we focus here on 3243A>G and 8344A>G mutations. The search yielded a total of 275 unique data pairs for the 3243A>G mutation [44, 47, 187-189, 211-228] and 48 unique data pairs for the 8344A>G mutation [229-233]. A subset of the blood heteroplasmy papers gathered for 3243A>G mutation also reported muscle heteroplasmy data [47, 211-213, 215, 220, 221, 226, 227]. Some papers did not report raw data but reported the heteroplasmy data in graphical form. In such cases, we use the software *Engauge Digitizer* to determine the approximate numerical values. Since we found only one paper that reported blood heteroplasmy for 3243A>G mutation over relatively longer time scales of 9 to 19 years [188], our collaborators gathered this data for further 11 subjects [187].

4.5 Section 4.5: Results

4.5.1 The rate of loss of heteroplasmy from blood stem cells is exponential

As we simulate the heteroplasmy dynamics in the stem cell population, the heteroplasmy distribution widens due to the processes of relaxed replication of mtDNA, mtDNA degradation, and cell divisions. Over time, some stem cells develop high heteroplasmy levels and exceed the m_{thresh} for the mutation. Such stem cells are removed from the simulated stem cell population. This stem cell loss over time gradually results in the decrease of the mean heteroplasmy level of the simulated stem cell population. Our simulations suggest that this decrease in stem cell heteroplasmy is exponential and not a constant linear rate as reported in literature [188, 189].

The mean mutation level as a function of time is described by a decaying exponential with an initial transient (Figure 13A). By conducting several simulations for a range of input parameter values, we find the dependence of exponential decay on the model parameters T_{half} and N_{target}. The dependence is given by the function,

$$m(t) = m(0) \times \exp[\frac{-t}{B}] \tag{3}$$

Where B is a value derived from exponential curve fitting given by:

$$B = \frac{N_{target} \times T_{half}}{C} \tag{4}$$

C is a dimensionless constant whose value is determined from simulations as $C = 1.45 \pm 0.07$ (Table 3).

$$m(t) = m(0) \times \exp[-(\frac{C \times t}{N_{target} T_{half}})] \tag{5}$$

For short times, $\left(\dfrac{C \times t}{N_{target} \times T_{half}} \right) \ll 1$ and the decay will appear to be linear.

$$m(t) \approx m(0)(1 - \frac{C \times t}{N_{target} \times T_{half}}) \tag{6}$$

So the apparent linear rate of loss of mtDNA mutation in blood is approximately

$$m(t) = m(0) - (\frac{m(0)}{B})t$$
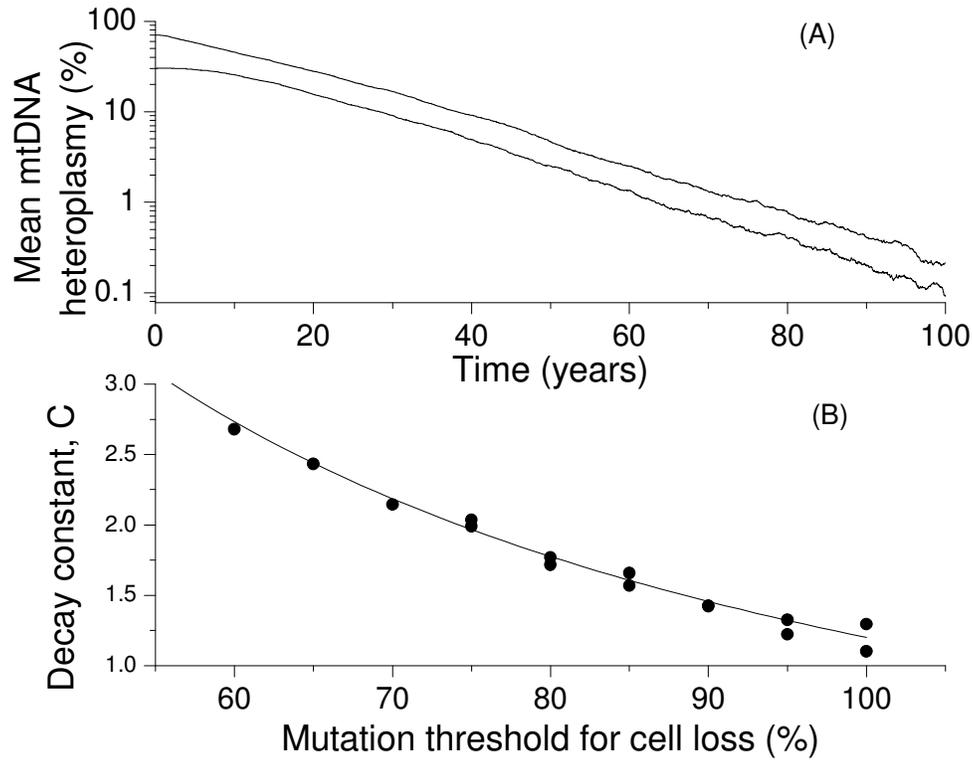
Figure 13: Simulation results for the blood stem cell model. (A) An exponential decrease in mean mutation level in blood stem cell model. Results are shown for two simulations with different initial mutation levels, 70% and 30%. Other simulation parameters are T_{half} = 10 days, N = 1000 and m_{thresh} = 90%. (B) Dependence of the decay constant C, defined in equation (5), on the mutation threshold for loss of the stem cell, m_{thresh}. The line is a fit to the data using equation (7), (with R_2 = 0.968 and p < 0.0001).

To study the dependence of the decay constant on mutation threshold for cell removal, m_{thresh}, we setup repeat experiments by varying m_{thresh} over a range of values $60\% \leq m_{thresh} \leq 100\%$. The simulations show that the decay constant C is a function of m_{thresh} (Figure 13B). Lower values of m_{thresh} cause faster loss of the mutation from the stem cell population, an intuitively reasonable behavior. The functional form of this dependence is given by,

$$C = C_0 - \left(\frac{A}{m_{thresh}} \right) \tag{7}$$

Where constant C_0 = -1.1 ± 0.1 and A = (230 ± 8) are determined by a linear fit. The exponential decay was consistent even at an m_{thresh} value of 100% (Figure 13B) which requires the simulated cell to fix at 100% heteroplasmy before the cell is removed.

Table 3: Values for the exponential decay constant C in equation(5), is computed for a range of values of the simulation parameters. The parameters N_t, T_{half}, and the initial heteroplasmy levels are varied. The mean decay constant in these simulations is, $C = 1.45$ with standard deviation = 0.07.

Number of stem cells	MtDNA copy number, N_{target}	MtDNA half life, T_{half} (days)	Initial mutation level, m (%)	C
20,000	1,000	10	30	1.4251
20,000	1,000	10	70	1.4212
20,000	1,000	20	30	1.5234
20,000	1,000	20	70	1.5459
20,000	2,000	10	30	1.3870
20,000	2,000	10	70	1.3662
20,000	2,000	20	30	1.5530
20,000	2,000	20	70	1.4423
2,000,000	1,000	10	30	1.4075

To check the effects of initial conditions on the rate of decay, the initial mutation level is set to a range of values from 20% to 75%. These lines were nearly parallel (Figure 13), i.e., the initial condition does not noticeably impact the slope of the decay. The explanation is that the amount of time needed for the cells to exceed the mutation threshold for loss of cell function is proportional to the initial M level at which each cell starts. But, the decay constant does not depend on the initial heteroplasmy of the cell.

4.5.2 Mean heteroplasmy in peripheral blood is about the same as the mean heteroplasmy in the blood stem cell population

In order to relate the results from the stem cell model to the heteroplasmy measurements from blood samples, we need to understand the heteroplasmy changes during the formation of mature blood cells from the stem cell population. The progenitor cell expansion model simulates a series of over 20 rapid cell divisions with a mean time between cell divisions being 1 day [205]. Ten simulation runs with different random number seeds are setup with typical simulation parameters tabulated in Table 2. One set of five simulation runs begin with a 70% initial heteroplasmy and another set of five simulations begin with 30% initial heteroplasmy (Figure 14B). Figure 14A shows the exponential increase in the number of progenitor cells due to a series of cell divisions with time. The variation in the time required for progenitor cell expansion across these ten simulations is indicative of the sensitivity of the model to the timing of the first few cell divisions in the series. This variation, however, is not critical to the heteroplasmy results of these simulations. Despite the threshold mechanism to model cell loss in effect, the mean mtDNA heteroplasmy level of all cells resulting from the expansion of a single progenitor cell does not differ significantly from that of the progenitor cell itself (Figure 14B). Hence, we conclude that the mean heteroplasmy measured in peripheral blood is about the same as that measured in the blood stem cell population.
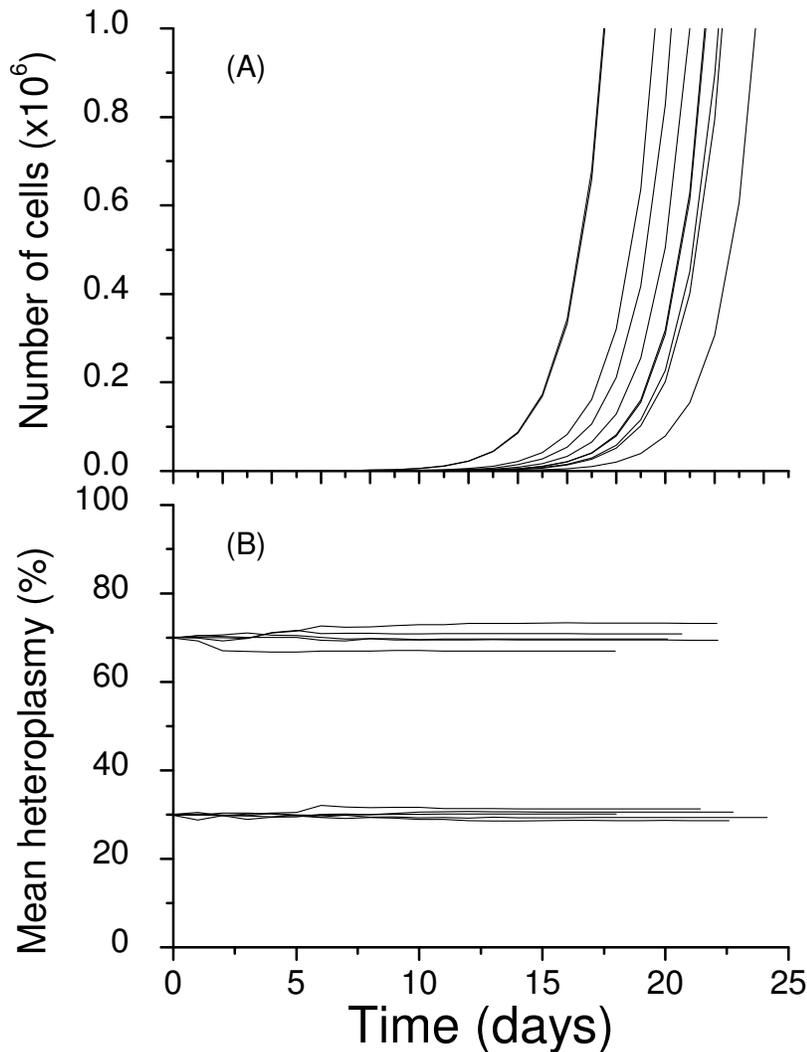
Figure 14: Simulation results for the progenitor cell model. Results are shown for five repetitions of the simulation starting at 70% mutant and five repetitions starting at 30% mutant. (A) The exponential increase in the number of simulated cells, starting from a single progenitor cell and dividing on average once per day. (B) The mean heteroplasmy of the cells over the course of the expansion in the number of cells.

Earlier studies [190] speculated that random genetic drift and selection at the molecular or cellular levels are acting in the decay of blood heteroplasmy. Population genetic models [234] have shown that selection does not act significantly on an exponentially expanding population. Hence, from our collective analysis of blood stem cell and progenitor cell models, we hypothesize that the selection against mutant mtDNA occurs at the cellular level and that this selection occurs in the stem cell population and not in the progenitor cells.

4.6 Section 4.6: Analysis of experimental data

In order to test the hypothesis that the mtDNA heteroplasmy decreases exponentially, we need to analyze published clinical data. Since the decrease in blood heteroplasmy is quite slow, we need data measurements separated in time by around a decade. We did not find many longitudinal studies reporting a series of heteroplasmy measurements over long time scales in the literature. The existing clinical data report pairs of heteroplasmy measurements separated by a few years at most. *Rahman, et al*. [188] reported the best available clinical data on the 3243A>G blood heteroplasmy with measurements separated by 9 to 19 years. Using pairs of heteroplasmy measurements, we can only calculate the rate of change of heteroplasmy. If the heteroplasmy decreases linearly as reported in literature, the rate of change of heteroplasmy should be a constant. Hence, a plot of the rate of change of heteroplasmy versus initial heteroplasmy will be a horizontal line with zero slope. However, if the heteroplasmy actually decreases exponentially as predicted by our simulations (Equation 3), then the rate of change of heteroplasmy should be proportional to the initial heteroplasmy itself. Therefore, a plot of the rate of change of heteroplasmy versus initial heteroplasmy should be a straight line with negative slope and zero intercept.

Since Rahman, *et al.* [188] report data for only six subjects, our collaborators in order to extend this dataset, carried out repeat blood heteroplasmy measurements in 11 individuals with 3243A>G mutation to compare to measurements made five or more years earlier for the same individuals. This dataset is separately published by Pyle, *et al.* [187]. As expected from our simulations, the Pyle, *et al.* [187] and Rahman, *et al.* [188] data fit with an exponential decay in blood heteroplasmy measurements (Figure 15) over time. Note that these are two separate studies conducted on different set of subjects at different times.

4.6.1 Theoretical limit on blood heteroplasmy

Exponential decay of blood heteroplasmy suggests that older individuals should not have high blood heteroplasmy levels for 3243A>G mutation. We define a theoretical maximum limit on the heteroplasmy for a given age t as

$$\max\left[m(t)\right] = \left(100\%\right)\exp\left(-St\right) \tag{8}$$

where $S = 0.020 \pm 0.003$ (1/years) is the slope measured from the data in Figure 15. Hence, we expect blood heteroplasmy measurements for 3243A>G mtDNA mutations to always fall under this predicted maximum limit.

To further test this hypothesis arising from our simulations, we plot the data from 23 published studies [44, 47, 187-189, 211-221, 223-228, 235] reporting 3243A>G blood mtDNA heteroplasmy levels together with the subjects' age, with a total of 275 unique

data points (Figure 16). These data points span from zero mutation up to the predicted maximum value. As expected, most data lie below the predicted maximum heteroplasmy (Figure 16) except for five measurements (not included in the plot) that lie above the predicted limit. Four of these five exceptional data points are reported in a single study by Hammans, *et al*. [213] and are recognized by the authors as being unusual. All four cases come from a single small pedigree that also contain a homoplasmic 3290T>C mutation within the same tRNA gene as the 3243A>G mutation. Hammans, *et al*. [213] note that this family had a unique clinical phenotype and propose that the 3290T>C variant may be altering the pathology of 3243A>G mutation. This idea is supported by an independent study by El Maziene, *et al*. [236] who show experimentally that a second mutation at position 12300 can suppress the pathogenicity of 3243A>G mutation. Hence, these exceptional cases do not affect the conclusions of our analysis.
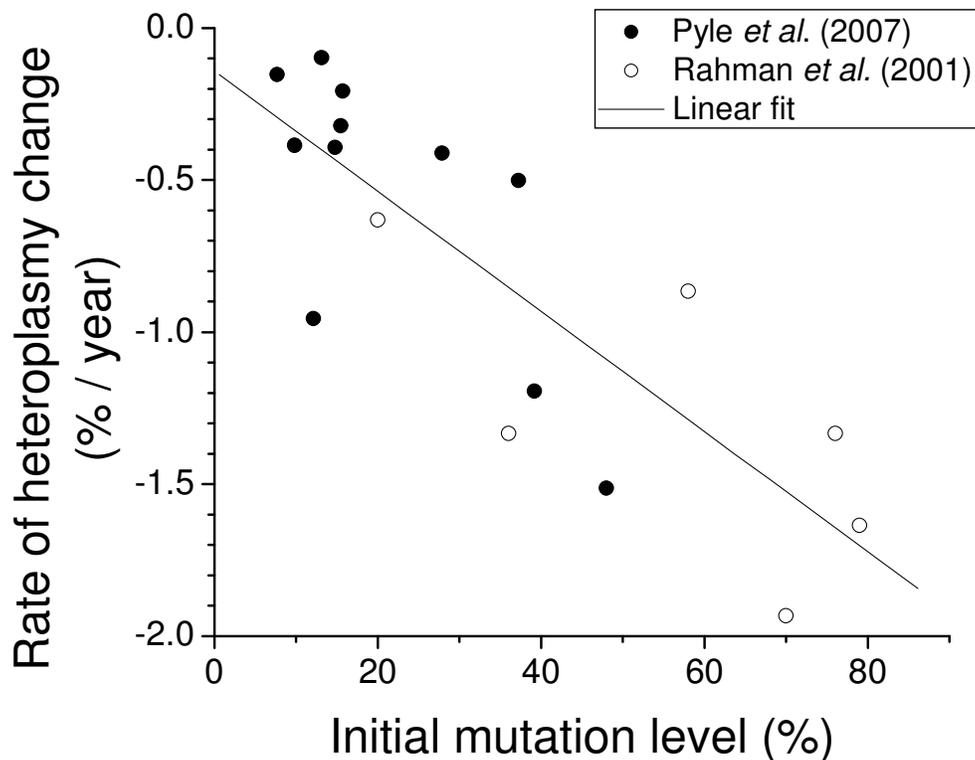
Figure 15: Analysis of two sets of clinical data [187, 188] to test for an exponential decrease in peripheral blood heteroplasmy. The line is a linear fit to the data, with slope -0.020 ± 0.003 (1/year) and intercept -0.14 ± 0.14 (%/year) (R^2 = 0.68 and $p < 10^{-4}$). A linear plot of this data with negative slope indicates an exponential decay of the blood heteroplasmy.

The sparse data region for subjects at young age and low heteroplasmy in Figure 16 is likely because most patients with 3243A>G mutation express symptoms at older ages.
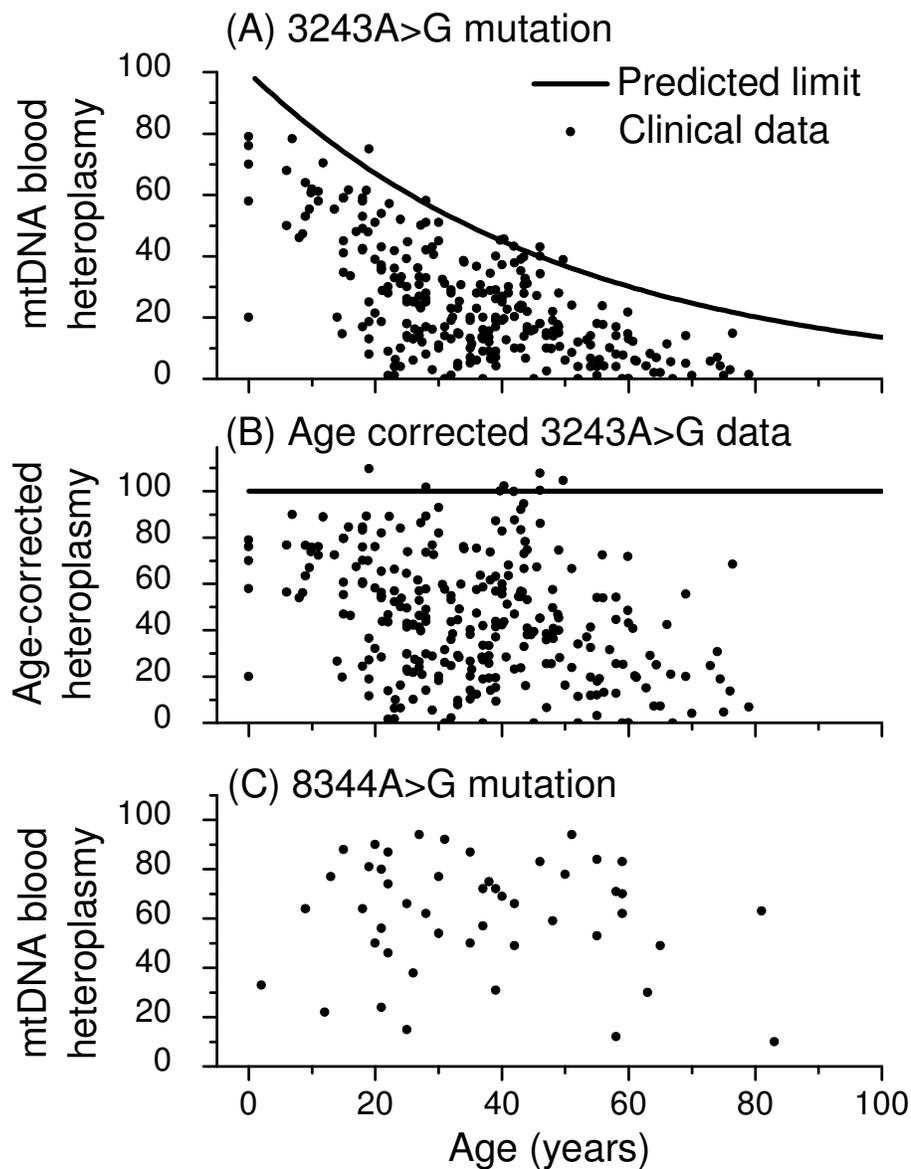
Figure 16: Comparison of clinical data to a predicted maximum mutation heteroplasmy in peripheral blood. **(A) The theoretical maximum blood mutation level (Equation (8)) and 275 measured values from 23 independent studies [44, 47, 187-189, 211-221, 223-228, 235] on subjects with the 3243A>G mutation. The theoretical upper limit is set using an initial heteroplasmy of 100%. (B) The 3243A>G data modified by the age correction (Equation (9)). (C) Blood heteroplasmy data (48 measured values) for the 8344A>G mutation [229-233]. The clinical results plotted here show no indication of a decrease in blood heteroplasmy with the subjects' age for this mutation.**

4.6.2 Age-correction in blood heteroplasmy measurements

Based on our analysis of the published clinical data, we propose a method for correcting for a subject's age in blood heteroplasmy measurements.

An age-corrected mutation level is defined as

$$m_{age-corrected} = m(t)\exp(St) \tag{9}$$

The age-corrected heteroplasmy measurements derived from Equation (9) are plotted in Figure 16B.

The 3243A>G heteroplasmy in blood is almost always lower than the muscle heteroplasmy [47]. To test whether the age-corrected blood heteroplasmy is consistent with muscle heteroplasmy, we use a subset of the blood heteroplasmy data for which muscle heteroplasmy data is also reported [47, 211-213, 215, 220, 221, 226, 227]. The plot of blood heteroplasmy versus muscle heteroplasmy for the 3243A>G mutation are plotted in Figure 17A. All subjects plotted in Figure 17, had lower blood heteroplasmy compared to their muscle heteroplasmy and this difference seems to get larger with a subject's age. Assuming muscle heteroplasmy is relatively constant over time, we apply the age correction of Equation 6 to the blood heteroplasmy levels in Figure 17B. We found a statistically significant ($p < 0.0001$) correlation between both, the blood heteroplasmy and the age-corrected blood heteroplasmy, with the muscle heteroplasmy measurements. The difference between raw blood heteroplasmy and age-corrected blood heteroplasmy is that the latter data points are closer to the line of equal heteroplasmy (for muscle and blood). The age-corrected blood heteroplasmy still tend to be lower than the muscle heteroplasmy, particularly for higher muscle heteroplasmy levels. However, age-correction resulted in the overlapping of data from all three age groups and eliminated the age dependent behavior of the blood heteroplasmy data.

4.6.3 Low penetrance mtDNA mutations behave differently

It is clear from our results that for 3243A>G mutation, the heteroplasmy decreases exponentially in blood stem cells with age due to the loss of stem cells that exceed the mutation threshold m_{thresh}. In certain cases, certain neutral or even pathogenic mtDNA mutations may not lead to loss of stem cells even when homoplasmic for the mutation. In all such cases involving low-penetrance mutations, we do not expect an exponential decay of heteroplasmy over time in blood. The second mutation 8344A>G, for which we collected data [229, 230, 232, 233, 237], falls under this category. A plot of blood heteroplasmy measurements for 8344A>G (Figure 16C) does not show an age dependent exponential upper limit for the 8344A>G mutation in blood.
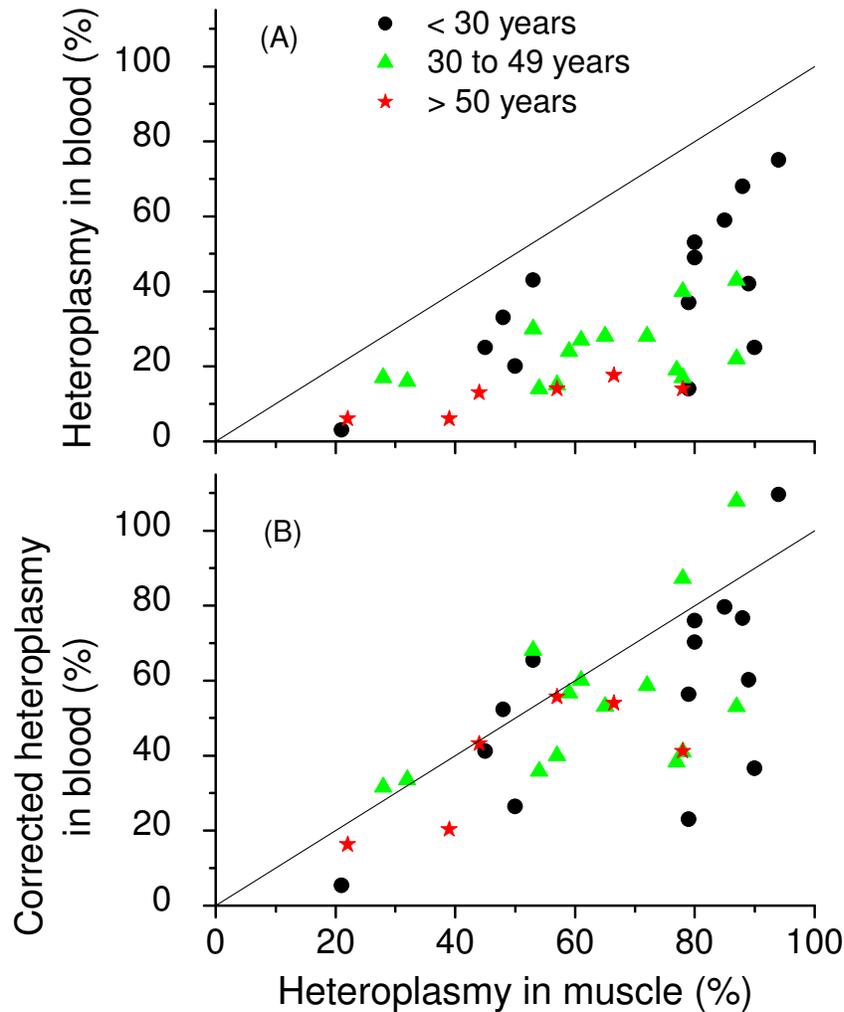
Figure 17: An application of the age correction for blood heteroplasmy. (A) Comparison of 3243A>G heteroplasmy levels in muscle and in blood. (B) Comparison using the age-corrected blood heteroplasmy from equation (9). The corrections are made using a value of S = 0.020 year⁻¹, the value determined from the data in Figure 15. The solid lines represent the lines of equal blood and muscle heteroplasmy.

4.7 Section 4.7: Discussion

Based on our integrative analysis of simulations together with clinical data exclusive to 3243A>G mutation, the most commonly occurring [36] heteroplasmic pathogenic mtDNA point mutation, we illustrate (Figure 15 and Figure 16) the exponential loss of pathogenic mtDNA heteroplasmy from human blood (Hypothesis 1). To determine whether Hypothesis 1 holds for other pathogenic mtDNA mutations, we need either a number of pairs of longitudinal blood heteroplasmy measurements spaced by around 10

years (Figure 15) or a much larger number of single time point heteroplasmy measurements for that mutation (Figure 16) for subjects covering a wide range of ages.

The analysis presented here are particular to the 3243A>G mutation. Other mtDNA mutations causing low-penetrance diseases (e.g., Leber's Hereditary Optic Neuropathy) may also show an exponential decrease in the blood heteroplasmy. A couple of cases of decreasing blood heteroplasmy of LHON mutations are reported in literature [238, 239]. In these individuals, the loss of heteroplasmy can still occur due to yet unknown cofactors leading the blood stem cells to disease. Hudson, *et al.* [240] report a case where an interacting genetic locus may act as a co-factor for the development of LHON. There are conflicting reports that exposure to environmental toxins such as excess alcohol or tobacco may [241] or may not [242] act as cofactors for the development of LHON.

Based on the availability of published experimental data, we focus our study on blood samples here. We expect the exponential decay of mtDNA heteroplasmy to occur in other dividing tissues that lose cells with high heteroplasmy. For example, reports [44, 243] indicate a decrease in the 3243A>G mutation heteroplasmy with age in the epithelial tissue and buccal mucosa. However, in post-mitotic tissues such as skeletal muscle, there is little loss of muscle cells even in patients who are homoplasmic to the 3243A>G mutation [244]. Our analysis here offers explanation for the accumulation of mutant mtDNA in post-mitotic tissues such as skeletal muscle [51, 245] as discussed by Chinnery and Samuels [43]. Accumulations of mutant mtDNA with age are reported in gastric [246] and colonic [247] stem cells. Our simulations may be applied to such stem cell systems that lead to disease phenotypes in the peripheral cells.

Blood samples are commonly used to determine heteroplasmy levels, especially in asymptomatic individuals. The variation in blood heteroplasmy can mislead scientists studying the inheritance of mtDNA mutations, if other tissues are also not co-examined. For example [190], increase in the heteroplasmy of a pathogenic mtDNA mutation has been reported across generations based on the relatively smaller blood heteroplasmy measured in mothers. Although such concerns were raised before [239], this is the first time that a practical age-correction method is proposed.

Based on our simulations, we hypothesized that the blood mtDNA heteroplasmy decreases exponentially with age. By analyzing our simulation results together with a vast pool of clinical data, we confirmed that this is true for the 3243 A>G mutation (Figure 15 and Figure 16). The key mechanism that leads to exponential decay is the loss of stem cells with high mutation level. However, there may be other mechanisms that could also lead to an exponential decrease. For example, an exponential decay of a natural non-pathogenic mtDNA genotype has been reported in murine models (BALB/c and NZB) by Battersby, *et al.* [248]. The authors report the loss of NZB mtDNA in these mice blood with a very high decay constant of $S_{mouse} = 1.387$ year^{-1} (compared to the value $S_{human} = 0.02$ year^{-1} from Figure 15). The authors conclude that the selection against NZB mtDNA is not due to an immune mechanism. A lack of correlation between oxidative phosphorylation and the cellular heteroplasmy level in these mice indicates that

the cell-loss mechanism proposed from our analysis here is not playing a role in these mice. The mechanisms leading to the rapid loss of NZB heteroplasmy in the blood of these mice still remain unexplained.

In this study, at an early stage, one experimental patient data (with about 10% heteroplasmy change/year) from our collaborator (data not shown) did not fit to the rest of the data. When we asked our collaborators to repeat that particular experiment, without revealing what was expected, it turned out to be an experimental error with the new data point fitting well with the rest of the data. Examination of the measurements on the other subjects showed that this experimental error only occurred in this one subject. This is an encouraging case for our simulation approach as it helped rectify an experimental error.

4.8 Section 4.8: Issues and limitations

4.8.1 The problem of initial transient

We simulate the stem cell model on cell population sizes from 20,000 to an estimated full population of 2 million cells [203]. Since the actual number of mtDNA per stem cell is not known, we simulate with a range of 1000 to 2000 mtDNA per cell for a maximum duration of 100 years. All stem cells are initialized to a uniform value P_0 for simplicity. The distribution of heteroplasmy in the stem cell population spreads out over time (Figure 18) due to the occurrence of stochastic events (relaxed mtDNA replication, mtDNA degradation, and segregation to daughter cells). Before the model can eliminate this initial artifact, there is an initial transient (Figure 13: the decay curves during the first five years or so) on the measurement of the heteroplasmy decay rate. To remove the effect of this initial transient, we only use simulation data after the heteroplasmy has dropped to below 90% of its initial value. As the mean heteroplasmy in the simulation decreases over time, we observe noise due to discreteness at low levels of mtDNA copy number per cell. To remove this effect, we drop all values below 10% heteroplasmy. It takes longer for the individual cells starting at 30% heteroplasmy to exceed the 90% mutation threshold for loss of cell function. The current procedure to determine the end of transient period is rather ad hoc. To eliminate the effect of initial transient, we only keep data after mutation level has fallen to 10% of its initial value. A cleaner way of handling this issue of initial transient is still of interest.

The stem cell population distribution for a simulation run starting with 70% initial mutation level, after 2, 6 and 60 years is shown in Figure 18. The distribution after 6 years shows a spread around the mean 70% level from 40% to 90%. However, after 60 years, the heteroplasmy in the population has spread the entire spectrum from 0 to 90% with more than 1500 cells fixed at all W type mtDNA.

4.8.2 Memory scalability

The choice of data structure chosen to model the array of cells affects the scalability of the simulations. The maximum size of the cell array that can be statically declared at the beginning of the program is about half a million. This is because memory for static data structures is allocated on the stack. Since the requirement was to simulate a million cell objects ($\sim 2^{20}$) or more, array data structure was a limitation to overcome. One option is to shift to dynamic memory allocation. Programmatically, this means significant complexity in managing garbage collection and the CPU time spent in traversing linked lists containing more than a million nodes at every time step.
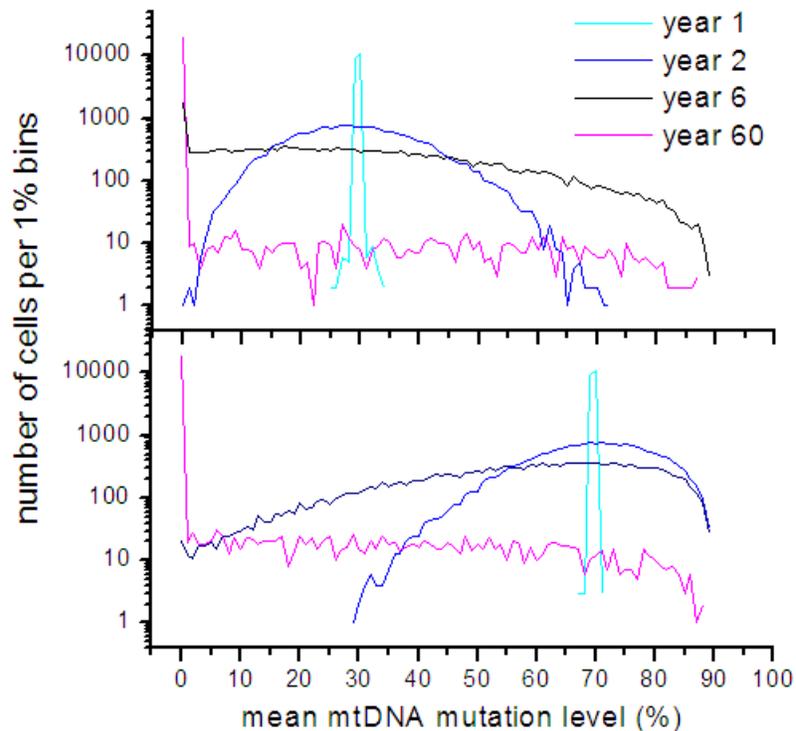
Figure 18: Distribution of the stem cell population based on their heteroplasmy levels

A workaround this problem is to still declare the large array of cell objects, but force the heap memory allocation rather than the stack.

i.e., instead of declaring:

```
// This allocates memory on the stack
Cell cell[MAXCELLS];
```

declare this way:
```
// This allocates memory on the heap
```

```
Cell *cell;
cell = new Cell[MAXCELLS];
```
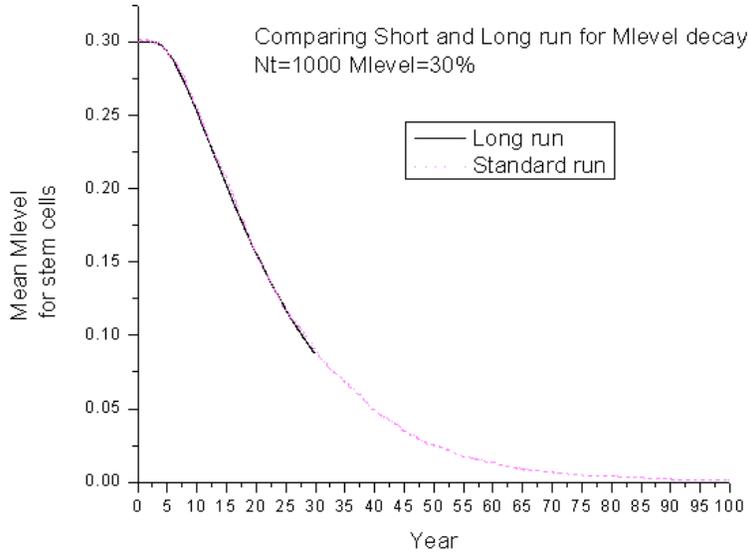

Figure 19: Comparison of a blood stem cell simulation run for a full number of 2 million blood stem cells with a blood stem cell simulation run for the standard number of 20,000 blood stem cells.
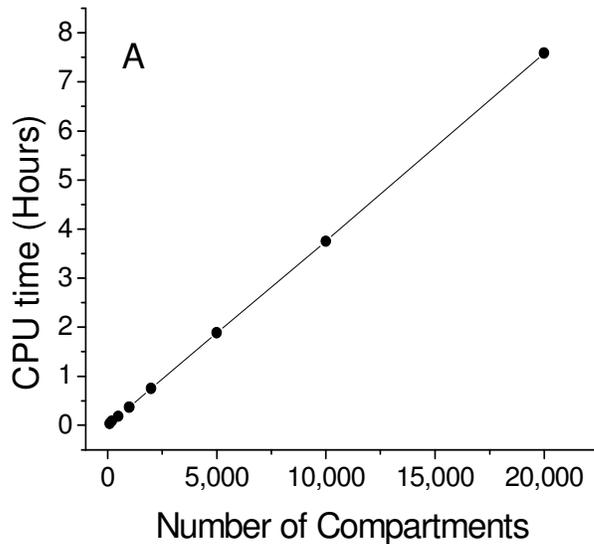
Figure 20: CPU time required as a function of the number of simulated cells (or compartments).

In this case, the maximum number of cell objects (MAXCELLS) is limited by the available secondary memory on the hard disk. Using this approach, we are able to simulate the progenitor cell expansion model for up to 7 million cells or 2 million stem

cell over a century, a big improvement over the earlier models developed by Chinnery and Samuels [43].

4.8.3 Simulation CPU and memory requirements

In Figure 19, we show a simulation of 2 million stem cells, the estimated size for the human adult blood stem cell population in the bone marrow [203]. This simulation run takes more than a couple days to simulate for 100 years. All simulations presented in this chapter are run for 20,000 stem cells. We do not expect any effect of simulating the smaller number on our results (Figure 19).

In Figure 20 and Figure 21, we show the CPU time and memory performance of the simulation. The simulations are run on a 2.0 GHz Pentium 4 CPU, with 512 MB RAM running Linux. Both the required CPU time (Figure 20) and the required RAM (Figure 21) increase linearly with the number of simulated cells. Tens of thousands of compartments can be simulated for a century in less than one day of CPU time. On a PC with 512 MB RAM, we have simulated up to ~8 million cells or compartments.
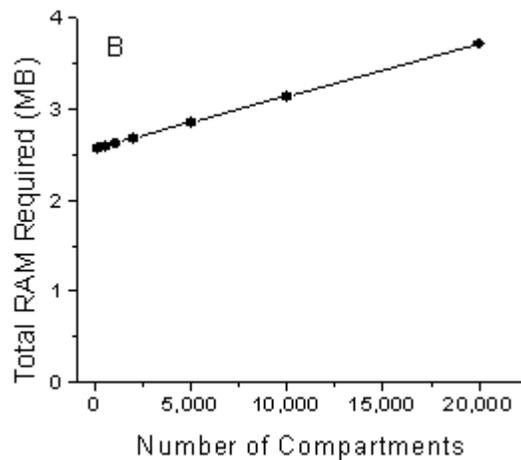
Figure 21: Total RAM required for simulation runs. Each compartment here represents a cell containing approximately 1,000 mtDNA molecules.

In Figure 22, we show the dependence of the CPU time on the number of mtDNA molecules per cell. Note the sharp contrast between the linear increase in CPU time required up to 10,000 mtDNA per cell and the relatively constant CPU time required above ~10,000 mtDNA per cell. This is due to the shifting of the Poisson and Binomial distribution subroutines [198] from direct methods to rejection methods for higher than 10,000 mtDNA per cell. Hence, we can simulate populations of 20,000 cells for a century, with no practical limit to the number of mtDNA molecules per cell. This means,

we can now simulate oocyte cells (containing 10^5 mtDNA per cell) for a century (if there is a biological motivation, of course) in less than a day.
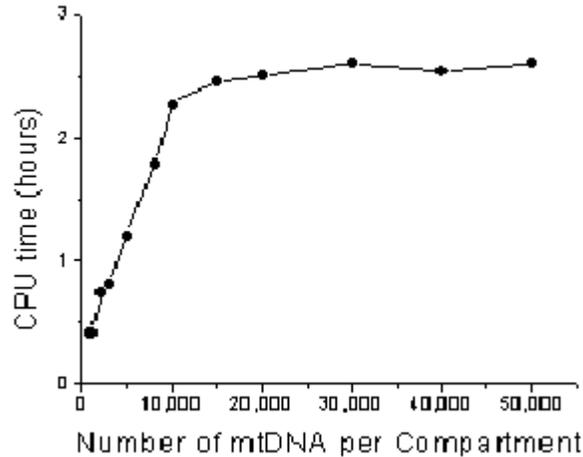
Figure 22: Dependence of the simulation CPU time on the number of mtDNA molecules per compartment (or cell). 1000 compartments (cells) are simulated for 100 years.

4.9 Model applications

Currently, the mtDNA are assumed to be uniformly distributed through out the cell. We can model the spatial compartmentalization of these mtDNA within the cell into mitochondria or nucleoids by adding another level of abstraction between the cell and mtDNA. The blood stem cell model can be adapted to simulate other stem cell types.

In Chapter 5, we adapt the progenitor cell expansion model to study the mitochondrial genetic bottleneck during mouse embryogenesis. In Chapter 6, the progenitor cell model is modified to simulate the segregation of mutant mtDNA during passages of cell culture growth to provide "control" for the experimental studies of our collaborators.

5 Chapter 5: Mitochondrial Genetic Bottleneck Model in Mouse Embryo

Chapter 5 presents the simulation to model mouse embryo to answer specific questions related to the mitochondrial genetic bottleneck motivated in Chapter 2. The results of this study are currently in press in Nature Genetics (Cree, *et al.* [186]).

5.1 Section 5.1: Introduction

A general introduction to the mitochondrial genetic bottleneck is provided in Section 2.1. In mammals, mitochondrial DNA is primarily inherited maternally. The mechanisms involved in this non-Mendelian inheritance are not fully understood [27]. Heteroplasmic mothers transmit varying proportion of mutant mtDNA to their offspring. In patients with mtDNA disorders, disease severity appears to correlate with the proportion of mutant mtDNA inherited from the mother [249-251]. Studies in cattle [193, 252], report rapid changes in allele frequency in a single generation indicating that the bottleneck size can be very small (a few mtDNA molecules). Jenuth, *et al.* [191] report that the heteroplasmy level of mouse offspring is determined at an early stage during oogenesis in mother, even before the formation of primary oocytes. The authors predict the bottleneck size in mice to be around 200 segregating units [191]. Subsequent studies [237, 249, 251, 253] confirm the observation of rapid changes in heteroplasmy in several other mammalian species, including humans.

Three mechanisms [191, 254, 255] are suggested in the literature to explain this genetic bottleneck. In one model, a dramatic reduction in the mtDNA copy number in cells followed by stochastic partitioning of mtDNA at cell division leads to marked segregation in mtDNA genotype between daughter germ cells. In the second model, multiple mtDNA molecules organize into segregating units called nucleoids. Since each nucleoid harbors a small mtDNA copy number, stochastic segregation can quickly lead to homoplasmy in individual nucleoids. This reduces the total number of segregating units and increases the variability [255]. In the third model, a group of mtDNA is selected to re-populate the next generation [256, 257]. These possibilities raise several important questions: What is the size of the mitochondrial genetic bottleneck? What is the mechanism by which mammalian offspring from the same mother inherit dramatically variable levels of mtDNA heteroplasmy? Do mtDNA segregate as individual molecules or as nucleoids?

To address these questions, previous studies have used either the *single-sampling binomial model* or the *multiple-sampling model*. The *single-sampling binomial model* (Figure 23**a**) models the process of formation of primary oocytes and predicts the probability of transmitting a particular level of heteroplasmy to offspring [258, 259]. The underlying assumption is that a selected number of mtDNA repopulate all of the primary

oocytes. However, the model does not provide any insights into the underlying biological mechanisms. Jenuth, *et al.* [191] adapt and apply a population genetics [260] based *multiple-sampling model* (Figure 23**b**) assuming that the numerous generations of binary cell divisions result in cells containing moderately low amounts of mtDNA. This model also does not accurately model biology because primordial germ cells (PGCs) do not arise from a single precursor, but rather from a random sample of cells (~40) out of the blastomere cells. Experimental observations [186] indicate that the mtDNA copy number within the PGCs increases between 7.5 dpc and 14.5 dpc (Figure 24**c**). In order to best model the underlying biological process, we adapt these two models from literature together with the experimental data from collaborators [186] (Figure 23**c**).
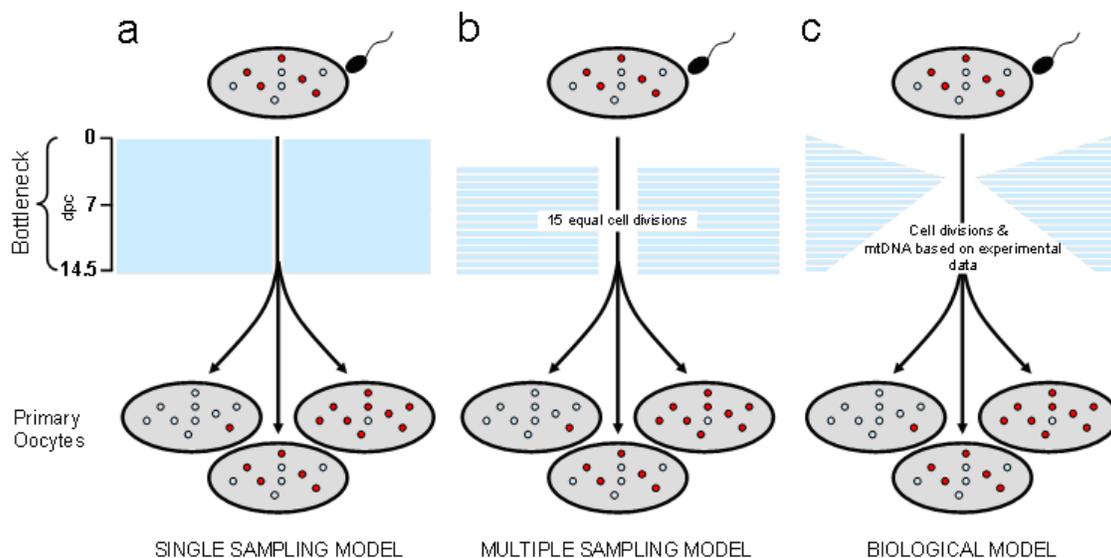
Figure 23: Models of the mitochondrial genetic bottleneck. Schematic diagram showing a heteroplasmic fertilized oocyte (top), a model of the mitochondrial genetic bottleneck (middle) and subsequent primary oocytes (bottom). Blue circles = wild type mtDNA. Red circles = mutated mtDNA. Time scale shown on the left in days post coitus (dpc). (a) Single-sampling model. A single random sample of mtDNA molecules is assumed to repopulate each primary oocyte. This model describes the whole bottleneck process well, and can be used to predict the variance in heteroplasmy levels amongst offspring, but it is biologically implausible, giving no insight into the underlying mechanism. (b) Multiple-sampling model. Using an adaptation of the population genetic model of Sewall-Wright [260], this approach assumes that an identical moderate genetic bottleneck is present over multiple cell divisions, G. In mice, G = 15, which is the number of divisions required to produce the 25,791 primary oocytes present by 13.5 dpc [261] from a from a single blastomere. This model is inaccurate because the germ line does not arise from a single precursor cell, and the experimental data [186] shows that the amount of mtDNA within single cells is different at different time points during development. (c) Complex biological model based upon the number of cell divisions leading up to the formation of 40 primordial germ cells (PGCs) at 7.25 dpc, followed by 9-10 cell divisions required to generate the 25,791 PGCs required to form a full complement of primary oocytes. The number of mtDNA molecules per cell in the pre-implantation embryo and subsequent primordial germ cells is based upon experimental observations of our collaborators (Table 4 and Table 5). This biologically plausible model forms the basis of the simulation described in the text.

5.2 Section 5.2: Modeling methods

It is important to emphasize the special interaction between experiments and simulation in this study. Since none of the earlier models accurately represent the underlying biology, our goal is to model the biological process by directly utilizing relevant experimental data. Our experimental collaborators [186] conducted experiments in mouse models specifically designed for the study of the mitochondrial genetic bottleneck. The experiments are focused on measuring specific quantitative data required for modeling this process. Earlier predictions [191] of the bottleneck are based on an assumed number of mtDNA per cell. But here, our experimental collaborators provide us with laboratory measurements for the mtDNA copy number and the number of PGCs during embryogenesis of mice (Table 4, Table 5, and Table 6). Heteroplasmic mice were produced with the two mtDNA alleles NZB and C57BL/6J by using cytoplast fusion techniques. The isolation of precursor cells is based on a fluorescent dye that specifically colors precursor cells, but not others. Data from a total of 246 offspring from 22 litters are reported. For detailed experimental methods, we refer the reader to the publication Cree, *et al.* [186]. Modeling and simulation methods for this study are presented here.

Since our collaborators [186] report varying mtDNA copy numbers across blastomeres, instead of using the earlier population genetics based model [191], we develop a model to directly simulate the population of cells with random mtDNA segregation during cell divisions. This approach allows us to accurately model what is known about the underlying biology as follows:

Pre-implantation
1. Start the simulation with a single cell, representing the fertilized oocyte, initialized to 5×10^5 mtDNA copies with 50% mutant and 50% wild-type mtDNA. This cell and all resulting generations of cells divide at a rate of one division every 15 hours, a value derived from literature [249-251, 262] and consistent with the new experimental data. MtDNA replication is blocked during this process [263].
2. During each cell division, mtDNA are randomly distributed between the two daughter cells. As a result, the mtDNA copy number decreases exponentially to a value of 314 ± 24 that compares well with experimental data from collaborators (Table 4).

At implantation
3. At 7 days post coitus (dpc), the total number of cells after about 10 generations of cell divisions = 2^{10} = 1024 cells representing a blastocyst. MtDNA replication is resumed in all simulated cells at 7 dpc with a minimum rate required, so as to populate the exponentially growing PGC population [261, 264].

Post-implantation
4. To model the development of primordial germ cell (PGC) line, we randomly sample 40 cells (to mimic laboratory observation [265]) from the total population of 1024 simulated cells and discard the remaining 984 cells.

5. The 40 cells selected to form PGCs continue to divide at the same rate of 15 hours to produce 25,791 primary oocytes by 13.5 dpc [261], with an ongoing mtDNA replication.
6. We follow the expansion process for 10 more cell generations to a final cell population of 40,960 at 13.4 dpc (). During this process, the mtDNA copy number per cell rises to about 1500. This matches with the experimentally observed range of 2152 to 1376 mtDNA per cell (Table 5).
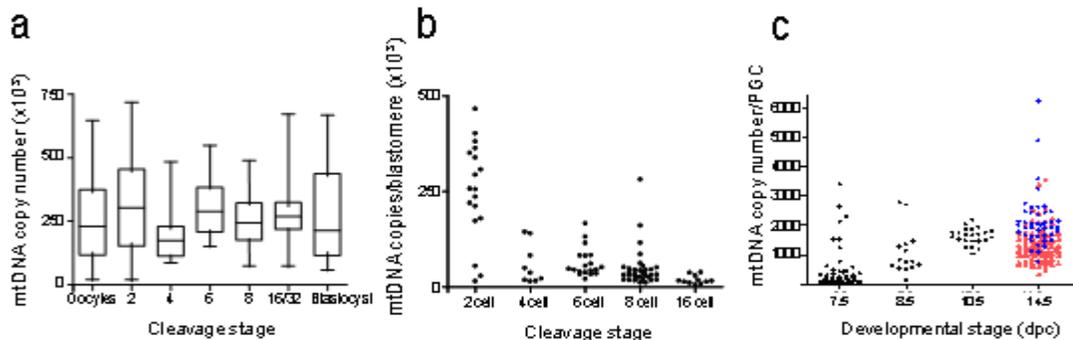
Figure 24: Experimental data [186]: The amounts of mtDNA in mature mouse oocytes and pre-implantation mouse embryos. (a) Mature oocytes and whole embryos. Box and whisker plot showing the median, +/- 1 SD, and the range from maximum to minimum values. (b) Single blastocyst cells (blastomeres) from pre-implantation embryos. Each data point corresponds to a single blastomere. (c) Primordial germ cells (PGCs) from post-implantation mouse embryos. Each data point corresponds to a single PGC. dpc = days post coitus. Data from male and female embryos is shown separately for 14.5-dpc which is shortly after the first point at which the gender can be determined. Blue circles = males, red triangles = females.

5.3 Section 5.3: Results

The random processes of distribution of wild-type and mutant mtDNA to daughter cells, mtDNA replication and mtDNA degradation cause the heteroplasmy level in each simulated cell to drift. Over time, this drift generates a heteroplasmy variance across all of the simulated cells. During the first phase of embryogenesis, while the mtDNA copy number per cell is still relatively high, very little heteroplasmy variance is generated (Figure 27c). As the mtDNA copy number per cell falls to a few hundred copies, heteroplasmy variance begins to rise. After mtDNA replication begins, and the PGC line is formed, mtDNA copy number per cell increases to approximately 1500 per cell. The heteroplasmy variance slows its rate of increase but continues to increase at a steady rate as long as the PGCs continue to divide at a rapid pace (Figure 27c).

To compare and test the predicted genetic bottleneck size of ~200 segregating units [191], our collaborators measured mtDNA copy numbers during early stages of development (Table 4). Based on an estimate for mtDNA copy number per cell at 5.5 dpc, the mtDNA copy number per cell among blastomeres before implantation was

estimated at about 4000, about 20 fold greater than the earlier prediction [191]. However, based on our simulations of the model described in Section 5.2, the number of mtDNA per cell before pre-implantation falls down to about 200 (Figure 27b), the predicted bottleneck size [191].
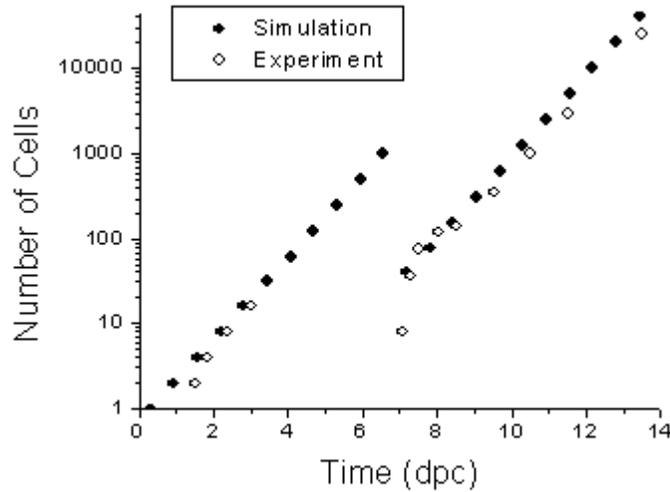
Figure 25: Comparison between the number of cells simulated and the actual number of cells observed experimentally by our collaborators [186]. The rate of cell division in pre-implantation embryos is derived from Streffer, *et al.* [262] and for post-implantation embryos from literature [261, 264]. PGCs are first detectable at 7.25 dpc. Note the logarithmic Y-axis indicating exponential growth to a final figure of 25,791 primary oocytes at day 13.5 [261].
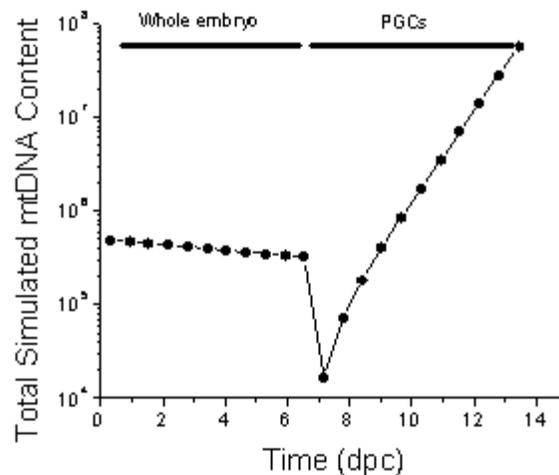
Figure 26: The total mtDNA copy number in the simulated mouse embryos up to 7dpc, followed by the total mtDNA copy number in the entire PGC population.

Table 4: Experimental data [186]: The amounts of mtDNA in mature oocytes and pre-implantation mouse embryos. n = number of embryos / oocytes studied. CV = coefficient of variance.

		Whole Embryo				Individual Cells		
Stage	N	Mean copy number (x10^3)	Range (x10^3)	CV	n	Mean copy number (x10^3)	Range (x10^3)	CV
Oocyte	-	-	-	-	22	249.4	26.9-645.7	0.63
2 cell	24	347.7	112.9-676.8	0.54	18	247	14.6-465.6	0.52
4 cell	13	196	85.9-483.2	0.55	9	57.7	15.1-143.6	0.9
6 cell	8	308.6	150.5-547.6	0.41	19	63.2	20.4-166	0.6
8 cell	23	244.5	73.8-488.2	0.41	33	47.9	11.0-281	1.07
16-32 cell	12	286.1	73.8-671.3	0.52	11	18.4	4.9-38.0	0.61
Blasto-cyst	15	280.8	56.7-667.1	0.68	-	-	-	-

Table 5: Experimental data [186]: the amount of mtDNA in primordial germ cells at different embryonic stages in mice. CV = coefficient of variance. n = number of primordial germ cells studied.

Stage dpc – days post coitus	N	Mean copy number (x10^2)	Range (x10^2)	CV
7.5	596	4.51	0.26-34.02	1.55
8.5	165	10.65	1.28-27.78	0.72
10.5	96	16.01	10.26-21.93	0.18
14.5 Male	1087	21.52	7.56-62.41	0.44
14.5 Female	1528	13.76	3.42-34.13	0.44

Table 6: Experimental data [186]: Variation in the level of heteroplasmy between the offspring of heteroplasmic female mice.

Proportion of NZB genotype in mother	Number of offspring	Variance in heteroplasmy amongst offspring	Coefficient of variation
0.01	9	0.0001	0.9274
0.01	17	0.0000	0.6856
0.03	9	0.0086	3.0872
0.05	11	0.0420	4.0999
0.1	6	0.0135	1.1605
0.11	11	0.0068	0.7478
0.16	8	0.0266	1.0475
0.16	4	0.0281	1.0201
0.16	16	0.0227	0.9412
0.18	15	0.0065	0.3219
0.18	7	0.0034	0.4462
0.26	20	0.0199	0.5428
0.27	10	0.0066	0.3013
0.28	10	0.0244	0.4586
0.28	4	0.0165	0.5579
0.3	5	0.0215	0.4882
0.31	10	0.0233	0.4921
0.34	8	0.0115	0.3155
0.35	18	0.0208	0.4122
0.4	17	0.0093	0.2411
0.48	17	0.0125	0.2333
0.58	14	0.0118	0.1869
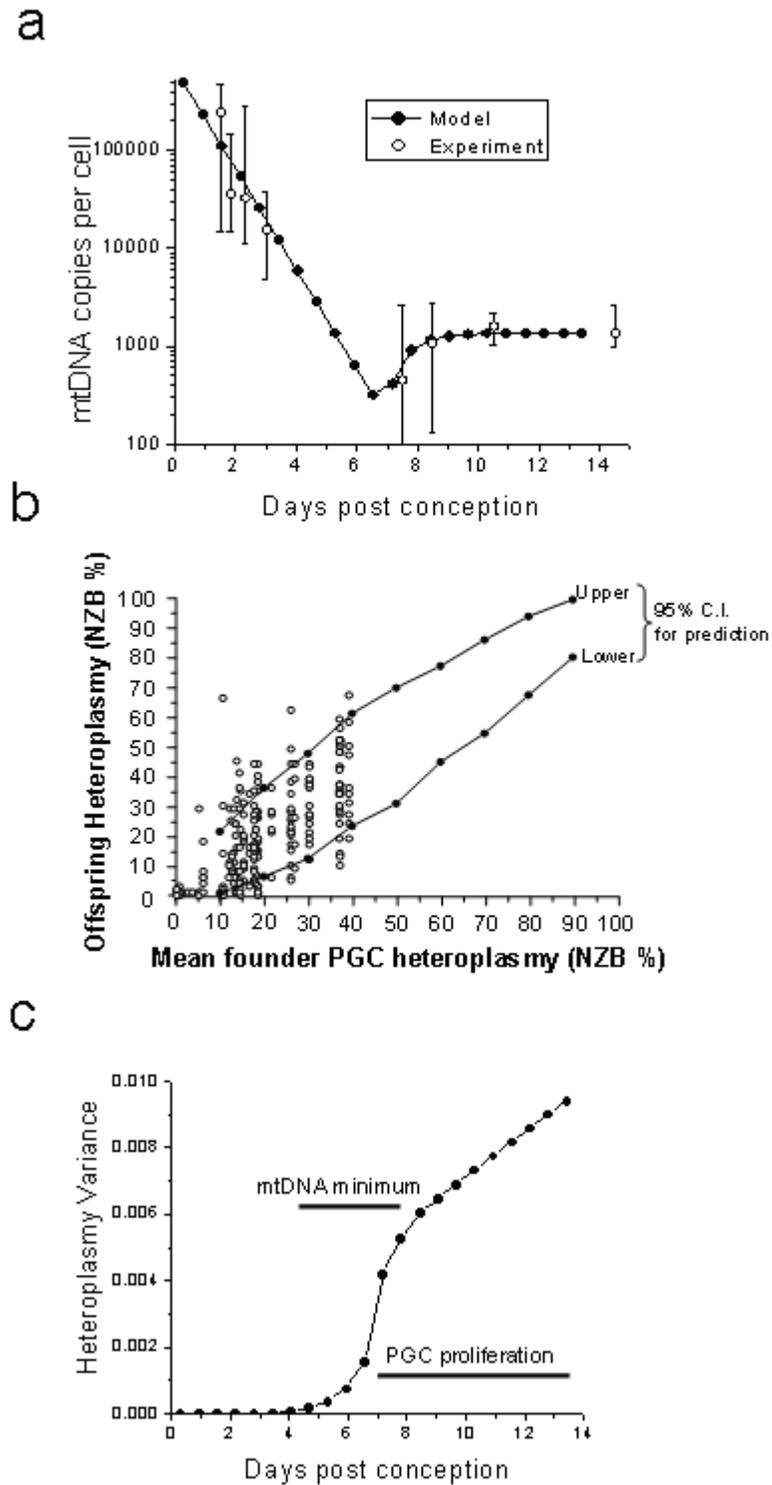
Figure 27: (a) Comparison between the simulated number of mtDNA in each cell (solid circles) and the actual number measured in pre-implantation embryos and primordial germ cells (open circles = mean, with 95% confidence intervals for the laboratory data [186]). (b) The simulation model reliably predicts the transmission of mtDNA heteroplasmy. At birth there is no significant difference in the proportion of NZB mtDNA between different tissues, but post-natal segregation of mtDNA genotypes leads to significant differences between the tail mtDNA and other tissues in adult mice

(Dahl, *et al*. unpublished, and Ref. [254]). Given that the transmission of NZB heteroplasmy is determined by random genetic drift [266], with an equal likelihood of an increase or decrease in the proportion of mtDNA, we estimate the NZB % in the maternal primordial germ cell founders as the mean level of heteroplasmy from the offspring at birth. Y axis = the percentage of NZB mtDNA in the offspring. X axis = estimated NZB mtDNA in the founding primordial germ cells (PGCs) in a single mother. Solid symbols and lines = 95% confidence interval (C.I.) for the predicted heteroplasmy level using the simulation model (Figure 23c), based on the actual measurement of mtDNA copy numbers during mouse development (Table 4 and Table 5). (c) Generation of the heteroplasmy variance in the blastomeres and primordial germ cells in a mother with 50% mutated mtDNA. Simulation shows that much of the variation is generated around the time of implantation and during PGC development. The predicted value corresponds with the actual value for a mother with 58% NZB mtDNA (Table 6).

From our analysis of simulation output, we define the 95% confidence interval (CI) for the mean NZB heteroplasmy data in founder PGCs and in the offspring. Based on a conservative model of the median number of mtDNA per cell at 7.5 dpc, Figure 27b shows that 91% of the experimental offspring NZB heteroplasmy levels fall within the predicted 95% CI for the model. Delaying the onset of mtDNA replication by 12 hours in the model (to simulate the variation observed in implantation time [267]), reduces the mtDNA copy number at implantation approximately to the lower end of the measured range in PGCs (Table 5) and increases the offspring heteroplasmy variance (Figure 27c). From the analysis of these results (Figure 27), we estimate about 70% of variance in offspring heteroplasmy is due to the drastic reduction in the number of mtDNA per cell (~200) owing to physical partitioning of mtDNA into daughter cells during pre- and early post-implantation development. The remaining 30% variance develops during the exponential growth of the PGC population with high mtDNA replication rate leading to an average mtDNA copy number of ~1500 per PGC. It is important to note that within these 70% and 30% contributions to variance, there are several contributors such as the relaxed replication of mtDNA and mtDNA degradation.

Taken together, these results suggest that individual mtDNA molecules segregating during the mouse embryogenesis is enough to explain the mitochondrial genetic bottleneck. Segregation of mtDNA grouped into nucleoids or mitochondria, as proposed by some [255], or selection of a group of mtDNA, is not a requirement for the mitochondrial genetic bottleneck.

6 Chapter 6: MtDNA Dynamics in Cell Culture

In chapter 5, we conclude that the segregation of individual mtDNA molecules during mouse embryogenesis is enough to explain the mitochondrial genetic bottleneck. This does not mean that groups of mtDNA compartmentalized into *nucleoids or mitochondria* could not segregate as one unit at other times. While no studies have reported a direct observation of the mtDNA segregation in the form of nucleoids during mammalian embryogenesis, Cao, *et al.* [255] predict that such segregation is required to explain the genetic bottleneck size.

To experimentally study the nature of mtDNA segregation in mammalian cell cultures, an experimental group lead by Dr. Anton K. Raap approached us for simulations to act as control for their experiments. The group is developing cell cultures of trans-mitochondrial human cybrid cells derived from patients harboring inherited pathogenic mtDNA mutations to study the segregation patterns of mtDNA during cell divisions. How do we expect the mutant mtDNA proportion to vary if mtDNA segregate purely randomly? If we produce the expected heteroplasmy variation assuming random mtDNA segregation using simulation, the collaborators will have a scale to compare to, to help in the interpretation of experimental results. Chapter 6 presents the mtDNA segregation model developed to support these cell culture experiments.

6.1 Section 6.1: Model of heteroplasmy changes in cell culture

Based on the cell culture requirements from the experimental group, we begin with a single cell and simulate the formation and maintenance of a culture of heteroplasmic cells over a time scale of 4 months. The initial cell undergoes cell division with a set mean time between divisions. The cells divide until the simulated cell culture population exceeds 1 million cells. The time required to achieve this population size is about 23 days with a mean cell division time of 24 hours. This marks the end of first passage and 10% of the cells are randomly sampled to initialize the next passage. In second passage, the population is again allowed to grow to a population size of 1 million cells. Note that the second passage will only require about 3.5 days. Again, a randomly sampled 10% cells are taken from second passage to initialize the third sample. Each time the cell population is randomly sampled at the end of each passage, the frequency of cells based on heteroplasmy is computed and saved in twenty bins of 5% mutation load each (0-100%) to produce the heteroplasmy distribution in cell culture. This simulation of cell culture passages is continued for 4 months, modeling about 30 passages of the cell culture.

Table 7: Description of the cell culture simulation parameters and their typical values

Parameters	Values	Description
STARTCELLNUMBER	100,000	Number of cells sampled at the end of each passage and initialized to heteroplasmy values derived from experimental data
PASSAGESIZE	3.5 days (84 hours)	We allow cells (100,000) to grow and divide for exactly 3.5 days
EXPECTEDCELLNUMBER	1,000,000	We allow the cells to grow and divide in culture for 3.5 days (a passage) during which we expect about 10 times increase in cell count.
SAMPLESIZE	100,000	At the end of each passage, we randomly sample exactly 100,000 cells to bring back the total number of cells in the system to 100,000. Same as STARTCELLNUMBER.
PASSAGECOUNT	31	The maximum number of passages of cell culture to simulate
T_{half}	10 days (240 hours)	Half life of mtDNA
D	24 hours	Mean time between cell division (all cells divide randomly with mean time separating their divisions being D hours).
N_{target}	1500	Target total number of mtDNA per cell
Time step	1 hour	Fixed time increments of simulation
No symbol	1 cell to 1 million for first passage. 100,000 to 1 million for all other passages	Total number of simulated cells

The following events are modeled in cell culture: relaxed mtDNA replication, mtDNA degradation, and cell division. Cell death due to high heteroplasmy levels is not modeled here because the medium in which the cells are cultured do not require functional mitochondria for their growth and survival. However, the cell death mechanism is easy to turn on programmatically if desired in future.

Table 7 describes the typical parameter values used in the cell culture simulations. All these events are modeled as described in Section 4.2 and are tabulated in Table 8. A typical 4 months simulation run of the cell culture requires about 2 hours of CPU time on an Intel Pentium 4, 2.40 GHz CPU with 1GB RAM.

Table 8: Description of the events occurring in the cell culture simulation model

EVENT	Description
Cell division	Every cell has a fixed probability of dividing during each timestep, $\Delta t = (ln(2)*\Delta t)/D$ When a cell divides, W and M mtDNA are distributed to daughter cells using binomial distribution and the total number of cells in the system is incremented by 1.
MtDNA replication	All mtDNA (both W and M) replicate with rate $Ro = ln(2)*N_{target}/T_{half} + ln(2)*N_{target}/D$ The number of W and M type mtDNA to replicate is chosen using a binomial distribution
MtDNA degradation	Number of W (and M type) mtDNA to degrade in one time step is calculated using a Poisson distribution with mean = $ln(2)*W*\Delta t / T_{half}$ $(ln(2)*M*\Delta t / T_{half})$

6.2 Section 6.2: Cell culture simulation results

We simulate the cell culture model (Section 6.1) for different input parameter values to enable direct comparison with in vitro experiments. Since the cell culture experiments are still in progress, we are keeping the preliminary experimental data confidential. However, we present simulation results here.

In Figure 28, we show two simulation runs starting with a single cell with 50% mutation load in culture, once with 1000 mtDNA per cell and once with 5000 mtDNA per cell. The initial cell undergoes a series of cell divisions increasing the number of cells exponentially. Due to the stochastic events of relaxed replication of mtDNA, mtDNA degradation, and segregation of mtDNA to daughter cells during cell division, the heteroplasmy in the simulated cells vary over time. At the end of each passage, the numbers of cells with heteroplasmy within a range of mutation load are counted. As we would expect and as is evident from Figure 28, the heteroplasmy in the simulated cell culture spreads faster for the simulation run with smaller number of mtDNA per cell. Since the experimental data was expected to be in the form of heteroplasmy distributions

at the end of certain passages (in between 1 to 31), we save the frequency data at the end of each simulated passage.
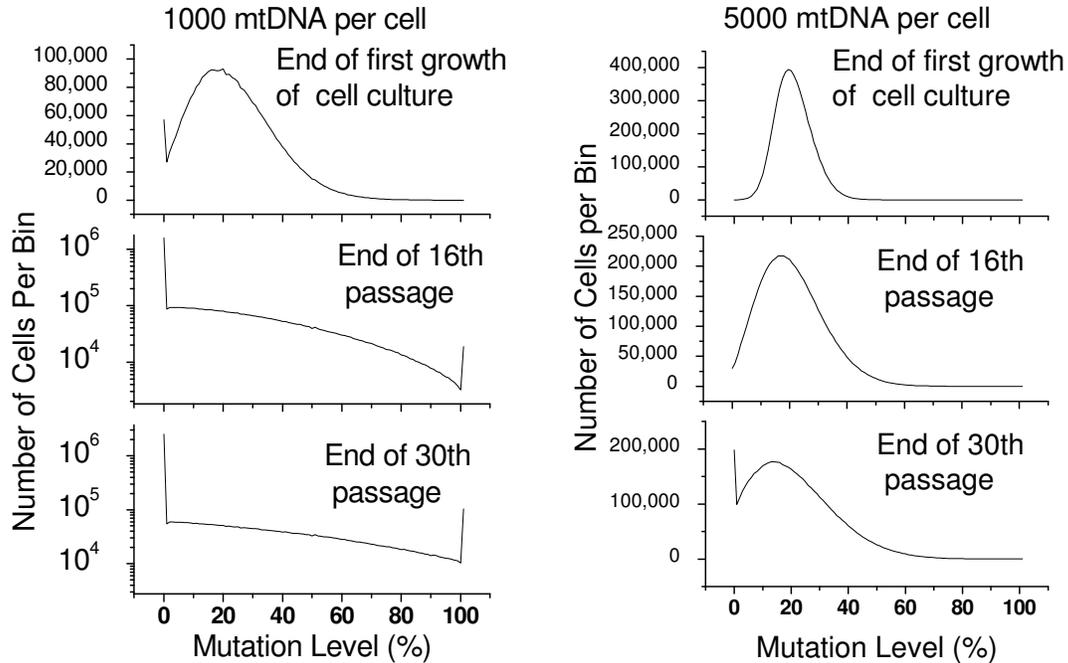
Figure 28: Simulation results for two different mtDNA copy numbers (1000 and 5000) per cell beginning with a 20% heteroplasmic cell. The population distribution is measured at the end of each passage, just before the 10% sampling is taken. The width of each bin is 1% mutation level. There are two special bins, at 0 and 100% mutation, for the cells that are fixed on wild-type and mutant respectively. The random drift in the cell mutation level is fastest in the simulation with the lower number of mtDNA per cell. In both simulations, the average mutation level taken over all the cells remains steady at the initial value, since in this simulation there is no advantage or disadvantage to the mutation.

Figure 29 shows the heteroplasmy distribution of simulated cells (initial cell at 50% heteroplasmy) at the end of several passages. The mean mutation load of the first cell in the simulation is set based on the experimental value from collaborators. These distributions generated by simulations can then act as controls for the distributions derived from experiments. In this case, the distributions showed marked disagreement with experimentally obtained distributions (data not shown). We conclude that the mechanisms included in the simulation model are not sufficient to explain the cell culture experiment results of our collaborators. The exact hypotheses are being made by our collaborators and we keep these confidential until publication.
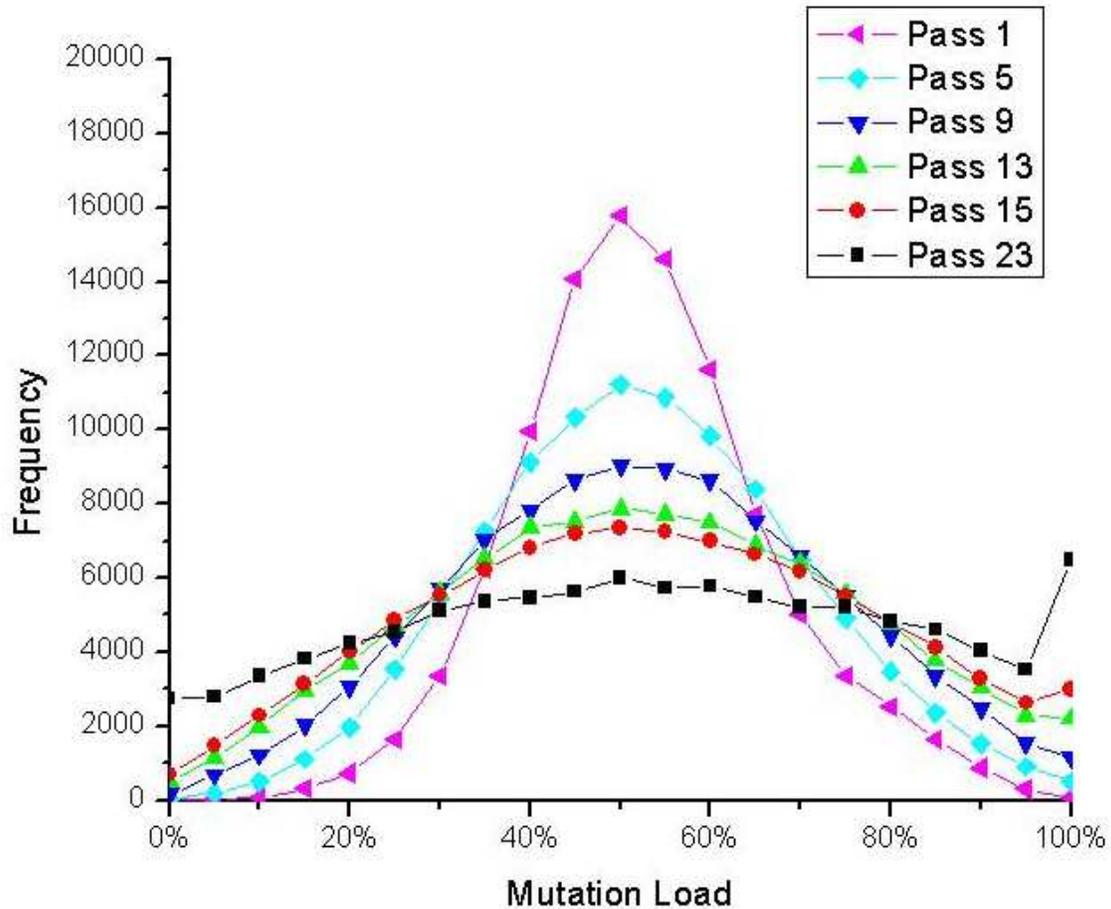
Figure 29: Simulation result showing the spread of heteroplasmy in cell culture due to the stochastic events of mtDNA replication, mtDNA degradation and distribution of mtDNA to daughter cells during cell division. The peaks in frequency at 0% and 100% heteroplasmy indicate the number of cells fixed at homoplasmy for wild-type or mutant mtDNA respectively. These distributions are to serve as controls for the distributions generated for cell cultures by our collaborators. The initial mutation load of the single cell that this simulation begins with, is set based on the input from experiments.

7 Chapter 7: Mitochondrial Morphologic Dynamics Model

Chapter 7 presents the mitochondrial morphologic dynamics model. Initially in this study, we aimed for a more complex model involving mitochondrial mass, growth, damage, and degradation in a dividing cell culture with the goal of analyzing the results reported by Jendrach, *et al.* [97]. However, from the model development process, it became apparent that it was too complex to understand the interplay between various mechanisms and simulation parameters simultaneously. We realized that a much simpler model was sufficient to address the basic question of how the cell controls mitochondrial morphological balance. So, we scaled down to a much simpler model focused on understanding the basic control process by which the cell balances the rates of occurrence of fission and fusion events. We present this simplified model and results here.

7.1 Section 7.1: A model of mitochondrial morphologic dynamics
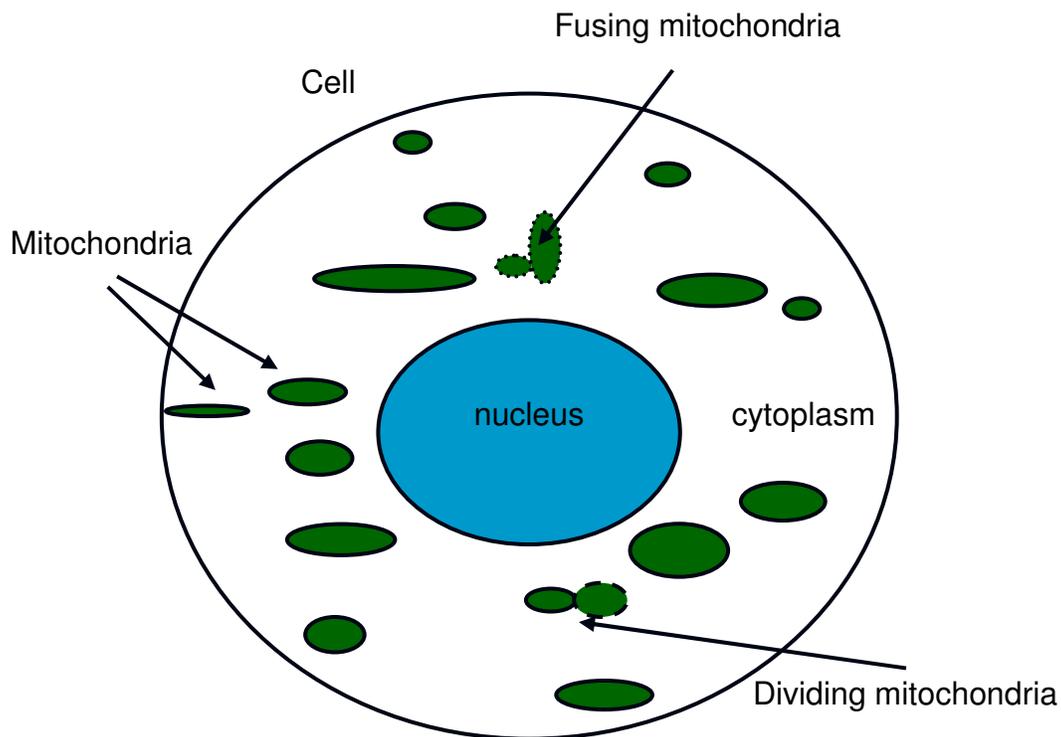
Figure 30: Diagrammatic representation of the mitochondrial morphologic dynamics model. Mitochondria of different masses are shown. Mitochondrial morphologic events fusion and fission are depicted. MtDNA are not modeled. This picture is a simplified version of the diagrammatic model in Figure 3.

We model about 100 to 200 mitochondria in a non-dividing post-mitotic cell with each mitochondrion initialized to a mass of 1 unit. These mitochondria undergo the stochastic events of fusion and fission. As an effect, these processes will cause the mitochondrial mass distribution in the cell to spread out. Each mitochondrion is modeled as a C++ object with its size or mass as an instance variable. Programmatically, it is easy to model additional mitochondrial characteristics such as the extent of damage accumulated in a mitochondrion or its inner membrane polarization state.

7.1.1 Mitochondrial fusion

Two mitochondria can fuse together to become one larger mitochondrion. When a fusion event occurs, the mass of the resulting mitochondrion will equal the mass of the two fusing mitochondria. The rate of occurrence of mitochondrial fusion event in a cell depends on the whether mitochondria fuse one end-to-one end (Figure 31), one-end-to-anywhere (Figure 32) or anywhere-to-anywhere (Figure 33). In order to keep the simulation flexible and to study the feasibility of the three fusion models, we have implemented all three alternatives and support the choice of using one of the three models during a simulation run. In any of the three fusion models, the following adjustments should happen in the system:

1. The mass of the resulting larger mitochondrion will be equal to the sum of the fusing mitochondria.
2. The total number of mitochondria in the cell is decremented by one.
3. The total mitochondria mass in the cell remains the same.

End-to-end fusion model: In this model (Figure 31), the assumption is that a mitochondrion can only fuse with another mitochondrion at one of its two "ends". Hence, if there are N_t number of mitochondria in the cell at time 't', then the mean number of fusion events occurring in the cell is proportional to the square of the number of ends (N_t x N_t).
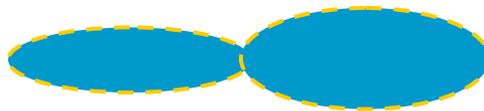
Figure 31: Illustration of the end-to-end fusion of mitochondria

The mean number of fusion events occurring in a time step at time t,

$$R_{fus} = FusA \times N_t^2 \tag{10}$$

where,

$$FusA = \frac{K_{fus}}{N^2_{target}} \qquad (11)$$

where K_{fus} is a constant and N_{target} is the target total number of mitochondria in the cell (). Hence,

$$R_{fus} = \frac{K_{fus} \times N_t^2}{N^2_{target}} \qquad (12)$$

End-to-anywhere fusion model: In this model (Figure 32), the assumption is that at least one end of one of the two mitochondria is needed for mitochondrial fusion. One end of a mitochondrion can fuse at any site on the surface of another mitochondrion. Hence, if there are N_t mitochondria in the system at time 't', then the mean number of fusion events occurring in a single time step in the cell is proportional to the number of ends times the mass of mitochondria at time 't' ($N_t \times M_t$). This assumes that the shape of the mitochondria is cylindrical, with constant diameter. Thus, increasing surface area corresponds to increasing mass.
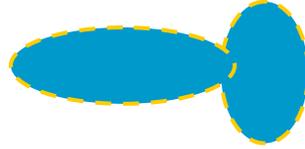
Figure 32: Illustration of the end-to-anywhere fusion of mitochondria

The mean number of fusion events occurring in a time step in the cell with end-to-anywhere fusion model at time t,

$$R_{fus} = \frac{FusA \times N_t \times M_t \times N_{target}}{M_{target}} \qquad (13)$$

where M_t is the total mitochondrial mass at time t and T_{arget} is the target mitochondrial mass in the cell (Figure 32). Hence, using the value for FusA from Equation (11),

$$R_{fus} = \frac{K_{fus} \times N_t \times M_t}{N_{target} \times M_{target}} \qquad (14)$$

Anywhere-to-anywhere fusion model: In this model (Figure 33), the assumption is that two mitochondria can fuse together at any sites on their surfaces. Hence, if there are N_t

mitochondria in the system with mass M_t at time 't', then the mean rate of fusion events occurring in the cell is proportional to square of their mass, i.e., M_t x M_t.
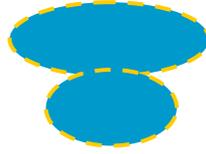
Figure 33: Illustration of the anywhere-to-anywhere fusion of mitochondria

The mean number of fusion events occurring in a time step in the cell with anywhere-to-anywhere fusion model at time t,

$$R_{fus} = \frac{FusA \times N^2_t \times M^2_t}{M^2_{target}} \qquad (15)$$

Hence,

$$R_{fus} = \frac{K_{fus} \times N^2_t \times M^2_t}{N^2_{target} \times M^2_{target}} \qquad (16)$$

7.1.2 Mitochondrial fission

Mitochondria undergo frequent fission or division to produce smaller mitochondria. The exact mechanism and sites of fission are yet to be ascertained. While inner membrane potential is shown to be a requirement for mitochondrial fusion [76], its role in mitochondrial fission is not decisive. It is generally believed that one of the two daughter mitochondria will lose its membrane potential and becomes depolarized upon fission [79]. It is not necessary that the two daughter mitochondria be identical or even of the same size. There are many ways we can choose the site of fission. For choosing the point of fission, we randomly choose somewhere within the middle 20% to 80% area of the mitochondrial mass. Mitochondria that undergo fission during a time step can either be sampled randomly or be sampled based on their masses. In our model, the probability of mitochondrial fission is proportional to its mass. A fission event increases the total number of mitochondria by one.

We model mitochondrial fission as a mechanistic event wherein the dynamin proteins pinch the mitochondrion at a specific site to result in two daughter mitochondria. The number of fission events in the cell in a given time step is modeled as a constant rate.

7.1.3   Balance between fission and fusion

To understand the balance in the rates of occurrence of fission and fusion events in a cell over time, we develop a simple model of the mitochondrial morphologic dynamics (Figure 30). We model a single non-dividing post-mitotic cell with no cell division events. The model does not account for the effects of cell cycle on the mitochondrial morphology as this is not relevant to the question we are trying to answer. The model also excludes mitochondrial damage, growth, and degradation. We had earlier implemented the effects of cell division, mitochondrial damage, growth and degradation in the model. We simply "switch off or disable" these processes from occurring in our simple model. We simulate all three models of mitochondrial fusion. We typically simulate about 100 mitochondria in a cell with the mass of each mitochondrion = 1.0. The mass is allowed to vary from 0.0 to 20.0. The mitochondrial mass varies only as a result of the stochastic occurrences of fission and fusion events. We assume that all mitochondria are initialized to a polarized state and that they will remain in that state throughout the simulation.

The key questions of interest for us from the model are

1. How does the cell tightly balance the rates of fission and fusion events as observed in literature [97] in human cells in culture?
2. The tight balance is shown to be at a much higher rate for young proliferative cells than for old post-mitotic cells in culture. What controls the rate at which the fission and fusion event rates are balanced at?

In answering these questions by utilizing experimental data, we need to pay particular attention to the time scales of measurements. The events occur almost instantaneously and the methods used to measure the rate of these events need to be carefully considered before directly comparing them to simulation results.

We will show that the process of simulation model development lead us to an analytical deterministic model as well. While the deterministic model is not useful to study the stochasticity of the system, it can be used to quickly compute mean values of the required parameters without having to do any simulation.

7.2 Section 7.2: Deterministic model

The process of development of the stochastic simulation model of mitochondrial morphology helped us arrive at a deterministic solution. In this section, we present the deterministic mathematical model for the morphologic dynamics model. In this model, the total mitochondrial mass in the simulated cell is a constant. The only variable in the model is the total number of mitochondria in the cell which varies as a function of fission and fusion events occurrences. The rate of occurrence of fission events is set to a constant value. The rate of occurrence of fusion events varies depending on the model chosen for mitochondrial fusion (Equations (10), (13), and (15)).

Table 9: Mitochondrial morphologic dynamics model parameters, descriptions and their values

Parameters	Typical Values	Description
R_{fis}	0.16	Constant rate of mitochondrial fission
R_{fus}	Depends on the chosen fusion model. Refer to equations (12), (14), and (16).	Rate of mitochondrial fusion is set depending on the fusion model chosen (end to end, end to anywhere, or anywhere to anywhere).
N_t	0-1000	Number of mitochondria in the cell at time 't'
N_{target}	100	Target total number of mitochondria in the cell
Δt	1.0 min	Simulation time step
M_t	100.0	Total mass of mitochondria in the cell at a given time t
M_{Target}	100.0	Target total mitochondrial mass
$FusA$	$K_{fus}/ N^2_{target} = 1000$ where $K_{fus} = 0.1$	

Let N_t be the number of mitochondria in the simulated cell at time t.
The number of mitochondria $N_{(t+\Delta t)}$ in a cell following end to end fusion model at time $(t+\Delta t)$ is given by

$$N_{(t+\Delta t)} = N_t + R_{fis} \times \Delta t - R_{fus} \times \Delta t \tag{17}$$

Where R_{fis} is the constant rate of mitochondrial fission and R_{fus} is the rate of mitochondrial fusion.

Case 1: End-to-end fusion of mitochondria

Using the R_{fus} value for end to end fusion model from Equation (12),

$$N_{(t+\Delta t)} = N_t + R_{fis} \times \Delta t - \frac{K_{fus} \times N_t^2 \times \Delta t}{N^2_{target}} \tag{18}$$

The change in the number of mitochondria in time step Δt is given by,

$$\frac{N_{(t+\Delta t)} - N_t}{\Delta t} = R_{fis} - \frac{K_{fus} \times N_t^2}{N^2_{target}} \tag{19}$$

Case 2: End-to-anywhere fusion model

The total number of mitochondria in a cell following end to anywhere fusion model at time $t+\Delta t$, is given by

$$N_{(t+\Delta t)} \;=\; N_t \;+\; R_{fis} \times \Delta t \;-\; FusA \times N_t \times N_{target} \times \frac{M}{M_{target}} \times \Delta t \qquad (20)$$

Where R_{fis} is the constant rate of mitochondrial fission and R_{fus} is the rate of mitochondrial fusion given by Equation (13).

The change in the number of mitochondria in time step Δt is given by,

$$\frac{N_{(t+\Delta t)} - N_t}{\Delta t} = R_{fis} - \frac{K_{fus} \times N_t \times M_t}{N_{target} \times M_{target}} \qquad (21)$$

Case 3: Anywhere-to-anywhere fusion model

The total number of mitochondria in a cell following anywhere to anywhere fusion model at time $t+\Delta t$, is given by

$$N_{(t+\Delta t)} \;=\; N_t \;+\; R_{fis} \times \Delta t \;-\; \frac{FusA \times N^2_{target} \times M_t^2}{M^2_{target}} \qquad (22)$$

Where R_{fis} is the constant rate of mitochondrial fission and R_{fus} is the rate of mitochondrial fusion given by Equation (15).

The change in the number of mitochondria in time step Δt is given by,

$$\frac{N_{(t+\Delta t)} - N_t}{\Delta t} = R_{fis} - \frac{K_{fus} \times M_t^2}{M^2_{target}} \qquad (23)$$

7.3 Section 7.3: Results

7.3.1 Steady state analysis

We present the results of the steady state analysis of the morphologic dynamics model for the three fusion cases. We prove that, of the two fusing mitochondria, at least one end of a mitochondrion is needed for the cell to balance mitochondrial fission and fusion (Equation (26)). We emphasize here that the deterministic model of morphological dynamics came as a desirable by-product of the simulation model development process. From the comparison of the results from stochastic simulations with those from the deterministic model, we show that fluctuations (standard deviation) in the mitochondria number can only be learned from the stochastic simulations. While the deterministic model is a simple solution to the mean number of mitochondria in the cell, stochastic simulations model the additional (natural) variation in the number of mitochondria in the cell. The steady state solution for the total number of mitochondria in the morphologic dynamics model at a given time t, is presented for the 3 cases representing the three different mitochondrial fusion models.

Case 1: Steady state solution for the total number of mitochondria with end–to–end fusion model

At steady state,

$$N_{(t+\Delta t)} = N_t$$

Hence, from Equation (19),

$$0 = R_{fis} - \frac{K_{fus} \times N_t^{\,2}}{N_{target}^{\,2}}$$

$$R_{fis} = \frac{K_{fus} \times N_t^{\,2}}{N_{target}^{\,2}}$$

Hence, the steady state solution to the mitochondria number in his case is given by:

$$N_t = \sqrt{\frac{R_{fis}}{K_{fus}}} \times N_{target} \tag{24}$$

Case 2: Steady state solution for the total number of mitochondria with end–to–anywhere fusion model

At steady state,

$$N_{(t+\Delta t)} - N_t = 0$$

Hence, from Equation (21),

$$0 = R_{fis} - \frac{FusA \times N_t \times N_{target} \times M_t}{M_{target}}$$

$$R_{fis} = \frac{K_{fus} \times N_t \times M_t}{N_{target} \times M_{target}}$$

Hence, the steady state solution to the mitochondria number in this case is given by:

$$N_t = \frac{R_{fis} \times M_{target} \times N_{target}}{K_{fus} \times M_t} \tag{25}$$

Case 3: Steady state solution for the total number of mitochondria with anywhere–to–anywhere fusion model

At steady state,

$$N_{(t+\Delta t)} - N_t = 0$$

Hence, from Equation (23)

$$0 = R_{fis} - \frac{K_{fus} \times M_t^2}{M_{target}^2}$$

$$R_{fis} = \frac{K_{fus} \times M_t^2}{M_{target}^2} \tag{26}$$

No steady state solution!

There is no N_t term in this equation. i.e., there is no steady state solution for N_t in the anywhere-to-anywhere fusion model. This is a mathematical proof for that at least one

end of a fusing mitochondrion should be involved for mitochondrial fusion in order for the cell to balance mitochondrial fission.

7.3.2 Comparison of steady state solutions from deterministic and stochastic models

Figure 34 shows the fluctuations in the number of mitochondria in the cell obtained by stochastic simulation. The mean value for the mitochondria number in cell obtained from simulation closely matches the value obtained from the deterministic steady state solution (Equation (24)).
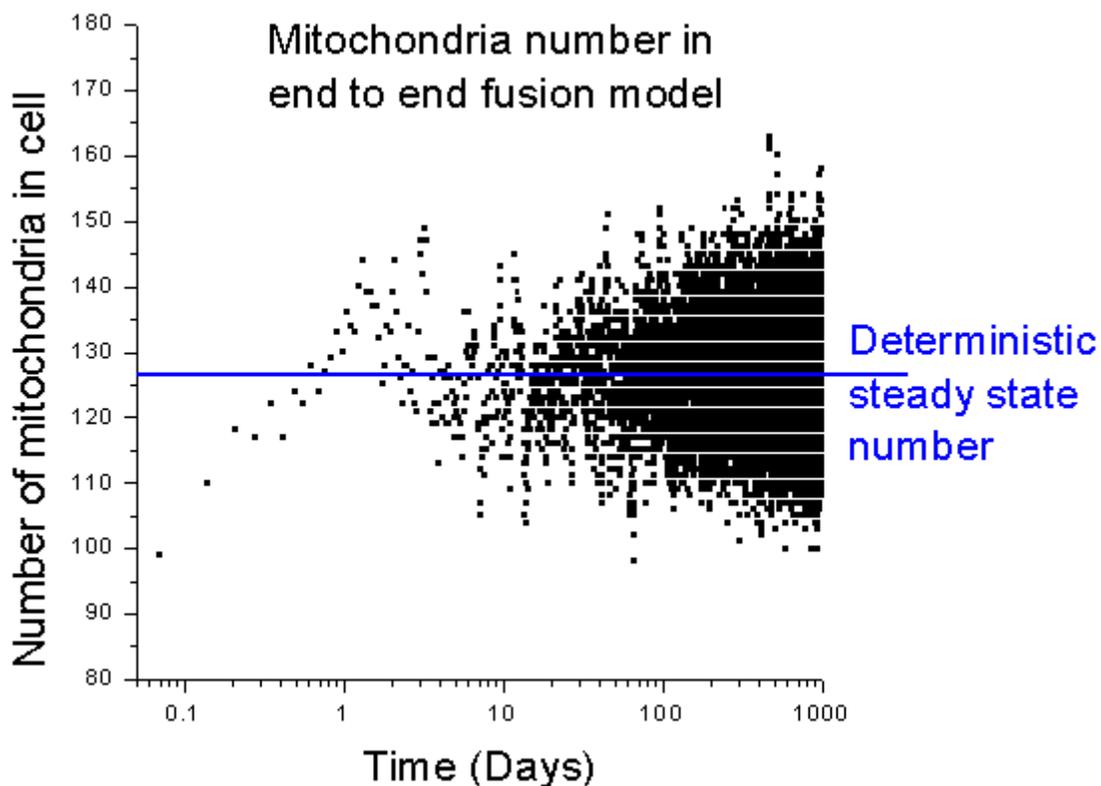
Figure 34: Simulation result: Fluctuations in the number of mitochondria in the cell due to stochastic occurrences of fission and fusion events. The fusion model chosen is end-to-end. The value for the steady state solution for the mean number of mitochondria in the cell derived from stochastic simulation = 126.06, very close to the value obtained from deterministic model (=126.5, indicated with a horizontal blue line). Note that the number predicted by simulation is slightly less due to the starting condition (start with 100 mitochondria).

7.3.3 Effects of changes in the rates of fission and fusion
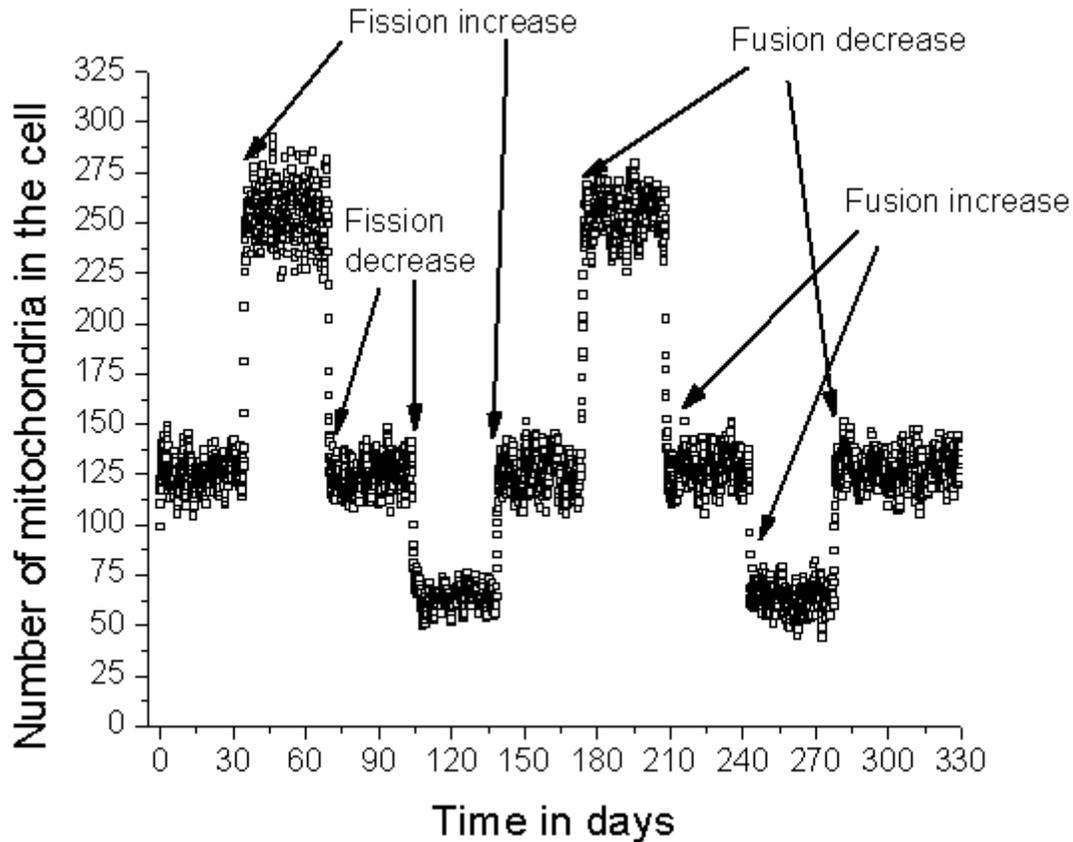
Figure 35: Variation in the number of mitochondria in the cell as a function of time. The simulation is setup to systematically vary the rates of fission and fusion in 9 passages (see text). Each increase and decrease in fission and fusion rates is done by a factor of 4.

To study the effects of changes in the rates of fission and fusion events on the number of mitochondria and mean mitochondrial mass in the cell, we set up a systematic simulation run as follows: We initialize the simulation parameters to values described in Table 9. Note that we start with an initial 100 mitochondria in the cell with the mass of each mitochondrion = 1.0. The number and mass of mitochondria in the cell vary during the course of the simulation due to the stochastic occurrence of fission and fusion events. We choose the end-to-end fusion model for this study. After some time, the number and mean mass of mitochondria reach steady state values of about 126 and 0.8 respectively.

The specific questions we are interested in here are: How does the cell respond to changes in the rates of fission and fusion events? If the cell needs to change the mitochondrial morphology, will it do so by altering the rate of fission or by altering the rate of fusion? To answer these questions illustratively, we systematically perturb the

steady state cell by subjecting it to 9 passages (each passage size of ~35 days) (Figure 35, Figure 36 and Figure 37):

1. In passage 1, mitochondria number reaches steady state value of 126.5.
2. In passage 2, we increase the rate of fission, R_{fis}, by 4 times. This results in doubling of the number of mitochondria in the cell and attains a new steady state. The result is consistent between stochastic and deterministic models (square root of 4 = 2 in equation(24)).
3. In passage 3, we decrease the rate of fission, R_{fis}, by 4 times. As we expect, the mitochondria number returns back to the initial steady state value of around 126.5.
4. In passage 4, we again decrease the rate of fission, R_{fis}, by 4 times. The mitochondria number now drops to half its initial value as we would expect from the deterministic solution in equation(24).
5. In passage 5, we increase the rate of fission, R_{fis}, by 4 times to bring back the mitochondria number to initial steady state value of around 126.5. This completes the perturbation of fission in both directions (increase and decrease).
6. Similarly, in passages 6-9, we perturb the regained steady state by altering the fusion rate to double and halve the mitochondria number. Since K_{fus} is in the denominator of equation(24), increasing fusion results in decreased mitochondria number and vice versa. The results are again consistent between deterministic model and stochastic simulation (Figure 35).

At regular intervals (every 100 minutes) during the simulation, we save the average number, mass of mitochondria, and the number of occurrences of fission and fusion events. We compute these numbers by averaging over a 100 minute window (note that each simulation time step = 1 min).

From data not shown, the standard deviation (=0.74204) for the steady state mean mitochondria mass in the cell as obtained from simulation is almost equal to the mean mass (0.7874) itself, suggesting that the mass of individual mitochondria follow exponential distribution. We verify this by plotting the masses of individual mitochondria saved at specific time intervals (every 900 time steps) during the simulation. Figure 36 shows the mitochondrial mass distribution at approximately, the beginning, middle and end of the simulation run.
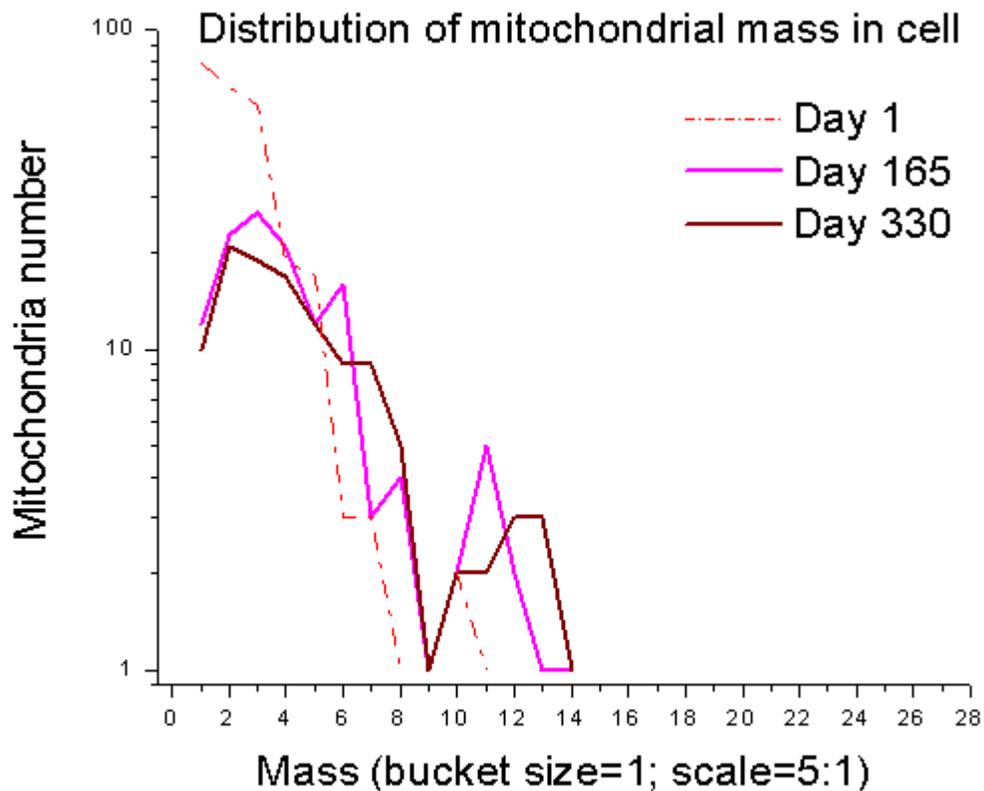
Figure 36: Mitochondrial mass distribution in the cell in passages 1, 5, and 9 of the simulation run. The rates of fission and fusion are varied as described for Figure 35.

Figure 37 shows the plot of actual number of fission and fusion events occurring in the cell counted in 100 min time slots. Observing at the regions of passages 6-9 in Figure 37, we conclude that the rate of fusion events adjusts itself to match the rate of fission events depending on the number of mitochondria at a given time. By substituting the steady state mitochondria number (126.5) in equation(24), we get the number of fusion events occurring at steady state.

7.4 Section 7.4: Discussion

Experiments [268] suggest that the cell switches its mitochondrial morphology between reticular and split mitochondria. When the cell needs to shift towards a split mitochondrial network (due to yet unknown signaling mechanisms), the cell has two ways of increasing its mitochondria count: (1) by increasing the rate of fission or (2) by decreasing the rate of fusion. Similarly, if the cell needs to change back to the reticular mitochondrial morphology (decrease the mitochondria number), the cell may either (1) decrease the rate of fission or (2) increase the rate of fusion. It is not clear yet, which one or both of these choices are made by the cell in controlling mitochondrial morphology.
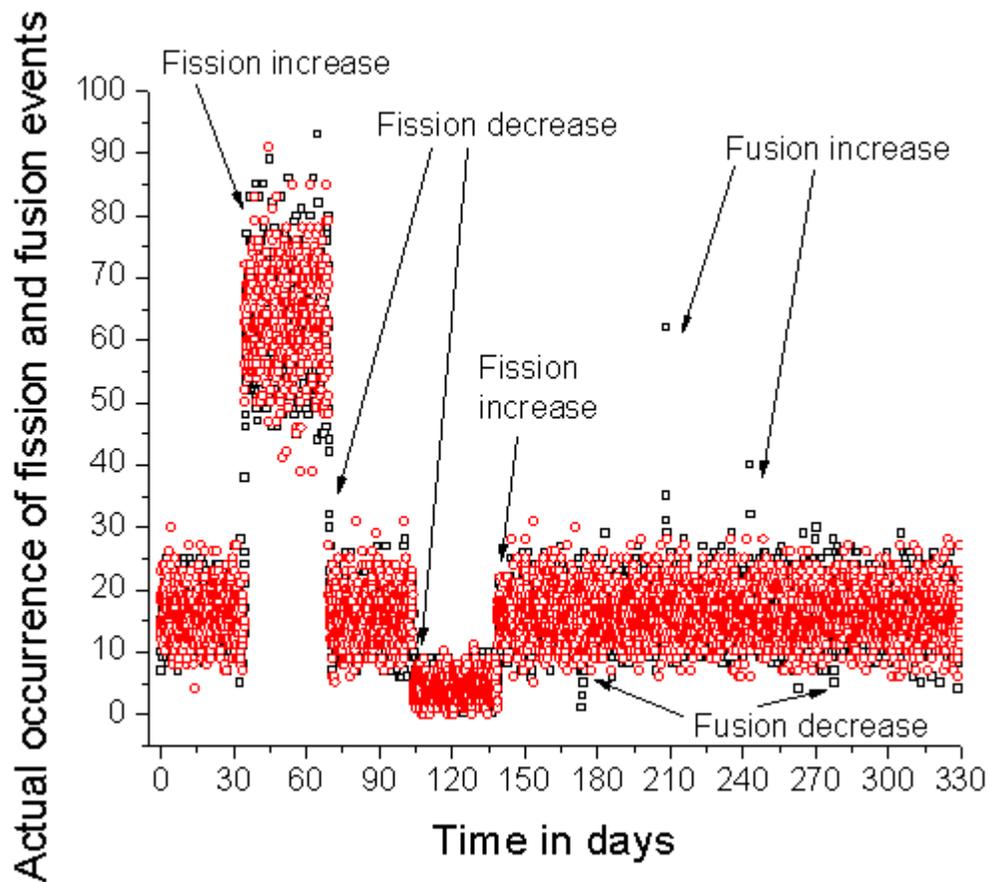
Figure 37: Actual number of fission and fusion events occurring in the cell through out the simulation run. Note that the number of fusion events adjusts itself to match the number of fission events, but not vice versa.

Our modeling study suggests that the effect of increasing (or decreasing) the rate of fission, produces the same effect on the steady state number of mitochondria in the cell as decreasing (or increasing) the rate of fusion. This is an intuitive result. However, an important result is that in this model, the cell adjusts the rate of fusion to match the rate of fission. But the cell cannot adjust the rate of fission to match the changing rate of fusion. Experimental data on the rates of mitochondrial fission and fusion at different phases of cell cycle will help in testing this hypothesis.

8 Chapter 8: Conclusions and Future Directions

Chapter 8 summarizes the results and original contributions of this dissertation. We highlight important research directions for focusing future efforts in the area of mitochondrial genetic and morphologic dynamics.

8.1 Section 8.1: Mitochondrial genetic dynamics model

In Chapter 4, we presented the mitochondrial genetic dynamics simulation model of mtDNA heteroplasmy variation due to the random processes of relaxed mtDNA replication, mtDNA degradation, mtDNA segregation during cell divisions, and cell death in a population of cells. By applying the mitochondrial genetic dynamics model to the hematopoietic stem cell system, we illustrated a powerful way of analyzing clinical data. Based on this analysis, we hypothesize that the decay of mtDNA heteroplasmy in blood is exponential, and not linear as reported in earlier literature. A clinically relevant result from the study was that the blood heteroplasmy measurements are a good approximation of the blood stem cell heteroplasmy. We propose for the first time, a way to correct for the age in the analysis of heteroplasmy data. We conclude from the simulation study that random genetic drift and selection at the cellular level explain the clonal expansion of mtDNA.

In Chapter 5, we developed simulation to directly model the mitochondrial genetic bottleneck during mouse embryogenesis by closely working with experimental collaborators. We demonstrated that grouped mtDNA segregation is not required to explain the genetic bottleneck. We conclude that partitioning of mtDNA into daughter cells during blastocyst formation and relaxed replication of mtDNA during the exponential growth phase of PGCs explain the variation in heteroplasmy inherited by different offspring from the same mother.

The cell culture model described in Chapter 6 is another application of the mitochondrial genetic dynamics model. The study highlights the importance of including simulation as a control in experimental design. Overall, we have contributed a novel and powerful *in silico* tool to study the mtDNA heteroplasmy variation occurring both in, *in vivo* and *in vitro* systems and also in *post-mitotic* and *proliferating* cell populations.

Mitochondrial genetic dynamics is an interesting field of research with several unsolved puzzles. We highlight some key questions to pursue as a follow up to our work. We showed that selection at the cellular level (cell loss above a certain threshold heteroplasmy) against pathogenic mtDNA mutation contributes to the exponential decay in blood heteroplasmy. Whether there is additional selection at the molecular level still remains a question. Since decay is observed mainly in blood, how do we explain the mechanisms leading to clonal expansion in post-mitotic tissues? We showed that the

decay for a specific MELAS mtDNA mutation (3243A>G) is exponential. Does the exponential decay apply to all mtDNA point substitution mutations? We addressed this question partially and showed that it does not apply to low penetrance mutations (LHON).

The genetic dynamics model described in this dissertation is focused around inherited mtDNA mutations and not acquired mtDNA mutations. We do know that mtDNA acquire new somatic mutations due to various DNA replication errors. One of the factors affecting the accuracy of mtDNA replication is the DNA precursor pool asymmetry [269]. Acquired mtDNA mutations have been observed in the muscle tissue of older humans [270-274]. Samuels, *et al.* [275] have previously simulated this process in post-mitotic cells and in the stem cells for colon crypts [276]. The basic idea here is, during each mtDNA replication event, there is a small probability of mtDNA acquiring new mutation(s). This can be easily incorporated into our current simulation by adding a Poisson process to the replication subroutine, to calculate the number of acquired mtDNA mutants during each time-step. Comparison of Samuels, *et al.* [277-279] previous models with experimental data indicates that a mutation probability of approximately 5×10^{-5} per replication reproduces the clonal expansion behavior seen in reality. Alternatively, acquired mtDNA mutations are independent of the replication mechanism. In this case, we will need to model the rate of acquiring a mutation by a constant rate instead of basing it on the replication rate. We will have to make a choice between the two models if we choose to pursue the study of acquired mutations.

With a genetic dynamics model for acquired mutations, we can ask the question, given the probabilities of occurrences of all known pathogenic mtDNA mutations, what is the probability of a mitochondrial disease occurring in an individual? in a population? We can then conduct population genetic studies on the rates at which these diseases are occurring in a particular geographic/ethnic group. Results from the stem cell model and the mouse embryo model have direct application to genetic counseling to elderly citizens and pregnant women on their risks of acquiring or passing on mtDNA diseases to offspring. Hence, enhancing our genetic dynamics model to study the effects of acquired mtDNA mutations is a valuable direction to pursue.

8.2 Section 8.2: Mitochondrial morphologic dynamics model

The mitochondrial morphologic dynamics model (Chapter 7) reveals that the cell's options in controlling mitochondrial morphology and function. We propose that the cell has the ability to adjust the rate of fusion to the independently changing rates of fission. We have proposed a simple deterministic model for the cell's balance between mitochondrial fusion and fission events.

The morphologic dynamics model described here has the potential and flexibility to be enhanced for further study of the mitochondrial morphology and its role in

apoptosis. In particular, we can extend the model to include mitochondrial damage and lysosomal degradation to study the feasibility of the *lysosomal-axis theory of ageing*. Because mitochondrial fission and fusion require mitochondrial inner membrane potential, we can add the inner membrane polarization state (polarized or depolarized). This may result in failed attempts of fission and fusion, since depolarized mitochondria cannot undergo these events. Study of the mitochondrial morphology changes, during different phases of the cell cycle is an exciting direction to pursue. Being able to simulate the effects of knocking out various proteins involved in fission and fusion (in terms of how each protein affects the probability of success of an attempted fusion or fission) would be a good goal to pursue.

Finally, the grand challenge is to integrate the mitochondrial genetic and morphologic dynamics model to study the combined effects at increasing levels of abstraction from molecular, cellular, tissue, organ, organism, up to population level.

References

1.	Dimauro, S. and M. Hirano, *Mitochondrial encephalomyopathies: an update.* Neuromuscular disorders 2005. **15**: p. 276-286.
2.	Nicholls, D., *Mitochondrial function and dysfunction in the cell: its relevance to aging and aging-related disease.* The International Journal of Biochemistry and Cell Biology, 2002. **34**: p. 1372-1381.
3.	Reichert, A. and W. Neupert, *Contact site between the outer and inner membrane of mitochondria - role in protein transport.* Biochimica et Biophysica Acta, 2002. **1592**: p. 41-49.
4.	Perkins, G. and T. Frey, *Recent structural insight into mitochondria gained by microscopy.* Micron, 2000. **31**: p. 97-111.
5.	Scheffler, I., *A century of mitochondrial research: achievements and perspectives.* Mitochondrion, 2001. **1**: p. 3-31.
6.	Dimauro, S. and G. Davidzon, *Mitochondrial DNA and disease.* Annals of Medicine, 2005. **37**: p. 222-232.
7.	Kroon, A. and C. Bogart, *Biogenesis of mitochondria and genetics of mitochondrial defects.* J Inherit Metab Dis., 1987. **10**(1): p. 54-61.
8.	Nass, S. and M. Nass, *Ultramitochondrial fibers with DNA characteristics.* J. Cell Biol., 1963. **19**: p. 593-629.
9.	Woodward, D. and K. Munkers, *Alterations of a maternally inherited mitochondrial structural protein in respiratory-deficient strains of neurospora.* PNAS, 1966. **55**: p. 872-880.
10.	Lightowlers, R., et al., *Mammalian mitochondrial genetics: heredity, heteroplasmy, and disease.* Trends Genet., 1997. **13**: p. 450-455.
11.	Poulton, J.a.M., DR, *Segregation of mitochondria DNA (mtDNA) in human oocytes and in animal models of mtDNA disease: clinical implications.* Reproduction, 2002. **123**: p. 751-755.
12.	Gray, M.W., *The evolutionary origins of organelles.* Trends Genet, 1989. **5**(9): p. 294-9.
13.	Anderson, S., et al., *Sequence and organization of the human mitochondrial genome.* Nature, 1981. **290**: p. 457-465.
14.	Samuels, D., et al., *A compositional segmentation of the human mitochondrial genome is related to heterogeneities in the guanine mutation rate.* Nucleic Acids Research 2003. **31**(20): p. 6043-6052.
15.	Barrientos, A., L. Kenyon, and C. Moraes, *Human xenomitochondrial cybrids - cellular models of mitochondrial complex I deficiency.* J. Biol. Chem., 1998. **273**: p. 14210-14217.
16.	Kenyon, L. and C. Moraes, *Expanding the functional human mitochondrial DNA database by the establishment of primate xenomitochondrial cybrids.* PNAS, 1997. **94**: p. 9131-9135.
17.	Moraes, C., L. Kenyon, and H. Hao, *Mechanisms of Human Mitochondrial DNA Maintenance: The Determining Role of Primary Sequence and Length over Function.* Molecular Biology of the Cell, 1999. **10**: p. 3345-3356.

18. Diaz, F., et al., *Human mitochondrial DNA with large deletions repopulates organelles faster than full-length genomes under relaxed copy number control.* Nucleic Acids Research, 2002. **30**(21): p. 4626-4633.

19. Moraes, C., *What regulates mitochondrial DNA copy number in animal cells?* TRENDS in Genetics, 2001. **17**(4): p. 199-205.

20. Graziewicz, M.A., M.J. Longley, and W.C. Copeland, *DNA Polymerase γamma in Mitochondrial DNA Replication and Repair.* Chemical Review, 2006. **106**: p. 383-405.

21. MITOMAP, *A Human Mitochondrial Genome Database.* www.mitomap.org, 2007.

22. *Map of the Human Mitochondrial DNA.* www.mitomap.org, 2005.

23. Kujoth, G., et al., *Mitochondrial DNA Mutations, Oxidative Stress, and Apoptosis in Mammalian Aging.* SCIENCE, 2005. **309**: p. 481-484.

24. *Mitochondrial encephalomyopathies: gene mutation.* Neuromuscular disorders, 2004. **14**(1): p. 107-116.

25. Miller, R., et al., *Evaluating Evidence of Aging.* SCIENCE LETTERS, 2005. **310**: p. 441.

26. Prolla, T. and R. Weindruch, *Evaluating Evidence for Aging.* SCIENCE, 2005. **310**: p. 441-443.

27. Smith, L.B., V Couto, MM Garcia, SM Yamazaki, W Meirelles, FV, *Mitochondrial genotype segregation and the bottleneck.* Reproductive BioMedicine online, 2002. **4**(3): p. 248-255.

28. Lightowlers, R.N., et al., *Mammalian mitochondrial genetics: heredity, heteroplasmy and disease.* Trends Genet, 1997. **13**(11): p. 450-5.

29. Chuenkongkaew, W.S., R, Vaeusorn, L Phasukkijwatana, N Lertrit, P and Suktitipat, B, *Proportion of 11778 Mutant Mitochondrial DNA and Clinical Expression in a Thai Population With Leber Hereditary Optic Neuropathy.* J Neuroophthalmol, 2005. **25**(3): p. 173-5.

30. Dunbar, D., et al., *Complex I deficiency is associated with 3243G:C mitochondrial DNA in osteosarcoma cell cybrids.* Human Molecular Genetics, 1996. **5**(1): p. 123-129.

31. Lynn, S., et al., *Heteroplasmic ratio of the A3243G mitochondrial DNA mutation in single pancreatic beta cells.* Diabetologia 2003. **46**: p. 296-299.

32. Moslemi, A.-R., et al., *Threshold expression of the tRNA^{Lys} A8344G mutation in single muscle fibres.* Neuromuscular disorders, 1998. **8**: p. 345-349.

33. Rahman, S.P., J Marchington, D and Suomalainen, A *Decrease of 3243 A->G mtDNA Mutation from Blood in MELAS Syndrome: A Longitudinal Study.* American Journal of Human Genetics, 2001. **68**: p. 238-240.

34. Tesarova, M., et al., *Variation in manifestations of heteroplasmic mtDNA mutation 8993 T>G in two families.* Cas Lek Cesk, 2002. **141**(17): p. 551-4.

35. Rossignol, R., et al., *Threshold effect and tissue specificity - Implication for mitochondrial cytopathies.* Journal Of Biological Chemistry, 1999. **274**(47): p. 33426-33432.

36. Chinnery, P.F., et al., *The epidemiology of pathogenic mitochondrial DNA mutations.* Annals Of Neurology, 2000. **48**(2): p. 188-193.

37.   Majamaa, K., et al., *Epidemiology of A3243G, the mutation for mitochondrial encephalomyopathy, lactic acidosis, and strokelike episodes: Prevalence of the mutation in an adult population.* American Journal Of Human Genetics, 1998. **63**(2): p. 447-454.

38.   Cock, H., J. Cooper, and A. Schapira, *Functional consequences of the 3460-bp mitochondrial DNA mutation associated with Leber's hereditary optic neuropathy.* Journal of the Neurological Sciences, 1999. **165**: p. 10-17.

39.   Smith KH, J.D., Heher KL, *Heteroplasmy in Leber's hereditary optic neuropathy.* Arch Ophthalmol 1993. **111**: p. 1486-1490.

40.   Barron, M.J., et al., *Cytochrome c oxidase deficient muscle fibres: Substantial variation in their proportions within skeletal muscles from patients with mitochondrial myopathy.* Neuromuscular Disorders, 2005. **15**(11): p. 768-774.

41.   Elson, J.L., et al., *The length of cytochrome c oxidase-negative segments in muscle fibres in patients with mtDNA myopathy.* Neuromuscular Disorders, 2002. **12**(9): p. 858-864.

42.   Shoubridge, E.A., *Mitochondrial-DNA diseases - Histological and cellular studies.* Journal Of Bioenergetics And Biomembranes, 1994. **26**(3): p. 301-310.

43.   Chinnery, P. and D. Samuels, *Relaxed Replication of mtDNA: A Model with Implications for the Expression of Disease.* American Journal of Human Genetics, 1999. **64**: p. 1158-1165.

44.   Frederiksen, A.L., et al., *Tissue specific distribution of the 3243A -> G mtDNA mutation.* Journal Of Medical Genetics, 2006. **43**(8).

45.   Kirches, E., et al., *Heterogeneous tissue distribution of a mitochondrial DNA polymorphism in heteroplasmic subjects without mitochondrial disorders.* Journal Of Medical Genetics, 2001. **38**(5): p. 312-317.

46.   Rossignol, R., et al., *Tissue variation in the control of oxidative phosphorylation: implication for mitochondrial diseases.* Biochemical Journal, 2000. **347**: p. 45-53.

47.   Chinnery, P.F., et al., *Nonrandom tissue distribution of mutant mtDNA.* American Journal Of Medical Genetics, 1999. **85**(5): p. 498-501.

48.   Dahl, H.H., D.R. thorburn, and S.L. White, *Towards reliable prenatal diagnosis of mtDNA point mutations: studies of nt8993 mutations in oocytes, fetal tissues, children and adults.* Hum Reprod, 2000. **15**(Suppl. 2): p. 246-255.

49.   Attardi, G., *Role of mitochondrial DNA in human aging.* Mitochondrion, 2002. **2**: p. 27-37.

50.   Orrenius, S., *Reactive Oxygen Species in Mitochondria-Mediated Cell Death.* Drug Metabolism Reviews, 2007. **39**(2): p. 443-455.

51.   Durham, S.E., D.C. Samuels, and P.F. Chinnery, *Is selection required for the accumulation of somatic mitochondrial DNA mutations in post-mitotic cells?* Neuromuscular Disorders, 2006. **16**(6): p. 381-386.

52.   Yaffe, M., *Dynamic mitochondria.* NATURE CELL BIOLOGY, 1999. **1**(October): p. E149-E150.

53.   Bereiter-Hahn, J. and M. Voth, *Dynamics of mitochondria in living cells: shape changes, dislocations, fusion and fission of mitochondria.* Microsocopy Research and Technique, 1994. **27**: p. 198-219.

54.   Hermann, G. and J. Shaw, *Mitochondrial Dynamics in Yeast.* Annual review of cell developmental biology, 1998. **14**: p. 265-303.

55.   Jendrach, M., et al., *Morpho-dynamic changes of mitochondria during aging of human endothelial cells.* Mechanims of aging and development 2005. **126**(813-821).

56.   Jensen, R., et al., *Yeast Mitochondrial Dynamics: Fusion, Division, Segregation, and Shape.* Microsocopy Research and Technique, 2000. **51**: p. 573-583.

57.   Legros, F., et al., *Mitochondrial Fusion in Human Cells Is Efficient, Requires the Inner Membrane Potential, and Is Mediated by Mitofusins.* Molecular Biology of the Cell, 2002. **13**: p. 4343-4354.

58.   Polyakov, V.S., MY Fais, D, *Fusion, Fragmentation, and Fission of Mitochondria.* Biochemistry, 2003. **68**(8): p. 838-849.

59.   Rube, D. and A. Bliek, *Mitochondrial morphology is dynamic and varied.* Molecular and Cellular Biochemistry 2004: p. 331-339.

60.   Shaw, J. and J. Nunnari, *Mitochondrial dynamics and division in budding yeast.* Trends in cell biology, 2002. **12**(4): p. 178-184.

61.   Westermann, B., *Mitochondrial membrane fusion.* Biochimica et Biophysica Acta 2003: p. 195-202.

62.   Logan, D., *Mitochondrial dynamics.* New Phytologist, 2003. **160**: p. 463-478.

63.   Simon, V., S. Karmon, and L. Pon, *Mitochondrial Inheritance: Cell Cycle and Actin Cable Dependence of Polarized Mitochondrial Movements in Saccharomyces cerevisiae.* Cell Motility and the Cytoskeleton, 1997. **37**: p. 199-210.

64.   Knowles, M., et al., *Cytoskeletal-assisted dynamics of the mitochondrial reticulum in living cells.* PNAS, 2002. **99**(23): p. 14772-14777.

65.   Bereiter-Hahn, J. and M. Voth, *Dynamics of mitochondria in living cells: shape changes, dislocations, fusion, and fission of mitochondria.* Microsc Res Tech, 1994. **27**(3): p. 198-219.

66.   Sazer, S. and S.W. Sherwood, *Mitochondrial growth and DNA synthesis occur in the absense of nuclear DNA replication in fission yeast.* Journal Of Cell Science, 1990. **97**(Pt 3): p. 509-516.

67.   Margineantu, D., et al., *Cell cycle dependent morphology changes and associated mitochondrial DNA redistribution in mitochondria of human cell lines.* Mitochondrion, 2002. **1**: p. 425-435.

68.   Arakaki, N., et al., *Dynamics of Mitochondria during the Cell Cycle.* Biol. Pharm. Bull., 2006. **29**(9): p. 1962-1965.

69.   Margineantu, D.H., et al., *Cell cycle dependent morphology changes and associated mitochondrial DNA redistribution in mitochondria of human cell lines.* Mitochondrion, 2002. **1**(5): p. 425-435.

70.   Jensen, R.E., et al., *Yeast mitochondrial dynamics: fusion, division, segregation, and shape.* Microsc Res Tech, 2000. **51**(6): p. 573-83.

71.   Brocard J.B, Rintoul G.L, and Reynolds I.J, *New perspectives on mitochondrial morphology in cell function.* Biology of the Cell, 2003. **95**(5): p. 239-242.

72.   Martinelli, C., et al., *Age-related quantitative changes in mitochondria of satellite cell sheaths enveloping spinal ganglion neurons in the rabbit.* Brain Res Bull, 2003. **61**(2): p. 147-51.

73.   Martinelli, C., et al., *A study of mitochondria in spinal ganglion neurons during life: quantitative changes from youth to extremely advanced age.* Tissue Cell, 2006. **38**(2): p. 93-8.
74.   Ledda, M., C. Martinelli, and E. Pannese, *Quantitative changes in mitochondria of spinal ganglion neurons in aged rabbits.* Brain Res Bull, 2001. **54**(4): p. 455-9.
75.   Terman, A., et al., *Mitochondrial recycling and aging of cardiac myocytes: the role of autophagocytosis.* Exp Gerontol, 2003. **38**(8): p. 863-76.
76.   Meeusen, S., J.M. McCaffery, and J. Nunnari, *Mitochondrial fusion intermediates revealed in vitro.* Science, 2004. **305**(5691): p. 1747-1752.
77.   Meeusen, S.L. and J. Nunnari, *How mitochondria fuse.* Curr Opin Cell Biol, 2005. **17**(4): p. 389-94.
78.   De Giorgi, F., L. Lartigue, and F. Ichas, *Electrical coupling and plasticity of the mitochondrial network.* Cell Calcium, 2000. **28**(5/6): p. 365-370.
79.   Twig, G., et al., *Tagging and tracking individual networks within a complex mitochondrial web with photoactivatable GFP.* American Journal Of Physiology-Cell Physiology, 2006. **291**(1): p. C176-C184.
80.   Griparic L. and Bliek A.M, *The Many Shapes of Mitochondrial Membranes.* Traffic, 2001. **2**: p. 235-244.
81.   Yaffe MP, *The machinery of mitochondrial inheritance and behavior.* SCIENCE, 1999. **283**: p. 1493-1497.
82.   Anesti V and Scorrano L, *The relationship between mitochondrial shape and function and the cytoskeleton.* Biochemica et Biophysica Acta, 2006. **1757**: p. 692-699.
83.   Hayashi, J.I., et al., *Human mitochondria and mitochondrial genome function as a single dynamic cellular unit.* The journal of cell biology, 1994. **125**(1): p. 43-50.
84.   Hermann, G.J. and J.M. Shaw, *Mitochondrial dynamics in yeast.* Annu Rev Cell Dev Biol, 1998. **14**: p. 265-303.
85.   Chen H and Chan D.C., *Critical dependence of neurons on mitochondrial dynamics.* Current Opions in Cell Biology, 2006. **18**: p. 453-459.
86.   Dimmer KS and Westermann B, *Solo or networked, mitochondria lead a complex life.* The ELSO Gazette, 2002(11): p. 3.
87.   Ratinaud, M.H. and R. Julien, *Variation of cellular mitochondrial activity in culture: analysis by flow cytometry.* Biol Cell, 1986. **58**(2): p. 169-172.
88.   Chen, H.C., et al., *Mitofusins Mfn1 and Mfn2 coordinately regulate mitochondrial fusion and are essential for embryonic development.* Journal Of Cell Biology, 2003. **160**(2): p. 189-200.
89.   Terman, A. and U.T. Brunk, *The aging myocardium: roles of mitochondrial damage and lysosomal degradation.* Heart Lung Circ, 2005. **14**(2): p. 107-14.
90.   Brunk, U.T. and A. Terman, *The mitochondrial-lysosomal axis theory of aging: accumulation of damaged mitochondria as a result of imperfect autophagocytosis.* Eur J Biochem, 2002. **269**(8): p. 1996-2002.
91.   Terman, A. and U.T. Brunk, *Oxidative stress, accumulation of biological 'garbage', and aging.* Antioxid Redox Signal, 2006. **8**(1-2): p. 197-204.
92.   Griffin E.E., Detmer S.A., and Chan D. C., *Molecular mechanism of mitochondrial membrane fusion.* Biochemica et Biophysica Acta, 2006. **1763**: p. 482-489.

93. Chan, D.C., *Mitochondria: dynamic organelles in disease, aging, and development.* Cell, 2006. **125**(7): p. 1241-52.

94. Chen, H. and D.C. Chan, *Emerging functions of mammalian mitochondrial fusion and fission.* Hum Mol Genet, 2005. **14 Spec No. 2**: p. R283-9.

95. Yang, H.-C., et al., *A rentention mechanism for distribution of mitochondria during cell division in budding yeast.* Current Biology, 1999. **9**: p. 1111-1114.

96. Hales, K.G., *The machinery of mitochondrial fusion, division, and distribution, and emerging connections to apoptosis.* Mitochondrion, 2004. **4**(4): p. 285-308.

97. Jendrach, M., et al., *Morpho-dynamic changes of mitochondria during ageing of human endothelial cells.* Mechanisms Of Ageing And Development, 2005. **126**(6-7): p. 813-821.

98. Savitha, S. and C. Panneerselvam, *Mitochondrial membrane damage during aging process in rat heart: Potential efficacy of L-carnitine and DL alpha lipoic acid.* Mechanisms Of Ageing And Development, 2006. **127**(4): p. 349-355.

99. Wong, Y.T., R.S. Ruan, and F.E.H. Tay, *Relationship between levels of oxidative DNA damage, lipid peroxidation and mitochondrial membrane potential in young and old F344 rats.* Free Radical Research, 2006. **40**(4): p. 393-402.

100. Lopes, G.S., et al., *Mitochondrial alterations and apoptosis in smooth muscle from aged rats.* Biochimica Et Biophysica Acta-Bioenergetics, 2004. **1658**(3): p. 187-194.

101. Pham, N.A., et al., *Altered mitochondrial structure and motion dynamics in living cells with energy metabolism defects revealed by real time microscope imaging.* Microscopy And Microanalysis, 2004. **10**(2): p. 247-260.

102. Bertoni-Freddari, C., et al., *A morphometric study on human muscle mitochondria in aging.* Journal Of The American Aging Association, 2002. **25**(2): p. 101-105.

103. Toescu, E.C., N. Myronova, and A. Verkhratsky, *Age-related structural and functional changes of brain mitochondria.* Cell Calcium, 2000. **28**(5-6): p. 329-338.

104. Bertonifreddari, C., et al., *Morphological Plasticity Of Synaptic Mitochondria During Aging.* Brain Research, 1993. **628**(1-2): p. 193-200.

105. Pieri, C., R. Recchioni, and F. Moroni, *Age-Dependent Modifications Of Mitochondrial Trans-Membrane Potential And Mass In Rat Splenic Lymphocytes During Proliferation.* Mechanisms Of Ageing And Development, 1993. **70**(3): p. 201-212.

106. Drew, B. and C. Leeuwenburgh, *Ageing and subcellular distribution of mitochondria: role of mitochondrial DNA deletions and energy production.* Acta Physiologica Scandinavica, 2004. **182**(4): p. 333-341.

107. Zhang, Y.P. and B. Herman, *Ageing and apoptosis.* Mechanisms Of Ageing And Development, 2002. **123**(4): p. 245-260.

108. Sastre, J., F.V. Pallardo, and J. Vina, *Mitochondrial oxidative stress plays a key role in aging and apoptosis.* Iubmb Life, 2000. **49**(5): p. 427-435.

109. Terman, A., B. Gustafsson, and U.T. Brunk, *The lysosomal-mitochondrial axis theory of postmitotic aging and cell death.* Chem Biol Interact, 2006.

110. Stroikin, Y., et al., *Testing the "garbage" accumulation theory of ageing: mitotic activity protects cells from death induced by inhibition of autophagy.* Biogerontology, 2005. **6**(1): p. 39-47.

111. Jendrach, M., et al., *Morpho-dynamic changes of mitochondria during ageing of human endothelial cells.* Mechanims of ageing and development 2005. **126**(813-821).

112. Yoon, Y., *Sharpening the scissors - mitochondrial fission with aid.* Cell biochemistry and biophysics 2004: p. 193-205.

113. Fannjiang, Y., et al., *Mitochondrial fission proteins regulate programmed cell death in yeast.* Genes & Development, 2004. **18**(22): p. 2785-2797.

114. Lee, Y.J., et al., *Roles of the mammalian mitochondrial fission and fusion mediators Fis1, Drp1, and Opa1 in apoptosis.* Molecular Biology Of The Cell, 2004. **15**(11): p. 5001-5011.

115. James, D.I., et al., *hFis1, a novel component of the mammalian mitochondrial fission machinery.* Journal Of Biological Chemistry, 2003. **278**(38): p. 36373-36379.

116. Hales, K., *The machinery of mitochondrial fusion, division, and distribution, and emerging connections to apoptosis.* Mitochondrion, 2004. **4**: p. 285-308.

117. Frank, S., et al., *The Role of Dynamin-Related Protein 1, a Mediator of Mitochondrial Fission, in Apoptosis.* Developmental Cell, 2001. **1**: p. 515-525.

118. Labrousse, A., et al., *C. elegans Dynamin-Related Protein DRP-1 Controls Severing of the Mitochondrial Outer Membrane.* Molecular Cell, 1999. **4**(November): p. 815-826.

119. De Vos, K., et al., *Mitochondrial Function and Actin Regulate Dynamin-Related Protein 1-Dependent Mitochondrial Fission.* Current Biology, 2005. **15**: p. 678-683.

120. Mozdy, A. and J. Shaw, *A fuzzy mitochondrial fusion apparatus comes into focus.* Nature Molecular Cell Biology 2003: p. 468-478.

121. Heath-Engel, H.M. and G.C. Shore, *Mitochondrial membrane dynamics, cristae remodelling and apoptosis.* Biochim Biophys Acta, 2006. **1763**(5-6): p. 549-60.

122. Karbowski, M. and R. Youle, *Dynamics of mitochondrial morphology in healthy cells and during apoptosis.* Cell Death and Differentiation 2003: p. 870-880.

123. Oakes, S. and S. Korsmeyer, *Untangling the web: mitochondrial fission and apoptosis.* Developmental Cell, 2005: p. 460-462.

124. Ly, J., D. Grubb, and A. Lawen, *The mitochondrial membrane potential in apoptosis; an update.* Apoptosis, 2003. **8**: p. 115-128.

125. Scorrano, L., *Proteins That Fuse and Fragment Mitochondria in Apoptosis: Con-Fissing a Deadly Con-Fusion?* Journal of Bioenergetics and Biomembranes, 2005. **37**(3): p. 165-170.

126. Mignotte B and Vayssiere J-L, *Mitochondria and apoptosis.* Eur J Biochem, 1998. **252**: p. 1-15.

127. Bossy-Wetzel, E., et al., *Mitochondrial fission in apoptosis, neurodegeneration and aging.* Current Opinion In Cell Biology, 2003. **15**(6): p. 706-716.

128. Krysko, D.V., et al., *Mitochondrial transmembrane potential changes support the concept of mitochondrial heterogeneity during apoptosis.* Journal Of Histochemistry & Cytochemistry, 2001. **49**(10): p. 1277-1284.

129. Youle, R.J. and M. Karbowski, *Mitochondrial fission in apoptosis.* Nature Reviews Molecular Cell Biology, 2005. **6**(8): p. 657-663.

130. Wesche, D.E., et al., *Leukocyte apoptosis and its significance in sepsis and shock.* Journal Of Leukocyte Biology, 2005. **78**(2): p. 325-337.

131. Perfettini, J.L., et al., *Mechanisms of apoptosis induction by the HIV-1 envelope.* Cell Death And Differentiation, 2005. **12**: p. 916-923.

132. van Empel, V.P.M., et al., *Myocyte apoptosis in heart failure.* Cardiovascular Research, 2005. **67**(1): p. 21-29.

133. Perfettini, J.L., T. Roumier, and G. Kroemer, *Mitochondrial fusion and fission in the control of apoptosis.* Trends In Cell Biology, 2005. **15**(4): p. 179-183.

134. Goldstein, J.C., et al., *Cytochrome c is released in a single step during apoptosis.* Cell Death And Differentiation, 2005. **12**(5): p. 453-462.

135. Youle, R.J., *Morphology of mitochondria during apoptosis: Worms-to-beetles in worms.* Developmental Cell, 2005. **8**(3): p. 298-299.

136. Sugioka, R., S. Shimizu, and Y. Tsujimoto, *Fzo1, a protein involved in mitochondrial fusion, inhibits apoptosis.* Journal Of Biological Chemistry, 2004. **279**(50): p. 52726-52734.

137. Crow, M.T., et al., *The mitochondrial death pathway and cardiac myocyte apoptosis.* Circulation Research, 2004. **95**(10): p. 957-970.

138. Eliseev, R.A., et al., *Diazoxide-mediated preconditioning against apoptosis involves activation of cAMP-response element-binding protein (CREB) and NF kappa B.* Journal Of Biological Chemistry, 2004. **279**(45): p. 46748-46754.

139. Oakes, S.A. and S.J. Korsmeyer, *Untangling the web: Mitochondrial fission and apoptosis.* Developmental Cell, 2004. **7**(4): p. 460-462.

140. Szabadkai, G., et al., *Drp-1-dependent division of the mitochondrial network blocks intraorganellar Ca2+ waves and protects against Ca2+-mediated apoptosis.* Molecular Cell, 2004. **16**(1): p. 59-68.

141. Kluza, J., et al., *Mitochondrial proliferation during apoptosis induced by anticancer agents: effects of doxorubicin and mitoxantrone on cancer and cardiac cells.* Oncogene, 2004. **23**(42): p. 7018-7030.

142. Tondera, D., et al., *Knockdown of MTP18, a novel phosphatidylinositol 3-kinase-dependent protein, affects mitochondrial morphology and induces apoptosis.* Journal Of Biological Chemistry, 2004. **279**(30): p. 31544-31555.

143. Lyamzaev, K.G., et al., *Inhibition of mitochondrial bioenergetics: the effects on structure of mitochondria in the cell and on apoptosis.* Acta Biochimica Polonica, 2004. **51**(2): p. 553-562.

144. Liu, C.Y., et al., *Mitochondrial DNA mutation and depletion increase the susceptibility of human cells to apoptosis*, in *Mitochondrial Pathogenesis: From Genes And Apoptosis To Aging And Disease*. 2004, New York Acad Sciences: New York. p. 133-145.

145. Karbowski, M., et al., *Quantitation of mitochondrial dynamics by photolabeling of individual organelles shows that mitochondrial fusion is blocked during the Bax activation phase of apoptosis.* Journal Of Cell Biology, 2004. **164**(4): p. 493-499.

146. Iverson, S.L. and S. Orrenius, *The cardiolipin-cytochromet c interaction and the mitochondrial regulation of apoptosis.* Archives Of Biochemistry And Biophysics, 2004. **423**(1): p. 37-46.

147. Skulachev, V.P., et al., *Thread-grain transition of mitochondrial reticulum as a step of mitoptosis and apoptosis.* Molecular And Cellular Biochemistry, 2004. **256**(1-2): p. 341-358.

148. Hu, Z.H. and M.M. Sayeed, *Suppression of mitochondria-dependent neutrophil apoptosis with thermal injury.* American Journal Of Physiology-Cell Physiology, 2004. **286**(1): p. C170-C178.

149. Kim, W.K. and P.E. Mirkes, *Alterations in mitochondrial morphology are associated with hyperthermia-induced apoptosis in early postimplantation mouse embryos.* Birth Defects Research Part A-Clinical And Molecular Teratology, 2003. **67**(11): p. 929-940.

150. Sovova, V., et al., *Alterations in mitochondria function and morphology in HT29 cells upon conditions inducing differentiation and apoptosis.* International Journal Of Oncology, 2003. **23**(6): p. 1755-1760.

151. Scorrano, L., *Divide et impera: Ca2+ signals, mitochondrial fission and sensitization to apoptosis.* Cell Death And Differentiation, 2003. **10**(12): p. 1287-1289.

152. Haga, N., N. Fujita, and T. Tsuruo, *Mitochondrial aggregation precedes cytochrome c 1release from mitochondria during apoptosis.* Oncogene, 2003. **22**(36): p. 5579-5585.

153. Kerkweg, U., et al., *Cold-induced apoptosis of rat liver endothelial cells: Contribution of mitochondrial alterations.* Transplantation, 2003. **76**(3): p. 501-508.

154. Lum, M.G. and P. Nagley, *Two phases of signalling between mitochondria during apoptosis leading to early depolarisation and delayed cytochrome c release.* Journal Of Cell Science, 2003. **116**(8): p. 1437-1447.

155. Dussmann, H., et al., *Mitochondrial membrane permeabilization and superoxide production during apoptosis - A single-cell analysis.* Journal Of Biological Chemistry, 2003. **278**(15): p. 12645-12649.

156. Olichon, A., et al., *Loss of OPA1 perturbates the mitochondrial inner membrane structure and integrity, leading to cytochrome c release and apoptosis.* Journal Of Biological Chemistry, 2003. **278**(10): p. 7743-7746.

157. Tolomeo, M., et al., *Mitochondrial disruption and apoptosis in lymphocytes of an HIV infected patient affected-by lactic acidosis after treatment with highly active antiretroviral therapy.* Journal Of Clinical Pathology, 2003. **56**(2): p. 147-151.

158. Karbowski, M., et al., *Spatial and temporal association of Bax with mitochondrial fission sites, Drp1, and Mfn2 during apoptosis.* Journal Of Cell Biology, 2002. **159**(6): p. 931-938.

159. McCormick, A.L., et al., *Disruption of mitochondrial networks by the human cytomegalovirus UL37 gene product viral mitochondrion-localized inhibitor of apoptosis.* Journal Of Virology, 2003. **77**(1): p. 631-641.

160. Pollack, M., et al., *The role of apoptosis in the normal aging brain, skeletal muscle, and heart*, in *Increasing Healthy Life Span: Conventional Measures And Slowing The Innate Aging Process*. 2002, New York Acad Sciences: New York. p. 93-107.

161. Frank, S., et al., *The role of dynamin-related protein 1, a mediator of mitochondrial fission, in apoptosis.* Developmental Cell, 2001. **1**(4): p. 515-525.

162.	Pollack, M. and C. Leeuwenburgh, *Apoptosis and aging: Role of the mitochondria.* Journals Of Gerontology Series A-Biological Sciences And Medical Sciences, 2001. **56**(11): p. B475-B482.

163.	Jagasia, R., et al., *DRP-1-mediated mitochondrial fragmentation during EGL-1-induced cell death in C. elegans.* letters to nature, 2005. **433**: p. 754-760.

164.	Szabadkai, G.S., AM Chami, M Wieckowski, MR Youle, RJ and Rizzuto, R, *Drp-1-Dependent Division of the Mitochondrial Network Blocks Intraorganellar Ca2+ Waves and Protects against Ca2+ - Mediated Apoptosis.* Molecular Cell, 2004. **16**: p. 59-68.

165.	Youle, R., *Morphology of mitochondria during apoptosis: worms-to-beetles in worms.* Developmental Cell, 2005: p. 298-299.

166.	Youle, R. and M. Karbowski, *Mitochondrial fission in apoptosis.* Nature Reviews Molecular Cell Biology, 2005. **6**: p. 657-663.

167.	Perfettini, J.-L.R., T and Kroemer, G *Mitochondrial fusion and fission in control of apoptosis.* Trends in cell biology 2005. **15**(4): p. 179-183.

168.	Shaw, J.M. and J. Nunnari, *Mitochondrial dynamics and division in budding yeast.* Trends Cell Biol, 2002. **12**(4): p. 178-84.

169.	Peck, S.L., *Simulation as an experiment: a philosophical reassesment for biological modeling.* TRENDS in Ecology and Evolution, 2004. **19**(10): p. 530-534.

170.	Breward, C., H. Byrne, and V. Lewis, *A Multiphase Model Describing Vascular Tumor Growth.* Bulletin of Mathematical Biology, 2003. **65**: p. 609-640.

171.	Colijn, C. and M.C. Mackey, *A mathematical model of hematopoiesis - I. Periodic chronic myelogenous leukemia.* Journal Of Theoretical Biology, 2005. **237**(2): p. 117-132.

172.	Takahashi, K.y., K Hashimoto, K Yamada, Y Pickett, CJF and Tomita, M, *Computational Challenges in Cell Simulation: A Software Engineering Approach.* IEEE Intelligent Systems, 2002(September/October): p. 64-71.

173.	Djafarzadeh, R., G. Wainer, and T. Mussivand, *DEVS Modeling and Simulation of the Cellular Metabolism by Mitochondria.* 2005: p. 8.

174.	Tyson, J., A. Csikasz-Nagy, and B. Novak, *The dynamics of cell cycle regulation.* Bioessays, 2002. **24**(12): p. 1095-1109.

175.	Novak, B., et al., *Mathematical model of the cell division cycle of fission yeast.* Chaos, 2001. **11**(1): p. 277-286.

176.	Sveiczer, A., J. Tyson, and B. Novak, *Modelling the fission yeast cell cycle.* Brief Funct Genomic Proteomic., 2004. **2**(4): p. 298-307.

177.	Zeigler, B., T. Kim, and H. Praehofer, *Theory of Modeling and Simulation.* Academic Press, 2000.

178.	Coller, H., et al., *High frequency of homoplasmic mitochondrial DNA mutations in human tumors can be explained without selection.* Nature Genetics, 2001. **28**: p. 147-150.

179.	Coller, H., et al., *Clustering of mutant mitochondrial DNA copies suggests stem cells are common in human bronchial epithelium.* Mutation Research, 2005. **578**: p. 256-271.

180. Reder, C., *Mutated mtDNA distribution in exponentially growing cell cultures and how the segregation rate is increased by the mitochondrial compartments.* Acta Biotheoretica, 2001. **49**: p. 235-245.
181. Aimar-Beurton, M., et al., *Virtual mitochondria: metabolic modelling and control.* DRAFT, 2005.
182. Takahashi, K., et al., *E-CELL System Version 3: A Software Platform for Integrative Computational Biology.* Genome Informatics, 2003. **14**: p. 294-295.
183. Yugi, K. and M. Tomita, *A general computational model of mitochondrial metabolism in a whole organelle scale.* Bioinformatics, 2004. **20**(11): p. 1795-6.
184. Rajasimha, H., D. Samuels, and R. Nance, *A Simulation Methodology in Modeling Cell Divisions with Stochastic Effects.* Proceedings of the Winter Simulation Conference, 2004.
185. Rajasimha, H.K., P.F. Chinnery, and D.C. Samuels, *Selection against pathogenic mtDNA mutations in a stem cell population leads to the loss of the 3243A>G mutation in blood.* American Journal of Human Genetics, 2008. **In Press**.
186. Cree, L.M., et al., *A reduction in the number of mitochondrial DNA molecules during embryogenesis explains the rapid segregation of genotypes.* Nature Genetics, 2007. **In Press**.
187. Pyle, A., et al., *Depletion of mitochondrial DNA in leucocytes harbouring the 3243A -> G mtDNA mutation.* Journal Of Medical Genetics, 2007. **44**(1): p. 69-74.
188. Rahman, S., et al., *Decrease of 3243 A-->G mtDNA mutation from blood in MELAS syndrome: A longitudinal study.* American Journal of Human Genetics, 2001. **68**: p. 238-240.
189. 't Hart, L.M., et al., *Heteroplasmy levels of a mitochondrial gene mutation associated with diabetes mellitus decrease in leucocyte DNA upon aging.* Human Mutation, 1996. **7**: p. 193-197.
190. Chinnery, P.F., et al., *The inheritance of mitochondrial DNA heteroplasmy: random drift, selection or both?* Trends In Genetics, 2000. **16**(11): p. 500-505.
191. Jenuth, J.P., et al., *Random genetic drift in the female germline explains the rapid segregation of mammalian mitochondrial DNA.* Nature Genetics, 1996. **14**(2): p. 146-151.
192. Hauswirth, W.W. and P.J. Laipis, *Rapid variation in mammalian mitochondrial genotypes: implications for the mechanism of maternal inheritance.* Mitochondrial Genes; Cold Spring Harbor Laboratory, 1982: p. 137-141.
193. Olivo, P.D., et al., *Nucleotide sequence evidence for rapid genotypic shifts in the bovine mitochondrial DNA D-loop.* Nature, 1983. **306**(5941): p. 400-2.
194. Ashley, M.V., P.J. Laipis, and W.W. Hauswirth, *Rapid segregation of heteroplasmic bovine mitochondria.* Nucleic Acids Research, 1989. **17**: p. 7325-7331.
195. Steffann, J., et al., *Analysis of mtDNA variant segregation during early human embryonic development: a tool for successful NARP preimplantation diagnosis.* Journal of medical genetics, 2005. **Online**.
196. Balci, O., *A Methodology for Certification of Modeling and Simulation Applications.* ACM Transactions on Modeling and Computer Simulation, 2001. **11**(4): p. 352-277.

197.	Sargent, R., *Some Approaches and Paradigms for Verifying and Validating Simulation Models.* Proceedings of the Winter Simulation Conference, 2001: p. 106-114.

198.	Press, W.H., et al., *Numerical Recipes in C: The Art of Scientific Computing.* 1988.

199.	Park, S. and K. Miller, Communications of the ACM, 1988. **31**: p. 1192–1201.

200.	Kopsidas, G., et al., *Tissue mitochondrial DNA changes - A stochastic system.* Molecular and cellular gerontology, 2000. **908**: p. 226-243.

201.	Balci, O., *The Implementation of Four Conceptual Frameworks for Simulation Modeling in High-Level Languages.* Proceedings of the Winter Simulation Conference, 1988: p. 287-289.

202.	Derrick, E.B., O and Nance, RE *A Comparison of Selected Conceptual Frameworks for Simulation Modeling.* Proceedings of the Winter Simulation Conference, 1989: p. 711-718.

203.	Lanza, R., et al., *Two-Volume Set with CD-ROM, Volume 1-2 : Volume 1-Embryonic Stem Cells; Volume 2-Adult & Fetal Stem Cells.* 2004.

204.	Vickers, M., et al., *Modelling haemopoietic stem cell division by analysis of mutant red cells.* British Journal of Haematology, 2000. **110**: p. 54-62.

205.	Mackey, M.C., *Cell kinetic status of haematopoietic stem cells.* Cell Proliferation, 2001. **34**(2): p. 71-83.

206.	Gross, N., G. Getz, and M. Rabinowitz, *Apparent turnover of mitochondrial deoxyribonucleic acid and mitochondrial phospholipids in the tissues of the rat.* J Biol Chem, 1969. **244**: p. 1552 - 1562.

207.	Matthews, P.M., et al., *Intracellular Heteroplasmy For Disease-Associated Point Mutations In Mtdna - Implications For Disease Expression And Evidence For Mitotic Segregation Of Heteroplasmic Units Of Mtdna.* Human Genetics, 1995. **96**(3): p. 261-268.

208.	Rossignol, R., et al., *Mitochondrial threshold effects.* Biochemical Journal, 2003. **370**: p. 751-762.

209.	Akala, O.O. and M.F. Clarke, *Hematopoietic stem cell self-renewal.* Current Opinion In Genetics & Development, 2006. **16**(5): p. 496-501.

210.	Shepherd, B.E., et al., *Estimating human hematopoietic stem cell kinetics using granulocyte telomere lengths.* Experimental Hematology, 2004. **32**(11): p. 1040-1050.

211.	Deschauer, M., et al., *Mitochondrial 3243 A -> G mutation (MELAS mutation) associated with painful muscle stiffness.* Neuromuscular Disorders, 1999. **9**(5): p. 305-307.

212.	Devries, D., et al., *Extreme variability of clinical symptoms among sibs in a MELAS family correlated with heteroplasmy for the mitochondrial A3243G mutation.* Journal Of The Neurological Sciences, 1994. **124**(1): p. 77-82.

213.	Hammans, S.R., et al., *The mitochondrial-DNA transfer RNA(Leu(UUR)) A->G((3243)) mutation - A clinical and genetic-study.* Brain, 1995. **118**: p. 721-734.

214.	Hotta, O., et al., *Clinical and pathologic features of focal segmental glomerulosclerosis with mitochondrial tRNA$^{Leu(UUR)}$ gene mutation.* Kidney International, 2001. **59**: p. 1236-1243.

215. Huang, C.C., et al., *MELAS syndrome with mitochondrial tRNA(Leu(UUR)) gene mutation in a chinese family.* Journal Of Neurology Neurosurgery And Psychiatry, 1994. **57**(5): p. 586-589.

216. Kato, Y., et al., *Age of onset possibly associated with the degree of heteroplasmy in two male siblings with diabetes mellitus having a A to G transition at 3243 of mitochondrial DNA.* Diabetic Medicine, 2002. **19**: p. 784-786.

217. Lien, L.M., et al., *Involvement of nervous system in maternally inherited diabetes and deafness (MIDD) with the A3243G mutation of mitochondrial DNA.* Acta Neurologica Scandinavica, 2001. **103**(3): p. 159-165.

218. Lu, J.X., et al., *Maternally transmitted diabetes mellitus associated with the mitochondrial tRNA(Leu(UUR)) A3243G mutation in a four-generation Han Chinese family.* Biochemical And Biophysical Research Communications, 2006. **348**(1): p. 115-119.

219. Majamaa-Voltti, K., et al., *Cardiac abnormalities in patients with mitochondrial DNA mutation 3243A>G.* BMC Cardiovascular Disorders, 2002. **2**(12): p. 7.

220. Martinuzzi, A., et al., *Correlation between clinical and molecular-features in 2 MELAS families.* Journal Of The Neurological Sciences, 1992. **113**(2): p. 222-229.

221. Mosewich, R.K., et al., *The syndrome of mitochondrial encephalomyopathy, lactic-acidosis, and stroke-like episodes presenting without stroke.* Archives Of Neurology, 1993. **50**(3): p. 275-278.

222. Ng, M.C.Y., et al., *Mitochondrial DNA A3243G mutation in patients with early- or late-onset type 2 diabetes mellitus in Hong Kong Chinese.* 2000, 2000. **52**: p. 557-564.

223. Olsson, C., et al., *Level of Heteroplasmy for the Mitochondrial Mutation A3243G Correlates with Age at Onset of Diabetes and Deafness.* Human Mutation, 1998. **12**: p. 52-58.

224. Saitoh, S., et al., *Single-cell analysis of mitochondrial DNA in patients and a carrier of the tRNA$^{Leu(UUR)}$ gene mutation.* Journal of Inherited Metabolic Disease, 1999. **22**: p. 608-614.

225. van Essen, E.H.R., et al., *HLA-DQ polymorphism and degree of heteroplasmy of the A3243G mitochondrial DNA mutation in maternally inherited diabetes and deafness.* Diabetic Medicine, 2000. **17**(12): p. 841-847.

226. Vilarinho, L., et al., *The mitochondrial A3243G mutation presenting as severe cardiomyopathy.* Journal Of Medical Genetics, 1997. **34**(7): p. 607-609.

227. Wilichowski, E., et al., *Pyruvate dehydrogenase complex deficiency and altered respiratory chain function in a patient with Kearns-Sayre/MELAS overlap syndrome and A3243G mtDNA mutation.* Journal Of The Neurological Sciences, 1998. **157**(2): p. 206-213.

228. Zhong, S., et al., *Presence of mitochondrial tRNA Leu(UUR) A to G 3243 mutation in DNA extracted from serum and plasma of patients with type 2 diabetes mellitus.* Journal of Clinical Pathology, 2000. **53**: p. 466-469.

229. Canter, J.A., et al., *Degree of heteroplasmy reflects oxidant damage in a large family with the mitochondrial DNA A8344G mutation.* Free Radical Biology And Medicine, 2005. **38**(5): p. 678-683.

230. Hammans, S.R., et al., *The mitochondrial-DNA transfer RNA(Lys) A-]G(8344) mutation and the syndrome of myoclonic epilepsy with ragged-red fibers (MERRF) - Relationship of clinical phenotype to proportion of mutant mitochondrial-DNA.* Brain, 1993. **116**: p. 617-632.

231. Larsson, N.G., et al., *Segregation and manifestations of the mtDNA trans RNA lys A->G(8344) mutation of myoclonus epilepsy and ragged-red fibers (MERRF) Syndrome.* American Journal Of Human Genetics, 1992. **51**(6): p. 1201-1212.

232. Piccolo, G., et al., *Myoclonus epilepsy and ragged-red fibers - Blood mitochondrial-DNA heteroplasmy in affected and asymptomatic members of a family.* Acta Neurologica Scandinavica, 1993. **88**(6): p. 406-409.

233. Traff, J., et al., *Ekboms syndrome of photomyoclonus, cerebellar-ataxia and cervical lipoma is associated with the tRNA(Lys) A8344G mutation in mitochondrial-DNA.* Acta Neurologica Scandinavica, 1995. **92**(5): p. 394-397.

234. Avise, J.C., J.E. Neigel, and J. Arnold, *Demographic Influences On Mitochondrial-Dna Lineage Survivorship In Animal Populations.* Journal Of Molecular Evolution, 1984. **20**(2): p. 99-105.

235. Ng, M.C.Y., et al., *Mitochondrial DNA A3243G mutation in patients with early- or late-onset type 2 diabetes mellitus in Hong Kong Chinese.* Clinical Endocrinology, 2000. **52**: p. 557-564.

236. El Meziane, A., et al., *A tRNA suppressor mutation in human mitochondria.* Nature Genetics, 1998. **18**(4): p. 350-353.

237. Larsson, N.G., et al., *Segregation and manifestations of the mtDNA tRNA(Lys) A-->G(8344) mutation of myoclonus epilepsy and ragged-red fibers (MERRF) syndrome.* American Journal of Human Genetics, 1992. **51**(6): p. 1201-12.

238. Howell, N., et al., *Longitudinal analysis of the segregation of mtDNA mutations in heteroplasmic individuals.* Journal Of The Neurological Sciences, 2000. **172**(1): p. 1-6.

239. Jacobi, F.K., et al., *Segregation patterns and heteroplasmy prevalence in Leber's hereditary optic neuropathy.* Investigative Ophthalmology & Visual Science, 2001. **42**(6): p. 1208-1214.

240. Hudson, G., et al., *Identification of an X-chromosomal locus and haplotype modulating the phenotype of a mitochondrial DNA disorder.* American Journal Of Human Genetics, 2005. **77**(6): p. 1086-1091.

241. Sadun, F., et al., *Ophthalmologic findings in a large pedigree of 11778/Haplogroup J Leber hereditary optic neuropathy.* American Journal Of Ophthalmology, 2004. **137**(2): p. 271-277.

242. Kerrison, J.B., et al., *A case-control study of tobacco and alcohol consumption in Leber hereditary optic neuropathy.* American Journal Of Ophthalmology, 2000. **130**(6): p. 803-812.

243. Olsson, C., et al., *The level of the mitochondrial mutation A3243G decreases upon ageing in epithelial cells from individuals with diabetes and deafness.* European Journal Of Human Genetics, 2001. **9**(12): p. 917-921.

244. Sciacco, M., et al., *Lack of apoptosis in mitochondrial encephalomyopathies.* Neurology, 2001. **56**(8): p. 1070-1074.

245.   Bidooki, S.K., et al., *Intracellular mitochondrial triplasmy in a patient with two heteroplasmic base changes.* American Journal Of Human Genetics, 1997. **60**(6): p. 1430-1438.

246.   McDonald, S.A.C., et al., *Clonal expansion in the human gut - Mitochondrial DNA mutations show us the way.* Cell Cycle, 2006. **5**(8): p. 808-811.

247.   Taylor, R.W., et al., *Mitochondrial DNA mutations and aging in human colonic crypts and stem cells.* American Journal Of Human Genetics, 2003. **73**(5): p. 250-250.

248.   Battersby, B.J., M.E. Redpath, and E.A. Shoubridge, *Mitochondrial DNA segregation in hematopoietic lineages does not depend on MHC presentation of mitochondrially encoded peptides.* Human Molecular Genetics, 2005. **14**(17): p. 2587-2594.

249.   Holt, I.J., D.H. Miller, and A.E. Harding, *Genetic heterogeneity and mitochondrial DNA heteroplasmy in Leber's hereditary optic neuropathy.* Journal of Medical Genetics, 1989. **26**(12): p. 739-43.

250.   Bolhuis, P.A., et al., *Rapid shift on genotype of human mitochondrial DNA in a family with Leber's hereditary optic neuropathy.* Biochemical and Biophysical Research Communications, 1990. **170**: p. 994-997.

251.   Vilkki, J., M.L. Savontaus, and E.K. Nikoskelainen, *Segregation of mitochondrial genomes in a heteroplasmic lineage with Leber hereditary optic neuroretinopathy.* American Journal of Human Genetics, 1990. **47**(1): p. 95-100.

252.   Upholt, W.B. and I.B. Dawid, *Mapping of mitochondrial DNA of individual sheep and goats: rapid evolution in the D loop region.* Cell, 1977. **11**(3): p. 571-83.

253.   Chinnery, P.F., et al., *Molecular pathology of MELAS and MERRF. The relationship between mutation load and clinical phenotypes.* Brain, 1997. **120**(Pt 10): p. 1713-21.

254.   Jenuth, J.P., A.C. Peterson, and E.A. Shoubridge, *Tissue-specific selection for different mtDNA genotypes in heteroplasmic mice.* Nature Genetics, 1997. **16**: p. 93-95.

255.   Cao, L., et al., *The mitochondrial bottleneck occurs without reduction of mtDNA content in female mouse germ cells.* Nature Genetics, 2007.

256.   D'Herde, K., et al., *Homology between mitochondriogenesis in the avian and amphibian oocyte.* Reprod. Nutr. Dev., 1995. **35**: p. 305-311.

257.   Meirelles, F.V. and L.C. Smith, *Mitochondrial genotype segregation during preimplantation development in mouse heteroplasmic embryos.* Genetics, 1998. **148**: p. 877-883.

258.   Bendall, K.E., et al., *Heteroplasmic point mutations in the human mtDNA control region.* American Journal of Human Genetics, 1996. **59**: p. 1276-1287.

259.   Poulton, J., V. Macaulay, and D.R. Marchington, *Mitochondrial genetics '98: Is the bottleneck cracked?* American Journal of Human Genetics, 1998. **62**: p. 752-757.

260.   Wright, S., *Evolution and the genetics of populations.* 1969, Chicago: University of Chicago Press.

261.   Tam, P.P.L. and M.H.L. Snow, *Proliferation and migration of primordial germ cells during compensatory growth in mouse embryos.* Journal of Embryology and Experimental Morphology, 1981. **64**: p. 133-147.

262.   Streffer, C., et al., *Kinetics of cell proliferation in the pre-implanted mouse embryo in vivo and in vitro.* Cell and Tissue Kinetics, 1980. **13**: p. 135-143.

263.   Larsson, N.G., et al., *Mitochondrial transcription factor A is necessary for mtDNA maintenance and embryogenesis in mice.* Nature Genetics, 1998. **18**(3): p. 231-6.

264.   Ginsburg, M., M.H.L. Snow, and A. McLaren, *Primordial germ cells in the mouse embryo during gastrulation.* Development, 1990. **110**: p. 521-528.

265.   McLaren, A. and K.A. Lawson, *How is the mouse germ-cell lineage established?* Differentiation, 2005. **73**(9-10): p. 435-7.

266.   Jenuth, J., et al., *Random genetic drift in the female germ line explains the rapid segregation of mammalian mitochondrial DNA.* Nature Genetics, 1996. **14**: p. 146-151.

267.   Downs, K.M. and T. Davies, *Staging of gastrulating mouse embryos by morphological landmarks in the dissecting microscope.* Development, 1993. **118**: p. 1255-1266.

268.   Yaffe, M., *The cutting edge of mitochondrial fusion.* NATURE CELL BIOLOGY, 2003. **5**(6): p. 497-499.

269.   Martomo, S. and C. Mathews, *Effects of biological DNA precursor pool asymmetry upon accuracy of DNA replication in vitro.* Mutation Research, 2002. **499**: p. 197-211.

270.   Mullerhocker, J., *Cytochrome-C-Oxidase Deficient Fibers in the Limb Muscle and Diaphragm of Man without Muscular Disease - an Age-Related Alteration.* Journal of the Neurological Sciences, 1990. **100**(1-2): p. 14-21.

271.   Melov, S., et al., *Marked Increase in the Number and Variety of Mitochondrial-DNA Rearrangements in Aging Human Skeletal-Muscle.* Nucleic Acids Research, 1995. **23**(20): p. 4122-4126.

272.   Kovalenko, S.A., et al., *Deltoid human muscle MTDNA is extensively rearranged in old age subjects.* Biochemical and Biophysical Research Communications, 1997. **232**(1): p. 147-152.

273.   Lee, C.M., R. Weindruch, and J.M. Aiken, *Age-associated alterations of the mitochondrial genome.* Free Radical Biology and Medicine, 1997. **22**(7): p. 1259-1269.

274.   Cortopassi, G.A. and A. Wong, *Mitochondria in organismal aging and degeneration.* Biochimica Et Biophysica Acta-Bioenergetics, 1999. **1410**(2): p. 183-193.

275.   Elson, J.L., et al., *Random intracellular drift explains the clonal expansion of mitochondrial DNA mutations with age.* American Journal of Human Genetics, 2001. **68**(3): p. 802-806.

276.   Taylor, R.B., MJ Borthwick, GM Gospel, A Chinnery, PF Samuels, DC Taylor, GA Plusa, SM Needham, SJ Greaves, LC Kirkwood, TBL and Turnbull, DM, *Mitochondrial DNA mutations in human colonic crypt stem cells.* The journal of clinical investigation 2003. **112**(9): p. 1351-1360.

277.   Khrapko, K., et al., *Cell-by-cell scanning of whole mitochondrial genomes in aged human heart reveals a significant fraction of myocytes with clonally expanded deletions.* Nucleic Acids Research, 1999. **27**(11): p. 2434-2441.

278.   Fayet, G., et al., *Ageing muscle: clonal expansions of mitochondrial DNA point mutations and deletions cause focal impairment of mitochondrial function.* Neuromuscular Disorders, 2002. **12**(5): p. 484-493.

279.   Kraytsberg, Y., et al., *Mutation and intracellular clonal expansion of mitochondrial genomes: two synergistic components of the aging process?* Mechanisms of Ageing and Development, 2003. **124**(1): p. 49-53.

Vita

HARSHA KARUR RAJASIMHA B.E., M.S., Ph.D.
URL: http://www.linkedin.com/in/HarshaRajasimha
Email: hrajasim@vt.edu
Harsha is the second son of Mrs. Vani Rajasimha and Mr. Karur Rajasimha, M.Sc. born on December 21st, 1978 at Bellary city in India.

OBJECTIVE:
A full time position in bioinformatics research and software development for biomedical application

EDUCATION:
Doctor of Philosophy (PhD), Interdisciplinary program in Genetics, Bioinformatics, and Computational Biology (computer science track):   Fall 2007
Virginia Polytechnic Institute and State University (Virginia Tech), Blacksburg, VA
Dissertation: "Insights into Mitochondrial Genetic and Morphologic Dynamics Gained by Stochastic Simulation"; Advisor: Dr. David C. Samuels;   GPA: 3.6/4.0

Master of Science (MS), Computer Science and Applications: Dec 2004
Virginia Tech, Blacksburg, VA
Thesis: "PathMeld: A Methodology for the Unification of Metabolic Pathway Databases"   GPA: 3.7/4.0

Bachelor of Engineering (BE), Computer Science and Engineering: Sep 2000
Dr. Ambedkar Institute of Technology, Bangalore, India;   GPA: 75% (~3.7/4.0)

WORK EXPERIENCE:
Software Engineer (June 2004 - present), Cyber Infrastructure Group, Virginia Bioinformatics Institute, Blacksburg, VA 24061
  Point of contact for all biological pathways related resources and issues
  Design, develop, and deploy Java and XML based bioinformatics web-services.
  Develop visualization plugins in Java Swing to import pathways in XML and semantic web based standards – SBML and BioPAX.
  Mine biological pathway data from Metacyc, KEGG and Bnet databases. Software memory performance tuning using DevPartner package.
  Evaluate and recommend generic pipeline workflow development software for automating genomic sequence analysis pipelines.
  Lead a computer science based team effort on pathway data integration, curation, visualization, and analysis for drug target discovery.
  Project management using Vertabase software.

Harsha Karur Rajasimha

Graduate Research Assistant (Dec 2002 - May 2004), Virginia Bioinformatics Institute, Virginia Tech, Blacksburg, VA

Stochastic modeling and agent-based simulation of mitochondrial DNA (mtDNA), mtDNA mutation dynamics and mitochondrial morphologic dynamics in a cell, Nucleotide pool (dNTP) modeling, simulation of the mitochondrial toxicity of a HIV drug (AZT) and cell culture simulations.

All models are developed and applied to answer specific biological questions and the results are published in journals.

Programmer (Sep 2002 - Dec 2002), Information Systems and Insect Studies lab, Virginia Tech, Blacksburg, VA

Convert a Java application to applet. The application supported creation and editing of concept maps.

Microsoft Intern Summer 2002, XML Enterprise Services, Microsoft, Redmond, WA

Develop and implement test cases for the COM+ team.

Integrate multiple leak detection tools and identify potential memory leaks

Programmer (Feb 2001 - May 2002), Multimedia Lab, Virginia Tech, Blacksburg, VA

Java implementation of a movie scheduling system;

Text book conversion using Adobe Illustrator;

Develop online survey and web publish results of survey;

Java Developer Intern (Sep 1999 - Jul 2000), Center for Development of Advanced Computing (CDAC) [Government of India]

Develop webmail client using Java mail API, Jdk1.2, JWS2.0, and JSDK

Lecturer (Sep 2000 - Dec 2000), Department of Computer Science, Dr A.I.T, Bangalore, India

Teach Logic Design, Computer Networks, and Data Structures with C

PROJECTS ON WHICH EMPLOYED:

PATRIC: PAThosystems Resource Integration Center (http://patric.vbi.vt.edu)

Funded by NIH through NIAID to PI: Dr. Bruno Sobral (2004-2009). PATRIC is one of 8 Bioinformatics Resource Centers (BRCs) in USA funded by NIAID, NIH. The goal of the project is to analyze raw genomic sequences of pathogenic bacteria and viruses to enable the prediction of vaccines, diagnostics and therapeutics.

My contribution (06/2005 – present)**:** Lead a computer science based effort to evaluate and recommend software solutions to predict, annotate and visualize metabolic pathways in bacteria, given their genomic annotations.

Recommended and integrated Pathway tools software into the PATRIC system. We implemented the computational prediction of metabolic chokepoints and other pathways analyses targeted towards therapeutics.

PathPort: Pathogen Portal (http://pathport.vbi.vt.edu/main/home.php)
> Funded by DOD to PI: Dr. Bruno Sobral (2002-2007)
> The goal of the PathPort project is to develop sequence analysis and bioinformatics webservices and visualization plugins to study various pathogenic bacteria and viruses posing a biothreat.
> **My contributions** (06/2004-01/2006): Develop a webservice to mine metabolic pathway data, develop pathway visualization plugin to import pathway data in standard XML formats such as SBML and BioPAX, and perform software performance evaluation and tuning.

Biodefense Proteomics Resource (http://www.proteomicsresource.org/default.aspx)
> $8.7million grant awarded by NIH through NIAID to Social and Scientific Systems, Inc, teaming with VBI and Proteomics Information Resource
> The goal of the project is to accumulate, store, retrieve, and disseminate proteomic experimental data.
> **My contributions** (06/2005-01/2007): Integrate visualization plugin for yeast-2-hybrid experimental data and integrate proteomics data with the PATRIC project.

COURSE PROJECT WITH EXTERNAL CLIENT:
Global Market Research (GMR) Project: International Marketing Analysis and Market Entry Strategy for a Virginia based software firm
> GMR is a unique resource offered by Virginia Economic Development Partnership's (VEDP) Division of International Trade to link Virginia businesses interested in exporting international markets with the talent pool concentrated in graduate business schools throughout the commonwealth.
> GMR project is a 3 hour elective offered through the MBA program.
> Generally it is limited to MBA candidates, but since the project involved marketing a software product, students from computer science were invited into the project team of four - two from MBA and two from computer science.
> My team leader role in this project was a rewarding experience.
> The project involved international market research of document control software product, recommending the market with the greatest potential, developing market entry strategy and making recommendations on advertising.

PUBLICATIONS:
> **HK Rajasimha,** PF Chinnery, DC Samuels; Selection against pathogenic mtDNA mutations in a stem cell population: The loss of the 3243A>G mutation in blood; *American Journal of Human Genetics*; Feb 2008; Accepted for publication; In Press
> LM Cree, DC Samuels, SC de Sousa Lopes, **HK Rajasimha**, P Wonnapinij, JR Mann, HM Dahl & PF Chinnery; A reduction in the number of mitochondrial DNA molecules during embryogenesis explains the rapid segregation of genotypes. *Nature Genetics*; Dec 2007; Accepted for publication; In Press
> Snyder EE, Kampanya N, Lu J, Nordberg E, **Karur HR**, Eckart JD, Kenyon R, Will R, Setubal J, Sobral B: The VBI PathoSystems Resource Integration Center (PATRIC); *Nucleic Acids Research: Database Issue*; 2006

HK Rajasimha, DC Samuels, and RE Nance; A simulation methodology in modeling cell divisions with stochastic effects; *Proc. of the Winter Simulation Conference* 2004; Washington DC

SYMPOSIUMS AND WORKSHOPS:

Participant, BioPAX Development Meeting: June 20-21, 2006; Cold Spring Harbor Lab, NY
Presenter, First Annual Virginia Bioinformatics Institute Research Symposium.
March 23-24, 2006, Blacksburg, VA
Title: "Integration of metabolic pathway databases"
BioPAX Symposium and Workshop (International): Nov 15-18, 2005, Tokyo, Japan.
Title: "Pathways support in Pathogen Portal"

TALKS:

For a list of technical talks delivered, refer http://staff.vbi.vt.edu/hrajasim/talks.html

COMPUTER SCIENCE RELATED COURSES:

Information Visualization, Software Engineering, Internet Software, Usability Engineering, Operating Systems, Computer and Network Architecture, Design and Analysis of Algorithms

BIOINFORMATICS RELATED COURSES:

Algorithms in Bioinformatics, Computational Systems Biology, Statistics in Research, Continuous Models for Biological Applications, Problem Solving in Bioinformatics, Database design for signaling networks in plants, Cell Biology and Genetics, Computational Biochemistry for Bioinformatics, Issues in Bioethics, Seminars.

TECHNICAL SKILLS:

Languages: C, C++, C#, Java, XML, UML, 'R' statistics package, RDF/OWL
Source version control: CVS, SVN
Operating Systems: Windows 9x/2000/NT/. NET server, Linux
Databases: Postgres, Oracle, MS Access, SQl Server 2000
Servers: Apache Tomcat and Axis deployment, Blazix
Software performance & project management: DevPartner, Vertabase
Bioinformatics skills: Pathway tools, GO, SBML, BioPAX, KEGG, Integration of databases, Reactome, Cell designer, COPASI, Modeling & simulation

ACTIVITIES/HONORS:

Certification in training for human subjects protection, Virginia Tech, VA
Secretary of The Interior and Co-Social Director, Computer Science Grad Student Council, Virginia Polytechnic Institute and State University, Blacksburg, VA
First Place, district level inter-collegiate Elocution Competition, Gulbarga, India
Volunteer, International Mega event Bangalore.IT.COM

REFERENCES:

Dr. David C. Samuels, Assistant Professor, Virginia Bioinformatics Institute (dsamuels@vbi.vt.edu) Phone: 540-231-8999
Mr. Eric Nordberg, Senior software engineer, Virginia Bioinformatics Institute, (enordber@vbi.vt.edu) Phone: 540-231-5353
Dr. Joao Setubal, Associate Professor & Deputy Director of Virginia Bioinformatics Institute, (setubal@vbi.vt.edu) Phone: 540-231-9464